Quaternary Science Reviews 269 (2021) 107133

Contents lists available at ScienceDirect

Quaternary Science Reviews

journal homepage: www.elsevier.com/locate/quascirev

Invited review

Sea-ice reconstructions from bromine and iodine in ice cores

Paul Vallelonga [a, b, *], Niccolò Maffezzoli [a, c, d], Alfonso Saiz-Lopez [e], Federico Scoto [f], Helle Astrid Kjær [a], Andrea Spolaor [c, d]

[a] Physics of Ice, Climate and Earth (PICE), Niels Bohr Institute, University of Copenhagen, Tagensvej 16, Copenhagen N, 2200, Denmark
[b] Oceans Graduate School, The University of Western Australia, M470, Perth, WA, 6009, Australia
[c] Department of Environmental Sciences, Informatics and Statistics, University Ca' Foscari of Venice, via Torino 155, 30172, Venice, Italy
[d] Institute of Polar Sciences, National Research Council of Italy, via Torino 155, 30172, Venice, Italy
[e] Department of Atmospheric Chemistry and Climate, Institute of Physical Chemistry Rocasolano, CSIC. Serrano 119, 28006, Madrid, Spain
[f] Institute of Atmospheric Sciences and Climate, National Research Council of Italy, SPLecce - Monteroni Km 1.2 -73100, Lecce, Italy

ARTICLE INFO

Article history:
Received 14 February 2021
Received in revised form
19 June 2021
Accepted 30 July 2021
Available online 21 August 2021

Handling Editor: C. O'Cofaigh

Keywords:
Halogen
Ice core
Bromine
Iodine
Sea-ice
Sea-ice extent
Sea-ice reconstruction
Antarctica
Southern ocean
Greenland
Svalbard
Severnaya Zemlya
Nordic seas

ABSTRACT

As the intricacies of paleoclimate dynamics are explored, it is becoming understood that sea-ice variability can instigate, or contribute to, climate change instabilities commonly described as "tipping points". Compared to ice sheets and circulating ocean currents, sea-ice is ephemeral and continental-scale changes to sea ice cover occur seasonally. Sea-ice greatly influences polar albedo, atmosphere-ocean gas exchange and vertical mixing of polar ocean masses. Major changes in sea ice distribution and thickness have been invoked as drivers of deglaciations as well as stadial climate variability described in Greenland climate records as "Dansgaard-Oeschger" cycles and described in Antarctic climate records as "Antarctic Isotopic Maxima".

The role of halogens in polar atmospheric chemistry has been studied intensively over the past few decades. This research has been driven by the role of bromine, primarily as gas-phase bromine monoxide (BrO), which exerts a key control on polar tropospheric ozone concentrations. Initial findings led to the discovery of boundary-layer self-catalyzing heterogeneous bromine reactions fed by sunlight and ozone, known as bromine explosions. First-year sea-ice and blowing snow have been identified as key components for this heterogeneous bromine recycling in the polar boundary layer. This understanding of polar halogen chemistry – supported by an expanding body of observations and modeling – has formed the basis for investigating quantitative links between halogen concentrations in the polar atmospheric boundary layer and sea-ice presence and/or extent.

Despite the clear importance of sea-ice in paleoclimate research, the ice core community lacks a conservative and quantitative proxy for sea-ice extent. The most commonly applied proxy, methanesulphonic acid (MSA), is volatile and has not been demonstrated reliably for ice core records extending beyond the last few centuries. Sodium has also been applied to reconstruct sea-ice extent in a semi-quantitative manner although the effects of meteorological transport noise are significant. Contrary to *a priori* expectations, the halogens bromine and iodine appear to be stable in polar snow and ice over millennial timescales, addressing the temporal limitations of MSA records. Unfortunately, transport and meteorological variability influence sodium deposition as well as the deposition of halogens and the many other ionic impurities found in ice cores. The atmospheric chemistry of halogens is more complex than those of sodium or MSA due to the mixed-phase (gas and aerosol) nature of halogen photochemistry. Thus the application of halogen records in ice cores to sea-ice reconstruction overcomes some challenges posed by existing proxies, but also opens new challenges specific to halogens. Challenges common to all sea-ice proxies include the deconvolution of changes in emission source locations and changes in transport efficacy, particularly those occurring during climate transitions combining changes in sea-ice and atmospheric circulation, such as stadial/interstadial or glacial/interglacial climate variability.

In this review, we describe the rationale and available evidence for linking the halogens bromine and iodine found in polar snow and ice to sea-ice extent. Reported measurements of bromine and iodine in

* Corresponding author. Physics of Ice, Climate and Earth (PICE) , Niels Bohr Institute, University of Copenhagen, Tagensvej 16, Copenhagen N, 2200 Denmark.
E-mail address: vallelonga@nbi.ku.dk (P. Vallelonga).

https://doi.org/10.1016/j.quascirev.2021.107133

polar snow and ice samples are critically discussed. We also consider aspects of halogen transport and retention in polar snow and ice that are still poorly understood. Overall, there is a growing body of evidence supporting the application of bromine to sea-ice reconstructions, and the use of iodine to reconstruct marine biological activity mediated in part by sea-ice extent. These halogens complement existing sea-ice proxies but most crucially, offer the capacity to greatly extend the temporal and spatial coverage of ice core-based sea-ice reconstructions. We identify knowledge gaps existing in the current understanding of spatial and temporal variability of halogen distributions in the polar regions. We suggest areas where polar halogen chemistry can contribute to a better understanding of the halogen records recovered from ice cores. Finally, we propose future steps for establishing reliable and constructive sea-ice reconstructions based on bromine and iodine as observed in snow and ice cores.

1. Introduction

Ice cores provide sensitive and detailed records of past climate variability, with the unique ability to directly archive atmospheric gases and aerosols. Snow deposition and retention is the fundamental requirement for ice caps to form and eventually grow to large ice sheets such as those found in Greenland and Antarctica. Smaller ice caps form on mountain ranges although many are currently threatened by anthropogenic warming. The polar ice sheets are up to 4 km thick, while most mountain ice caps are not more than approximately 100 m thick (Bradley, 2015). Ice cores record climate on seasonal to millennial timescales, with the oldest ice cores recovered from central Antarctica (EPICA community members, 2006). The time period archived in an ice core primarily depends on the rate of snow accumulation at the site, the amount of glaciological thinning due to ice flow and the thickness of the ice sheet. Ice core chronologies are essential to the accurate interpretation of ice core impurities, and are established by a variety of complementary techniques, including the counting of annual layers determined by seasonally-varying impurities (Sigl et al., 2016; Winstrup et al., 2019), identification of known or notable volcanic eruptions (Sigl et al., 2015; Svensson et al., 2020), determination of globally-synchronous atmospheric events such as methane uptake/release from tropical wetlands (EPICA community members, 2006) and fluctuations in the Earth's magnetic field (Raisbeck et al., 2017), as well as the application of glaciological ice flow models (e.g.: Parrenin et al., 2007).

Climate records are typically obtained from ice sheets by drilling ice cores, often striking a compromise between the amount of ice sample obtained and the ability to access deep ice far below the surface (Johnsen et al., 2007). An electromechanical ice core drill is a hollow tube with cutters at the bottom, which rotates and draws cuttings up into a chamber above the ice core cylinder. The drill is suspended on a cable, providing power and control data as well as lowering and raising the drill. Once a suitable core length has been drilled, the drill is raised and upward-pointing core-dogs dig into the ice to break the ice cylinder and hold it in position. Electromechanical ice core drills typically produce 75–108 mm diameter cores with up to 30 m drilled per day (Sheldon et al., 2014). Deep ice core drillings conducted in central Greenland and Antarctica may require 3 or more drilling seasons to reach bedrock (Popp et al., 2014). Electromechanical drills can recover ice from a few hundred metres' depth typically within a week or two.

In the absence of excessive melt, impurities are preserved in the snow/ice matrix and can be determined to investigate a wide variety of climate parameters. The impurities are employed in a quantitative or semi-quantitative manner as proxies of earth system parameters including desert dust, storminess, wind speed, biomass burning, volcanism, and many others (Schüpbach et al., 2018). Key to the employment of such proxies is their sensitivity to source emissions, lack of ambiguity/alternate emission sources, reliability of transport and stability in the snow/ice matrix. Atmospheric transport processes may be investigated by deposition studies, in-situ analyses and/or model-based studies. Surface melting occurs in sites where a significant number of consecutive positive degree days are experienced or liquid precipitation events may occur due to atmospheric phenomena such as 'atmospheric rivers' (Nghiem et al., 2012). Such sites may be located hundreds of metres above the calculated equilibrium line altitude (e.g. Holtedahlfonna in Svalbard is located at 1150 m asl whereas the equilibrium line is 600–700 m a.s.l.). Meltwater produced at the surface is then able to mix with deeper, cooled layers and eventually refreezes in dense and/or cold layers in snowpack, typically corresponding to the previous winter strata. Surface melting can volatilize some unstable molecules such as MSA, iodine and nitrate, leading to unreliability in their use for climate reconstructions (Pohjola et al., 2002). Many ionic species appear to be unaffected by surface melt (Bonne et al., 2015; Nilsson et al., 2015).

Sodium has been studied extensively in ice and snow as it is relatively easy to determine, stable in the snow matrix and primarily represents sea-salt deposition to the sampling site. Early studies of sodium deposition, conducted on snow pit sites at central Greenland and coastal Antarctic locations, revealed a seasonal cycle peaking in winter (Legrand and Mayewski, 1997). This peak has been traditionally attributed to a peak in storminess, generating waves and transporting marine aerosols efficiently to the polar ice sheets. Later studies identified a sodium/sulphate fractionation indicative of sea-ice based frost flowers: mirabilite crystals that grow from the salty brine on the sea-ice surface and can be transported inland during wind gusts (Rankin et al., 2002). While the importance of sea-ice sea-salt aerosol emissions was recognized, the idea that frost flowers were the main sea-salt aerosol source was challenged by laboratory and model studies (e.g. Legrand et al., 2016; Levine et al., 2014). To date, the most efficient substrate for sea-salt aerosol emissions in the polar regions is attributed to the snow layer that deposits onto fresh sea-ice surfaces, known as salty blowing snow, that becomes enriched in brine and can be easily lofted by the strong polar winds (Frey et al., 2020). Given that sodium can be emitted from the open ocean as well as the sea-ice surface, modeling studies have been employed to better constrain the circumstances in which sodium in ice cores may be attributed to sea-ice (Levine et al., 2014; Rhodes et al., 2018). Such studies indicate that sodium, and likely other sea-ice related elements such as Br and MSA, could be controlled by meteorological effects on annual to decadal scales. Sea-ice reconstructions (SIR) based on sodium are highly dependent on individual site characteristics (Rhodes et al., 2018). Sodium has been demonstrated to be an effective sea-ice indicator primarily at coastal sampling locations (Mezgec et al., 2017).

Methanesulphonic acid (MSA) is an oxidation product of

dimethylsulfide (DMS) released by marine algae. The links between DMS and sea-ice were first investigated in the 1990s (Curran et al., 1998) and DMS is now identified as a credible indicator of sea-ice at some sites in Antarctica and the Arctic (Abram et al., 2013). Depending on the configuration of sea-ice cover and open water, different interpretations are applied to MSA records from different sampling sites, so MSA has been used variously to quantify open water extent (summer sea-ice absence), winter sea-ice extent or atmospheric transport conditions. Models overestimate the concentration of MSA in the snowpack of central Antarctica – most likely because of postdepositional loss of MSA from such zones of low snow accumulation – but do attribute the majority of MSA variability to sea-ice variability (Hezel et al., 2011). The stability of MSA in ice cores has been demonstrated to be problematic in some ice cores – MSA is volatile and will remobilize in the ice matrix with time (Curran et al., 2002; Osman et al., 2017). MSA is volatilized from ice core samples stored for several years but appears stable in samples that have been melted and then refrozen within a few months of ice core extraction (Abram et al., 2013). Studies of Antarctic and Arctic ice cores have shown that MSA migrates from summer deposition layers to impurity-laden winter layers, particularly those containing high levels of sea salt (Osman et al., 2017). MSA stability in ice cores is also promoted by the presence of dust (Legrand et al., 1997). Recently, it has been proposed that MSA found in Greenland ice is predominantly controlled by DMS emission due to North Atlantic ocean productivity (Osman et al., 2019). For central Antarctic sites, there is evidence that MSA is destroyed in-situ by photochemical processes (Legrand et al., 2016) particularly during the summertime. The longest MSA-based SIR for the northern hemisphere is from Lomonosovfonna, Svalbard (Isaksson et al., 2005) and covers the last few centuries. For the Southern Hemisphere, the longest MSA-based SIRs cover approximately 300 years (Thomas and Abram, 2016; Xiao et al., 2015) although several shorter records have also been reported (Abram et al., 2013 and references therein; Bertler et al., 2018; Murphy et al., 2014).

Sea-ice occurs in the polar regions, where atmospheric temperatures are sufficiently cold to freeze seawater (Thomas and Dieckmann, 2003). There are several different forms of sea-ice, but relatively stable water conditions are required for sea-ice to form as frazil and grease ice, and then conglomerate into larger forms such as pancake ice (Eicken, 2003). Sea-ice that forms during the autumn and winter is known as seasonal, first-year or fresh, sea-ice while sea-ice that remains frozen through the spring and summer is classified as multi-year sea-ice. Antarctica is primarily surrounded by first-year sea-ice, with pockets of multi-year sea-ice that remain in the Weddell Sea and some bays along the Antarctic coastline. In the Arctic, multi-year sea-ice is present as a mass located between Greenland and the North pole, with first-year sea-ice growing to cover the Arctic Ocean, Baffin and Hudson bays as well as often filling the Barents and Chukchi seas (Stroeve et al., 2012a). As sea-ice forms, salt is expelled into channels and pockets of brine collecting on the upper surface of the ice. Freeboarding of seawater onto the ice is another source of salt for the sea-ice surface. Sea-ice forms an important barrier to the exchange of heat, gas and aerosols from the ocean to the atmosphere and vice versa. Sea-ice is permeable to gases at temperatures above -5 °C and is a vital habitat for algae in polar ecosystems (Vancoppenolle et al., 2013).

Despite being observed for hundreds of years, Arctic sea-ice variability is still a topic of considerable interest with substantial uncertainty regarding its variability and future. The earliest sea-ice observations are drawn from the written records of Iceland fishermen, going back over 400 years (Ogilvie, 1984). With increasing emissions of greenhouse gases, the impact of recent climate change has led to renewed interest in the understanding of sea-ice variability (Kinnard et al., 2011). Since the start of the satellite era, Arctic sea-ice has been observed to decrease rapidly in extent and thickness. Past models of sea-ice decline have failed to capture the rapidity of change in the Arctic predicting that the Arctic will be free of summer sea-ice (sea-ice area<1 million km^2) before the end of the 21st century (Stroeve and Notz, 2015). The latest generation models, however, are able to provide a more realistic estimate of the sensitivity of September Arctic sea-ice area to a given amount of anthropogenic CO_2 emissions and to a given amount of global warming. Most simulations from the last Coupled Model Intercomparison Project (CMIP6) indicate the occurrence of sea-ice free September events in the Arctic Ocean by 2050 (SIMIP Community, 2020). In this perspective, reconstructions of sea-ice extending back to the penultimate interglacial warm period (the Eemian as it is known in the Northern Hemisphere) are of vital importance to understanding the extent of sea-ice in warm climate periods.

The majority of paleo-scale sea-ice reconstructions are based on sea-ice proxies preserved in marine sediment cores. Marine basins typically feature very low sedimentation rates, resulting in relatively poor time resolution – compared to ice cores – but much longer temporal coverage, combined with superior spatial coverage. The direct sedimentation of sea-ice debris onto the seafloor is also strongly favourable to the reconstruction of sea-ice presence from sediment records. Sea-ice reconstructions from ocean sediments have been produced from siliceous diatoms, phytoplankton markers and most recently from IP_{25}, a highly branched isoprenoid lipid biomarker associated with sea-ice-dwelling diatoms in the Arctic Ocean (Belt et al., 2007). IP_{25} is specific to seasonal sea-ice, as algal communities are not sustained below relatively thick and impermeable perennial sea-ice, where light and nutrients are unavailable. As the absence of IP_{25} may indicate either open water conditions, or perennial sea-ice, it is typically combined with a complementary phytoplankton biomarker to establish which extreme condition exists (i.e.: perennial sea-ice or open water). These are identified as P_BIP_{25} or P_DIP_{25} respectively, if Brassicasterol or Dinosterol phytoplankton biomarkers are employed. Reconstructions of Antarctic sea-ice extent are based on an equivalent biomarker present in the Southern Ocean, denoted as $IPSO_{25}$, and are presently limited to the Atlantic and Indian Ocean sectors due to the problem of carbonate dissolution primarily in the Pacific Ocean sector and near to the Subtropical Front (Gersonde et al., 2005).

Although it is a halogen element, chlorine is not considered as a sea-ice proxy in this review due to key issues regarding the emission, transport and deposition of this ubiquitous marine element. The emission of chlorine (and sodium) into the atmosphere is overwhelmingly driven through wave breaking/bubble bursting processes occurring at the ocean surface. This feature has been used in past attempts to semi-quantitatively evaluate sea-ice extent through the fluxes of sodium and chloride to central Antarctica (Levine et al., 2014; Röthlisberger et al., 2003; Wolff et al., 2006). The findings of this course of research indicate that at best, sea-salts may be used to infer sea-ice extent in a qualitative manner: meteorological (transport) “noise” exerts a strong influence on the sea-salt signal deposited to inland Antarctica, and this effect becomes stronger as the distance from the sampling site to the marginal ice zone increases. Furthermore, the stability of chlorine in the snow matrix is challenged by post-depositional dechlorination of snow due to acid reactions producing gas-phase HCl (Röthlisberger et al., 2003). The combination of these factors inhibits the general reliability of Cl as an environmental proxy in ice cores; and specifically degrades any quantitative link between chlorine and sea-ice extent specifically. In comparison, bromine and iodine enrichment processes can be directly linked to sea-ice, specifically first-year sea-ice. While still subject to meteorological noise (as are all

aerosols), the post-depositional effects demonstrated by chlorine appear to be far less significant for bromine (as discussed further in section 3.4.2). Post-depositional effects are observed for iodine and are described in section 3.4.3.

In this review we will present the current state of understanding on the applicability of Br to track the past sea-ice extent and variability from ice core records. Although some uncertainties remain, such as a detailed understanding of the interactions ongoing within the mixed gas- and aerosol-based phases during bromine transport, this halogen shows promise as a possible tracer of past sea-ice extent. We will provide a brief introduction to the polar photochemistry associated with iodine and bromine and evaluate their stability in the polar snow/ice matrix. We will then present the available bromine data on timescales relevant to ice core archives, and summarize the findings of sea-ice reconstructions based on mainly bromine in polar ice. The locations of relevant studies of bromine and/or iodine timeseries are shown in Fig. 1 and summarized in Table 1. We conclude with a summary of the state of the art and outline future directions in this field of research, relevant for future deep ice core drilling as well as complementary sea-ice reconstructions from proxies found in marine sediment records.

2. Determination of halogens in ice

2.1. Analytical techniques

Bromine and iodine are found in meteoric ice at trace levels, typically from tens of picograms per gram (pg/g) to tens of nanograms per gram (ng/g). Although the measures are not strictly identical, ng/g (weight/weight) concentrations are often also reported as ppb (part per billion), which is a more generic concentration metric. For consistency with the literature, here we will consistently report ng/g concentrations as ppb, and pg/g as ppt. The highest concentrations have been reported for ice cores from low altitude, coastal locations whereas the lowest concentrations have been found far inland on the high-altitude East Antarctic plateau (Table 2).

Bromine concentrations are typically determined in polar snow and ice by Ion Chromatography (IC) or Inductively-Coupled Plasma Mass Spectrometry (ICPMS). Both instruments accept liquid samples, so the snow/ice sample is melted prior to analysis. The melting may take place as a dedicated sampling or, more commonly, will form part of a Continuous Flow Analysis (CFA) setup. CFA is a technique in which firn/ice sticks are sequentially melted onto a melthead which separates the pristine inner section of the sample from the contaminated exterior (e.g.: Kaufmann et al., 2008). Meltwater from the inner section is pumped into various flow-through sensors or sent to optical flow cells for determination of soluble ionic impurities, or collected in sampling tubes or beakers for later analysis. Typically, these discrete samples will be refrozen and stored until ready for analysis by IC or ICPMS. These techniques will be further discussed below.

Inductively Coupled Plasma Mass Spectrometry is a standard technique for trace analysis, with good sensitivity in the ppb to ppt range. ICPMS comprises three fundamental steps: sample ionization, separation and detection. Sample ionization is conducted using an argon-fed plasma, operating at 6000–10000 K. For signal stability, a fine aerosol of uniform size is produced by the introduction system and fed into the plasma using a nebulizer with a typical pore size of 50–200 μm. The introduction system may consist of a Scott-type spray chamber or a cyclonic spray chamber, with cooling to assist the drying of the aerosols. Once introduced into the plasma and ionized, the target ions are separated from other ions by either a quadrupole (ICP-QMS) or sector-field magnet (ICP-SFMS). The quadrupole has a faster rate of scanning but lower mass resolution compared to the sector-field instrument. In both instruments the detector is usually a secondary electron multiplier (SEM), which absorbs the ion and in turn produces a photon that can be amplified by a sequence of cascading anodes. Typically, a helium-filled collision cell is added to the ICP-QMS instrument to boost measurement sensitivity and signal stability. ICP-QMS is suitable for ppb concentrations while ICP-SFMS is recommended for ppt concentrations. However, ICP-QMS capabilities have improved in recent years also allowing determination of halogens at sub-ppb level, closer to the performance obtained from the ICP-SFMS.

Ion chromatography is a standard technique for the determination of soluble ions in snow and ice. The heart of the instrument is the separation column, a resin-based high-pressure ion-exchange column through which the ions will pass at different rates, based on their charge and other properties determining their level of binding to the column resin. The IC will typically feature a guard column to remove particles from the sample stream, then a preparation column to conduct a broad removal of unwanted ions, and then the sample will be introduced into the analytical column. Once the column has been loaded, an eluent removes the ions from the column, which then pass through a sensitive conductivity meter. The concentration of a particular ion is determined as the corresponding area below the conductivity peak and is calibrated using standard solutions of the ions to be determined. Optimization of the elution time and separation of interferences is normally achieved by finding an ideal combination of temperature, eluent concentration(s) and flow speed(s) applied to the column. The sensitivity of the IC technique is suitable for determination of bromine and iodine species at ppb concentrations but is generally insufficient for determination of halogens at low ppb and ppt levels. Therefore, iodine species are usually determined by ICPMS systems or IC separation systems coupled to an ICPMS detection system.

For any analytical technique, contamination control and memory effects must be carefully evaluated to ensure accurate measurements are made. In laboratory settings, bromine may be found in some plastics and in fire control equipment (as BFRs, bromine fire retardants). Generally, these materials are easily isolated from sample preparation areas. Due to the volatility of halogens, samples should not be exposed to acids or acid vapour and ice samples should generally be kept frozen and in darkness until they are to be analyzed. Samples analyzed for bromine and iodine are therefore not readily prone to contamination, but a more common source of difficulty is the substantial memory effects associated with quartz glassware commonly used in MS introduction systems. Therefore a moderate level of regular cleaning with ammonium hydroxide is required once the sample introduction system has been cleaned to an acceptable level (Spolaor et al., 2012). An initial cleaning with ammonium hydroxide removes bromine and iodine from the quartz glassware of the ICPMS introduction system, however the ammonium hydroxide may lead to salt deposition within the introduction system that may potentially block the nebulizer. Therefore, after the ammonium hydroxide cleaning stage, the introduction system is cleaned with 2 % nitric acid for 90 s and then MilliQ-quality (>18.2 MΩ/cm) ultrapure water (UPW) for 90 s before sample analysis. The use of UPW before the sample analysis has two effects: firstly, to remove any nitrate salts that may be deposited by the nitric acid and secondly, to condition the instrument before introducing the unacidified samples for halogens analysis.

Fig. 2 shows an example of the extensive memory effect that occurs when only nitric acid is used in the cleaning procedure – a technique that is typical for analysis of trace metals by ICPMS. In the case shown, the ICPMS introduction system is washed between analyses for 45 s using only a 2 % nitric acid solution. Each

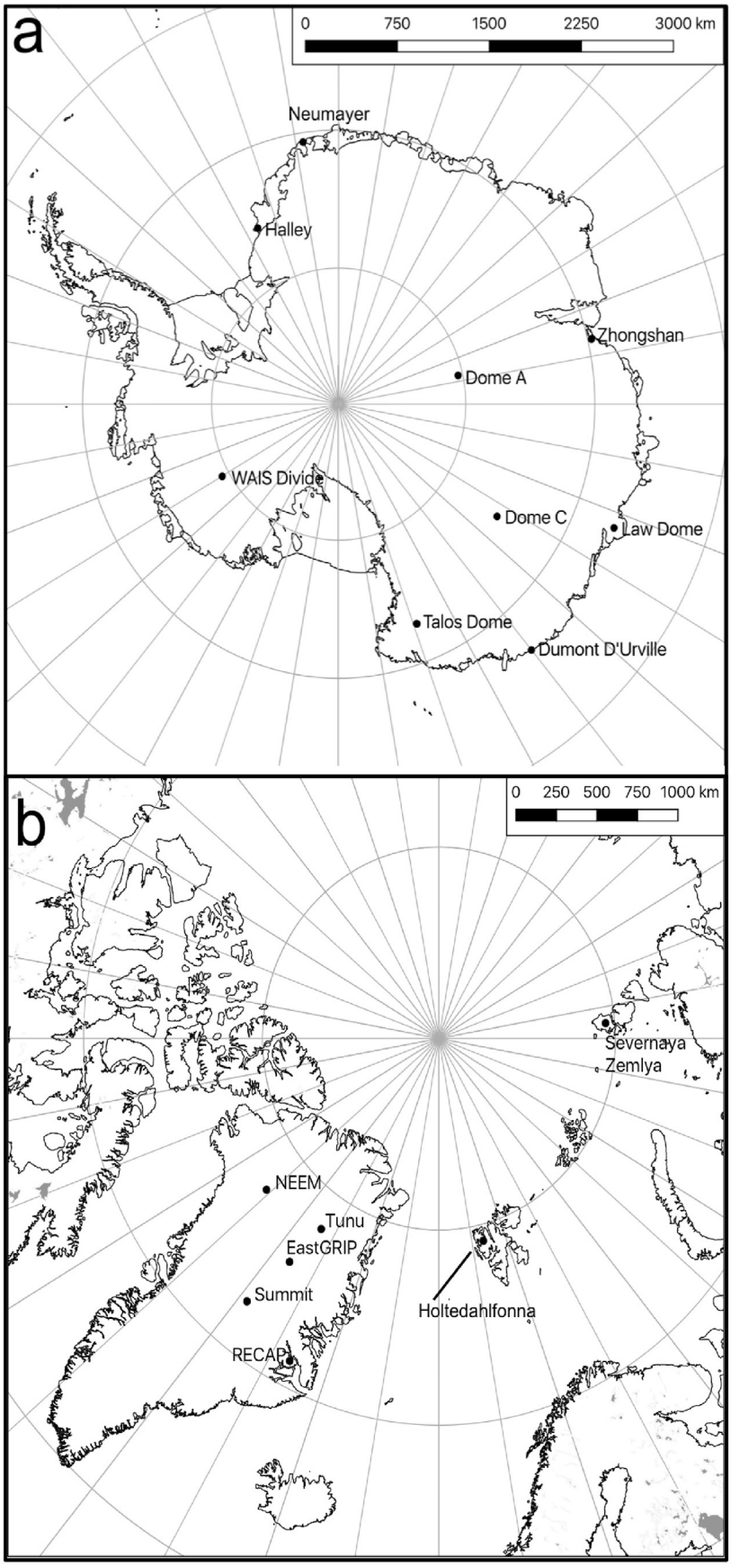

Fig. 1. Antarctic (a) and Arctic (b) sampling sites and research locations mentioned in the text.

Table 1
Summary information regarding halogen sampling sites mentioned in the text.

Location	Latitude, Longitude	Altitude (m asl)	Reference(s)	Resolution and duration of record	
				Bromine	Iodine
Antarctica					
Dome A	80°22'S, 77°21'E	4093	Li et al., 2014	annual	
Dome C	75°06'S, 123°33'E	3233	Legrand et al., 2016	seasonal	
			This work	seasonal	seasonal
Dumont D'Urville	66°40'S, 140°01'E	0	Legrand et al., 2016	seasonal	
Law Dome	66°46'S, 112°48'E	1370	Spolaor et al., 2014	seasonal	seasonal
			Vallelonga et al., 2017	seasonal-decadal	seasonal-decadal
Neumayer station	70°40'S, 8°16'W	40	Frieß et al., 2010		seasonal
Northern Victoria Land	72°48'S, 159°06'E	1781-2318	Maffezzoli et al., 2017	seasonal	seasonal
Talos Dome	72°49'S, 159°10'E	2318	Spolaor et al., 2013b	centennial-millennial	centennial-millennial
Arctic					
NEEM	77°45'N, 51°06'W	2450	Spolaor et al., 2014	seasonal	seasonal
			Spolaor et al., 2016b	centennial-millennial	
Renland	71°18'N, 26°43'W	2315	Cuevas et al., 2018		decadal-centennial
			Maffezzoli et al., 2019	centennial-millennial	
Severnaya Zemlya	80°31'N, 94°49'E	760	Spolaor et al., 2016a	seasonal-decadal	seasonal-decadal
Summit	72°20'N, 38°17'W	3200	Maselli et al., 2017	seasonal-decadal	
Svalbard (Holtedahlfonna)	79°09'N, 13°23'E	1150	Spolaor et al., 2013a 2014	seasonal-decadal	seasonal-decadal
Tunu	78°02'N, 33°52'W	2113	Maselli et al., 2017	seasonal-decadal	

Table 2
Summary of bromine and iodine results from Antarctica and the Arctic.

Antarctica	HOLOCENE / 20th century													
Location	Time period	Br min ppb	Br max ppb	Br mean ppb	Na min ppb	Na max ppb	I min ppb	I max ppb	Brenr min	Brenr max	Brenr mean	Brenr median	Reference	Relevance to Brenr
Talos Dome	10.7 - 4.2 ky BP	0.08	0.17	0.13	9	31	0.001	0.09	0.5	3.2	1.4	1.2	Spolaor et al., 2013b	Inland deposition zone
North Victoria Land	2011-2015 CE	0.2	2	0.66	8	200	0.03	0.05	1	12	4.4	3.9	Maffezzoli et al 2017	Coastal deposition zone
Law Dome	1927-1989 CE	0.8	20	3.2	22	162	0.03	0.2	3	71	17	11	Vallelonga et al 2017	Coastal deposition zone
Neumayer	2006-2008 CE						0.001	0.7					Frieß et al., 2010	Coastal deposition zone
Dome A	2012 CE			0.2		14					2.3		Li et al., 2014	Inland depletion zone
Dome C	2009-2010 CE	0.05	0.5		20	200	0.001	0.1	0.07	1.5	0.5		Legrand et al 2016	Inland depletion zone
Antarctica	**LGM**													
Talos Dome	34-17 ky BP	0.02	0.15	0.07	22	68	0.034	0.27	0.1	0.7	0.3	0.2	Spolaor et al., 2013b	Inland depletion zone during glacials
Arctic	**HOLOCENE / 20th century**													
Location	Time period	Br min ppb	Br max ppb	Br mean ppb	Na min ppb	Na max ppb	I min ppb	I max ppb	Brenr min	Brenr max	Brenr mean	Brenr median	Reference	Interpretation
Greenland (NEEM)	0.02-3 ky b2k	0.20	0.80	0.47	5	37			3.9	24	10.6	9.9	Spolaor et al., 2016b	Inland deposition zone
Greenland (RECAP)	0.02-10.6 ky b2k	0.06	0.40	0.34	7	27			1.8	47	3.8	3.4	Maffezzoli et al., 2019	Coastal deposition zone
Greenland (RECAP)	1750-2011 CE				4	227	0.007	0.06					Cuevas et al., 2018	Coastal deposition zone
Greenland (TUNU)	1750-2013 CE	0.08	0.98	0.34	2	200			0.2	36	5.7	4.4	Maselli et al., 2017	Inland deposition zone
Greenland (Summit2010)	1742-2010 CE	0.16	0.62	0.39	26§	245§			4.1	32	13.6	12.7	Maselli et al., 2017	Inland deposition zone
Svalbard (Holtedahlfonna)	2003-2011 CE	0.40	9.6	1.6	18	2744	0.005	0.25	0.06	540	14.0	3.9	Spolaor et al., 2014	Coastal deposition zone
Severnaya Zemlya	1950-1999 CE	0.30	81	5.2	15	1837	0.004	3.7	0.76	59	5.7	4.2	Spolaor et al., 2016a	Coastal deposition zone
Arctic	**LGM**													
Greenland (NEEM)	15-24 ky b2k	0.62	1.5	1	50	127			2	3.4	2.5	2.5	Spolaor et al., 2016b	Inland deposition zone
Greenland (RECAP)	17-27 ky b2k	0.3	0.81	0.58	10	34	0.04	0.09	2.8	8	3.8	3.7	Maffezzoli et al., 2019	Coastal deposition zone

§ Na values have been calculated from published Br and Brenr data.

calibration standard series results in a progressive coating of iodine and bromine onto the surface of the sample introduction system. During each sequence of Antarctic sample measurements (represented by black circles) the iodine and bromine in the introduction system is slowly and inefficiently removed. The memory effect is the main reason for the long cleaning step during the analysis between samples previously described. The duration of each analysis is approximately 5 min and each standard calibration sequence progressively increases from 0 to 600 ppt (10^{-12} g/g). In the absence of the ammonium hydroxide cleaning step, halogens are inefficiently removed from the ICPMS introduction system and substantial sample carry-over occurs.

The substantial memory effect of halogen elements in ICPMS sample introduction systems also reduces the suitability of coupled CFA-ICPMS systems for high-resolution analysis of halogens in ice cores. CFA systems typically involve sampling "runs" in which a sequence of ice up to 20 m in length is continuously melted. Between melting runs, the analytical systems are allowed to return to their baselines and are typically fed by a supply of UPW. The memory effect of halogens in ICPMS glassware leads to a "smoothing" of the ICPMS data and can be observed as a reduced sample variance. This effect was observed in bromine dataseries' reported for the Law Dome ice core, where overlapping ice core records drilled at the same location were measured using different techniques (See section 3.1 in Vallelonga et al., 2017). Greater variance was observed in the core that was sampled using a discrete cutting technique typically applied to IC samples, with the samples then measured individually by ICP-SFMS. Reduced variance was observed in the core that was melted continuously in a CFA system and then measured using an online ICP-SFMS instrument. The mean results from the cores were in agreement, but interannual variability of bromine concentrations was not fully resolved by the continuous-sampling technique. This is a counter-intuitive result, as one would expect data variance to increase as sampling resolution increases. Sodium – which does not suffer from memory effects in ICPMS sample introduction systems – was also measured in both cores, and showed the expected pattern of increased data variance with increased sampling resolution (See Table 1 in Vallelonga et al., 2017).

Interlaboratory comparisons are a valuable method of comparing analytical methods as well as investigating the long-term stability of halogens in samples. Fig. 3 shows the results of an interlaboratory measurement comparison for bromine and iodine. The samples were first melted as part of a CFA campaign, where discrete aliquots were collected for measurement of halogens (Maffezzoli et al., 2019). The refrozen samples were sent to the University Ca' Foscari of Venice (Italy, IT) where they were melted, sampled for measurement and then refrozen. The refrozen samples were then sent to Curtin University of Technology (Australia, AUS) to be melted once more for analysis of halogens using similar instrumentation. The laboratory intercomparison between sodium and bromine measurements was performed on a common set of samples (n = 140) to investigate differences between the analytical techniques and laboratories, as described in Vallelonga et al. (2017). The correlations and the gradients between the measured concentrations in the two set-ups are ρ(Na IT-Na AUS) = 0.99 (n = 140; p < 0.01), mean gradient Na = 1.084 ± 0.011 (1σ) for sodium; and ρ(Br IT-Br AUS) = 0.93 (n = 140; p < 0.01), mean gradient Br = 1.085 ± 0.011 (1σ) for bromine. Fig. 3 shows that sodium and bromine measurements in the two labs are in good agreement and are close to a 1:1 line, whereas there has been some loss of iodine

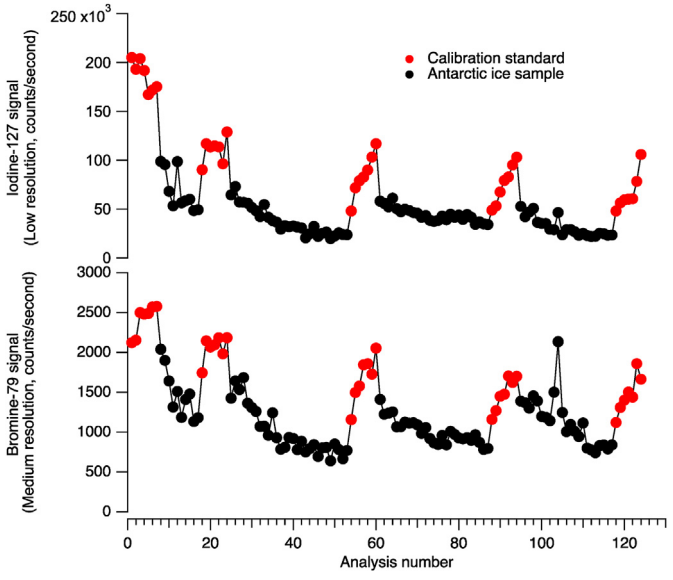

Fig. 2. Demonstration of a memory effect in an ICPMS sample introduction system when an inadequate cleaning technique is used. In this case, the cleaning technique includes nitric acid but omits ammonium hydroxide. The black circles show Antarctic ice core samples, bracketed by repeated calibration standard runs (red circles). (For interpretation of the references to colour in this figure legend, the reader is referred to the Web version of this article.)

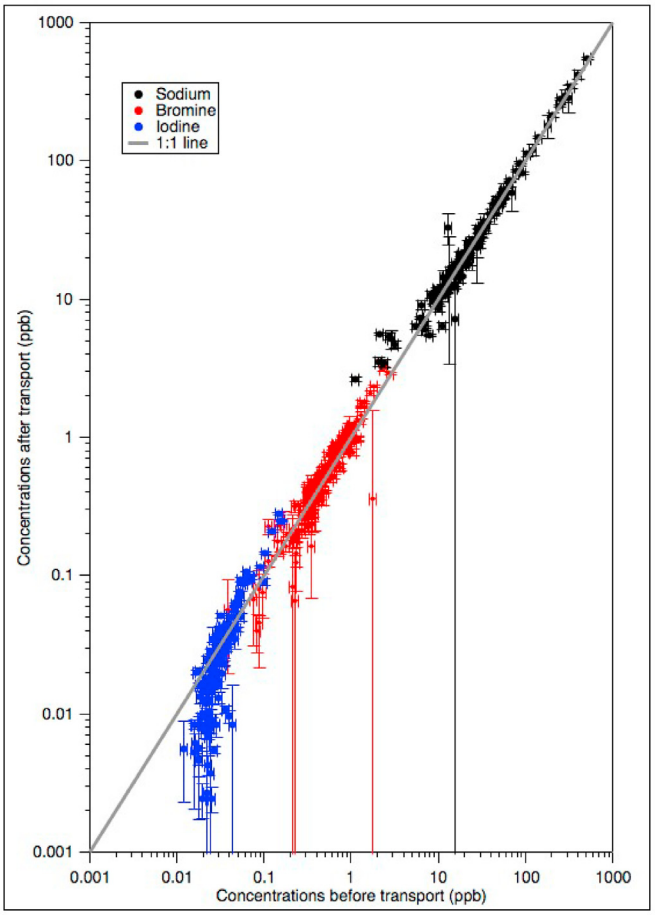

Fig. 3. Laboratory intercomparison for measurements of bromine, iodine and sodium in RECAP snowpit samples. Samples were first measured at the University Ca' Foscari of Venice in Italy, then transported to Curtin University of Technology in Australia and remeasured. Redrawn from data originally published in Vallelonga et al. (2017).

during the refreezing, transport and remelting processes that occurred between the measurements. This loss is most evident for the samples containing the lowest concentrations of iodine. Bromine concentrations may be accurately measured from repeatedly melted samples as long as the samples are kept frozen and away from light and the sample container is in a good condition. Repeated measurements of iodine samples is inadvisable and likely results in under-reported values subsequent to the first measurement.

2.2. Metrics of halogen enrichment

2.2.1. Element concentrations

The evaluation of halogen enrichment in ice and snow is primarily conducted by comparing bromine and iodine with corresponding sodium data. In the following discussion we will consistently refer to bromine but all equations are equally suitable to iodine. The concentration of bromine in ice is represented by [Br]. The standard approach is to calculate the concentration of sea-salt (ss) bromine based on the sodium concentration in ice (assuming the sodium in the sample to be purely of marine origin) and the bromine/sodium mass ratio commonly found in seawater. The latter has been reported in key studies of mean ocean water composition (e.g.: Millero, 1974; Millero et al., 2008; Turekian, 1968). The sea-salt component of bromine is determined using the following relation

$$[ssBr] = [Na] * W(Br)/W(Na)$$

where W(Br) is the sea water mass fraction of solute Br (grams of Br/grams of total solute), following the style of Millero et al. (2008).

If the site of investigation is located in a region affected by mineral dust input, sodium may contain some crustal input. In this case, the sea-salt sodium component (ssNa) must be calculated before it is used in the above sea-salt halogen calculation. Two different approaches can be used to evaluate ssNa. In general, when two elements have mixed crustal (non-sea-salt) and marine (sea-salt) input, the two contributions can be separately calculated if their elemental ratios in the sea-salt and in the dust source are known (Vallelonga et al., 2004). In the case of sodium, its non sea-salt contribution is usually calculated by using a crustal element such as aluminum (Boutron et al., 1991), calcium (Maselli et al., 2017; Schüpbach et al., 2018), cerium (McConnell et al., 2014), iron or direct dust measurements (Vallelonga et al., 2013). The source of uncertainty of this approach lies in the knowledge of the dust source elemental ratio, while the marine ratio can be assumed well known. To date, upper continental crust average elemental ratios have been widely used both in the Arctic and Antarctica, but in some ice records this has been shown not to be an accurate representation of the source dust (Maffezzoli et al., 2019). The second approach to evaluate ssNa makes use of departures from the sea-salt sodium-to-chlorine ratio (Hansson, 1994). However, chlorine concentrations in sea-salt aerosol are biased by dechlorination processes, which lead to loss of chlorine from the aerosol to the gas phase (Röthlisberger et al., 2003). Overall, the chlorine-to-sodium ratio could be enhanced (and therefore mask the decreasing behavior of the Cl/Na ratio due to the crustal sodium factor) because of the longer residence time of gas phase chlorine (HCl) compared to sodium, which remains in the aerosol phase. We recommend the use of elemental dust ratios, in preference to chlorine-based evaluations, as the best available method to represent mineral dust inputs to ice core records. The selection of elemental ratios to be used should be made carefully and the results should be evaluated based on the range of outcomes possible from each of the available crustal markers.

The non-sea-salt (nss) component of bromine (or iodine) can be calculated as:

$$[nssBr] = [Br] - [ssBr]$$

Note that this measurement combines uncertainties in the determination of bromine and sodium, as well as their ocean water compositions, so nssBr may be negative if [Br] is particularly low. In such cases, it is common practice to round up to zero and interpret the result as indicative of a negligible non-sea-salt contribution. Negative nss values may also be obtained if the element has been remobilized, re-emitted or otherwise lost from the snow surface.

The term nssBr expresses an abundance of bromine (or iodine) that cannot be attributed to the calculated sea-salt loading present in the sample. As such, it can be considered an *excess* (or depletion in case of a negative value) beyond the "direct" sea-salt input. The source of this excess must then be hypothesized. In the case of bromine, heterogeneous recycling over first-year sea-ice is a clearly demonstrated and well-constrained mechanism for enhancing bromine in the boundary layer (Abbatt et al., 2012). For iodine, we attribute non-sea-salt emissions to algal communities hosted by first-year sea-ice (Saiz-Lopez and Blaszczak-Boxe, 2016), particularly in the Antarctic. In the Arctic, an iodine-ozone feedback mechanism has recently been identified, in which oceanic iodine emissions are enhanced by ozone deposition to the sea surface (Cuevas et al., 2018). This process is most relevant to the Arctic, which is subject to perturbation of natural ozone levels due to industrial processes (Prados-Roman et al., 2015).

2.2.2. Element ratios

Bromine excess may also be expressed as a relative metric, rather than an absolute abundance. We consider this a relative *enrichment*, rather than the abundance *excess* mentioned in the previous section. Thus, fractional bromine (or iodine) enrichment may be calculated as a ratio:

$$Br_{enr} = [Br] / [ssBr]$$

Where a value of 1 indicates no enrichment of Br beyond the ss contribution (equivalent to nssBr = 0) and values greater than 1 indicate an additional quantity of Br that cannot be attributed to ss (equivalent to nssBr > 0). Values of Br_{enr} less than 1 indicate depletion, due to loss of Br from ss either during transport to the site or due to post-depositional processes. A value of $Br_{enr} = 2$ indicates that only half of Br in the sample can be explained by sea-salt, thus ssBr = nssBr. A Br_{enr} value greater than 5 indicates a substantial Br enrichment process has occurred. Br_{enr} can only approach zero if the concentration of Br is below the limit of determination or if ssBr $\gg$ Br.

As mentioned previously, values of Br_{enr} less than 1 indicate depletion of bromine relative to sea-salt inputs. The first published interpretation of bromine as a possible sea-ice proxy quantified this depletion metric as an indicator of sea-ice extent (Spolaor et al., 2013b). For clarity, we show that this depletion metric is effectively the inverse of the aforementioned Br_{enr} enrichment metric, and the two can be used equivalently. The depletion calculation employed by Spolaor et al. (2013b) was:

$$\%Br_{fi} = 100 * (([Na] * 0.006 - [Br]) / [Na] * 0.006)$$

where $\%Br_{fi}$ was called the bromide fractionation index. Rather than a percentage, this can be expressed as a fraction and more accurately labeled as Bromine depletion (Br_{dep}):

$$Br_{dep} = ([Na] * 0.006 - [Br]) / [Na] * 0.006$$
$$= ([ssBr] - [Br]) / [ssBr]$$

In section 4.4.1 we will further explore the data presented by Spolaor et al. (2013b). The interpretation of the data and its use to reconstruct sea-ice extent are described and considered further in section 5.1.1. At this point, we reiterate that the plotting of bromine depletion, rather than enrichment, should not alter the findings arising from the study and most importantly, arise from the same two data series of bromine and sodium concentrations.

The applicability of iodine enrichment metrics is still a matter of debate and uncertainty. For iodine enrichment (I_{enr}) and nss-I the same calculation can be applied as for Br but using the iodine/sodium ratio in seawater of 5.93×10^{-6} (Turekian, 1968). Unlike Br_{enr} and nssBr, iodine enrichment is infrequently used due to the many biological processes associated with iodine emission, in addition to direct sea spray emission (Saiz-Lopez and Blaszczak-Boxe, 2016). Thus while I_{enr} may, in principle, be used to apportion biotic and abiotic iodine emission pathways, in practice the complex heterogeneous reactions that take place above seasonal sea-ice invalidate any simple consideration of two independent biotic and abiotic pathways describing iodine in the polar environment. We refer the reader to Saiz-Lopez et al. (2012) for a more detailed description of iodine atmospheric chemistry.

2.2.3. Element fluxes

In general, upon measurement, ice core impurities are detected using instruments that provide concentration values: c_{ice}. Such concentrations are the parameter we referred to in the above sections 2.2.1 and 2.2.2 as [Br] in the specific case of bromine concentration determination. From the ice concentration, the air-to-snow depositional flux (J) can be calculated as:

$$J = c_{ice} * A$$

if the snow accumulation rate A is known (from experimental data or model results). A is expressed as the annual mass of deposited snow per m^2.

In general, the deposition of an impurity onto ice sheets or glaciers proceeds via both wet and dry deposition:

$$J = \left(v_{dry} * c_{air}\right) + (k * A * c_{air}) \quad \text{(Eq 1)}$$

where c_{air} is the concentration of impurity c in the air, v_{dry} is the dry deposition velocity, k is the snow scavenging factor and A is the accumulation rate. In Eq. (1), the first sum ($c_{air} * v_{dry}$) is the dry component of the deposition which is independent of A. The second sum, the wet component, is ($k*A*c_{air}$). Using the definition of J, we can express the ice concentration in Eq. (1) as:

$$c_{ice} = \left(v_{dry} / A\right) * c_{air} + k * c_{air} \quad \text{(Eq 2)}$$

When interpreting ice core records, we would like to consider a parameter which is linearly related to the air concentration c_{air} and ideally does not suffer from the effects of temporal changes in the other parameters. In general, all parameters in Eq. (2) can be a function of time, in particular across glacial-interglacial timescales. The particular effect of the accumulation rate A on c_{ice} can be investigated in two case limits:

- In the case of dominant wet deposition, $v_{dry}/A \ll k$, so from Eq. (2) $c_{ice} \rightarrow k*c_{air}$. In this case the ice concentration will be effectively linearly related to the air concentration and independent of accumulation changes. This case is most suitable for climatic interpretation as the potentially large glacial/interglacial variability in snow accumulation rate will not influence the analyte concentration in ice.
- In case of dominant dry deposition, $v_{dry} \gg kA$, so from Eq. (1), $J \rightarrow v_{dry}*c_{air}$. In this case the flux is the parameter linearly related to the air concentration and independent of accumulation changes. Therefore fluxes are most suitable for climatic interpretation of predominantly dry-deposited analytes.

Generally, for low accumulation sites and/or during periods of reduced accumulation (e.g. glacial periods), when dry deposition is believed to be the dominating mechanism, J is used to express the atmospheric loading of the analyte of interest. In contrast, if wet deposition is believed to be the dominating mechanism of deposition, c_{ice} is the parameter linearly related to c_{air} and independent of A. This general case works well for analytes which are reasonably conservative and do not undergo phase changes or excessive chemical changes in the atmosphere (Alley et al., 1995; Legrand, 1987)

In the case of an analyte which may be subject to a combination of wet and dry deposition, the relative strengths of each mode can be tested. This is done by assembling a suite of c_{ice} and accumulation data from snow/ice sampling locations encompassing a broad range of A values. If the flux deposition J can be modeled accurately by Eq. (1), one can estimate the dry deposition component $v_{dry}*c_{air}$ from the y-intercept of a linear regression of the data. From the same linear regression, the wet deposition component will be represented by the gradient $k*c_{air}$.

Antarctic records have been historically investigated using fluxes, as dry deposition is believed to be the dominating present-day mechanism at continental sites (e.g. Dome C) and even more so during glacial periods (Wolff et al., 2006). Other studies, however, have indicated that sodium is mainly wet deposited at more coastal Antarctic locations (McConnell et al., 2017, see Supplementary section 6) and have shown evidence of post-depositional bromine loss from the snowpack based on a negative dry flux result (these results are presented in detail in section 3.5.3).

If Antarctic records have shown that for some species, like sodium, dry deposition is probably dominant at inland sites while, at least for interglacial periods, wet deposition is dominant at the coast, Greenland records are even more challenging. Across Greenland, accumulation rates are typically greater than those found in Antarctica, hence wet deposition has a consistently greater influence on aerosol deposition, compared to Antarctica. Recent efforts based on analysis of the NEEM ice core, in northwestern Greenland, have employed a direct calculation of c_{air} from Eq. (2) (Schüpbach et al., 2018). Unfortunately, a limited knowledge of the variables, especially v_{dry} and k, result in a poorly constrained reconstruction of c_{air}. Such uncertainties particularly influence bromine and iodine, as these two impurities are emitted and transported in both gas and aerosol phases as well as different chemical species. Detailed field-based investigation campaigns – encompassing locations featuring a range of accumulation rates, and combining direct sampling of snow and atmospheric BrO and particulate loading - will be of great benefit for constraining bromine dry and wet deposition characteristics.

2.2.4. Considerations

In this section we describe some standard methods for determining and expressing deviations from the Br/Na ratio found in sea-salt. The interpretation of a data set should not change greatly if a deviation is expressed as an absolute excess or a relative enrichment, although there may be advantages to using one over the other, such as in the circumstances described below:

- When considering the concentrations of any aerosol deposited in snowpack, the relevant processes of deposition are critical to an accurate evaluation. It has been demonstrated that sea-salt aerosol (containing sodium and bromine) is transported as fine aerosol, whereas the transport of bromine includes chemical recycling processes occurring in mixed aerosol and gas phases. The relative contribution of the dry and wet components controlling bromine and sodium deposition are currently poorly constrained, and are dependent on snow accumulation as well as the chemical parameters of the many bromine species involved. With respect to Br_{enr} calculations, however, we can assume that dry deposition mechanisms are much more important for bromine than for sodium.
- When evaluating bromine recycling over long timescales involving significant snow accumulation changes (such as glacial/interglacial transitions and, in the case of Greenland, Dansgaard/Oeschger events) it is important to consider the effect that such accumulation changes may have on the relative dry and wet contributions of the analyte deposition, which may or may not influence the measured concentration. Considering element ratios rather than absolute abundances can minimize the effect of accumulation changes. Hence, bromine *enrichment* (i.e., Br_{enr}) is supposedly less biased by accumulation rate changes than bromine *excess* (i.e., nssBr), as the former incorporates element ratios rather than absolute quantities.
- Although Br_{enr} is less influenced by changes in accumulation over time, it is strongly influenced by changes in sodium concentration. For example, sodium concentrations display a strong gradient across Antarctica as aerosols travel inland (Bertler et al., 2005). Variability in Br_{enr} observed at an inland site may be artificially inflated due to the very small quantities of sodium deposited at that site. Furthermore, Br_{enr} variability observed along an inland traverse will be induced by the different deposition characteristics of Br and Na. These considerations are discussed in section 3.6. Hence, the geographical setting and absolute sodium concentration found in ice core records should be considered when interpreting Br_{enr} variability across sites.
- The same interpretation of a Br and Na data set should arise irrespective of whether the data are plotted as nssBr or Br_{enr}, as long as the sodium fraction is predominantly derived from sea-salt. The Br_{enr} metric incorporates sea-salt as the primary determinant of Br and therefore can be biased if a substantial proportion of sodium originates from non-sea-salt origins, such as mineral dust.
- The usage of Br_{enr} as indicator of past sea-ice variation employs a sea-salt correction based on sodium. The assumption behind this approach is that there is no fractionation of Br and Na prior to the emission "starting point", that is, the sea-ice surface. Therefore, the use of a "standard" sea-salt composition relies on this sea-salt composition being identical in the ocean and on sea-ice. First-year sea-ice is rich in sea-salt and available data indicates this sea-salt is not fractionated from its seawater composition (Vallelonga et al., 2020). Although there is no evidence of heterogeneous recycling of halogens over multi-year sea-ice, which is effectively drained of sea-salts, the content and composition of sea-salts in multi-year sea-ice should be comprehensively investigated.

Accurate analytical techniques are essential to the determination of iodine and bromine in polar snow and ice samples and to ensure they are reliably compared between sampling sites. It is also crucial to understand the various chemical and physical processes leading to the halogen concentrations found in the snowpack and in the ice core record. The following chapter will summarize the current state of knowledge regarding processes controlling halogens, in particular Br, in the polar atmosphere. These processes are divided into emission, transport, deposition and post-depositional processes.

3. Halogens in the polar boundary layer

Despite initial measurements conducted in the 1950s, it was not until the 1980s that Arctic ozone depletion events (ODEs) were associated with high levels of brominated compounds (Barrie, 1986). ODEs alter the oxidizing capacity of the atmosphere: minimizing the atmospheric oxidizers for which ozone is a precursor and promoting halogen oxidation pathways. Since the 1980s, several field measurement campaigns have been conducted in the Arctic and Antarctic, in conjunction with laboratory studies and model development necessary for parameterizing multiphase halogen chemistry in the polar boundary layer (PBL). The PBL, and its marine equivalent, the marine boundary layer (MBL), is the layer of the atmosphere directly impacted by processes or emissions originating from the corresponding ground/ice/seawater surface. The PBL or MBL may be quantified as the airmass within which a certain molecule [e.g., Na, bromine monoxide (BrO)] or parameter (temperature, humidity) falls to a specified percentage of its surface value. We provide here a brief overview of the current state of knowledge of emission sources, transport and deposition processes relevant to halogen-based sea-ice reconstructions from ice cores. Two previous review articles provide a comprehensive description of the atmospheric dynamics of the PBL (Anderson and Neff, 2008) and halogen chemistry of ODEs (Simpson et al., 2007b). The reader is also referred to Saiz-Lopez and von Glasow (2012) and Simpson et al. (2015) for overviews of the global context and broader relevance of tropospheric halogen chemistry. Saiz-Lopez et al. (2012) provide a thorough review of atmospheric iodine chemistry.

3.1. Sources of halogen emissions

Atmospheric bromine primarily originates from the open ocean surface, although volcanism may be a significant secondary source in some regions such as West Antarctica. The concentration of bromine in seawater is 67.3 ppm by weight (Turekian, 1968), and it is released to the atmosphere via sea-salt aerosol (SSA) or organobromine species produced by ocean biota. SSA is released through the common processes of ocean wave-breaking and bubble bursting, whereas organobromine species are released from the ocean through sunlight-driven processes. Although bromine originates from the oceans, the level of bromine in the PBL is controlled by heterogeneous halogen recycling processes which have been observed over the majority of polar substrates: first-year sea-ice, frost flowers, blowing snow and open-water leads (Abbatt et al., 2012). The activation of halides over sea-ice and snow is discussed in the following sections. The few available measurements of bromine emissions from volcanoes located at high latitudes indicate that volcanism may be a locally significant source of halogens to the polar atmosphere. The volcanoes that have been studied are Mt Erebus in Antarctica (Zreda-Gostynka et al., 1993, 1997) and Redoubt in Alaska (Kelly et al., 2013).

Similar to bromine, iodine in the PBL and MBL originates from the ocean surface (Carpenter et al., 2013; Saiz-Lopez and von Glasow, 2012), although biological processes are much more critical to the spatial and temporal distribution of iodine in the atmosphere. Many aspects of iodine emission and distribution still need to be better understood. It has not yet been conclusively explained why iodine oxide (IO) is observed at tens of ppt levels throughout coastal Antarctica, but in the Arctic IO is observed at levels in the low-ppt range near to detection limits: the so-called *polar iodine paradox* (Saiz-Lopez and Blaszczak-Boxe, 2016). The

difference has been tentatively attributed to the different proportions and extents of MY and FY sea-ice in each polar region, in additional to potentially different biological communities in each polar region. In the Arctic, an inorganic process also appears to be relevant to atmospheric iodine emissions. A feedback mechanism involving ozone-driven emission of iodine from the ocean surface has also recently been postulated (Prados-Roman et al., 2015), which may be of relevance to the large expanses of the North Atlantic and North Pacific oceans exposed to industrial emissions of NO_x pollutants (Cuevas et al., 2018). This ozone-iodine emission feedback loop is discussed further in section 4.3.2.

3.2. Halogen activation over sea-ice

3.2.1. Bromine

Substrates relevant for halogen chemistry in the polar regions include sea-ice, blowing snow, snowpack and aerosols. Gaseous bromine reservoir species such as hypobromous acid (HOBr), bromine nitrite ($BrNO_2$) and bromine nitrate ($BrONO_2$) are reactively taken up by these substrates leading to a sequence of reactions that liberate halogens (e.g. Br_2) from the condensed phase. This reaction cycle leads to the exponential growth of gas phase bromine as the uptake of one Br atom is followed by the release of two Br atoms. The photolysis of emitted precursors such as Br_2 and the subsequent oxidation by ozone of the bromine atoms leads to the formation of BrO, which is the most common bromine species measured in the atmosphere. Further reaction of BrO with hydrogen and nitrogen oxides leads to the formation of HOBr, $BrNO_2$, $BrONO_2$ and hydrobromic acid (HBr) reservoir species, thereby closing the cycle of polar bromine chemistry.

The importance of these substrates for halogen activation has been evaluated through a series of observation- and/or model-based studies (Abbatt et al., 2012; Pratt et al., 2013; Simpson et al., 2018). Primary criteria include salt concentration, activation surface area and micro environmental conditions such as acidity, humidity and wind speed. As sea-ice grows, the surface salt content is increased through brine rejection processes. Frost flowers may form and both seawater and blowing snow may contribute to the distribution of salts over the sea-ice surface. Sea-ice that persists through summer to become multiyear sea-ice is typically depleted of salts and therefore becomes less effective for halogen recycling. Satellite-based observations of BrO indicate that heterogeneous recycling occurs over freshly formed sea-ice, although more detailed studies have begun to elucidate the specific conditions contributing to such recycling (Abbatt et al., 2012). In particular, the role of multi-year sea-ice for bromine as well as for sodium emissions is still to be explored. Sea-ice salinity decreases with age, although some multi-year sea-ice snowpack measurements suggest that multi-year sea-ice regions have the potential to play an active role in Arctic boundary layer bromine chemistry (Peterson, 2019). Throughout the rest of the review we discuss the source of bromine and sodium in terms of first-year sea-ice surfaces although we acknowledge that multi-year sea-ice, particularly second-year sea-ice, could play an as-yet unquantified role in polar halogen chemistry.

Early studies of bromine recycling in polar regions proposed frost flowers as both a mechanism for enriching bromine and a substrate for heterogeneous recycling processes (Rankin et al., 2002). The enrichment of bromine and other salts in frost flowers was proposed as a means of ensuring fractionation of bromine beyond concentrations found in sea water. Furthermore, the complex structure of frost flowers was proposed to enhance the active surface area available for halogen chemical reactions to occur. Frost flowers are more prevalent in Antarctica than in the Arctic, and do not account for observed Arctic ozone depletion events (Simpson et al., 2007b). Analogous studies of sodium transport in Antarctica have demonstrated that frost flowers are relevant to the salt loading in areas of coastal Antarctica (Wagenbach et al., 1998) but can also influence sodium flux across continental Antarctica (Legrand et al., 2016).

As the role of frost flowers in bromine recycling became less clear, attention turned toward the influence of blowing snow and saline snow on sea-ice (Frey et al., 2020; Pratt et al., 2013; Yang et al., 2010). Blowing snow may be generated from moist marine air containing high quantities of marine aerosol. Furthermore, it may take up salts from the sea-ice surface, either from salty brine or seawater that has been rafted onto the sea-ice surface. Snow cover over sea-ice has been observed to be rich in sea-salts, particularly in the deeper layers that interact with open brine channels emerging from the sea-ice matrix. Both model and observational studies have linked blowing and saline snow to bromine heterogeneous recycling and ozone depletion events.

Currently, it is understood that blowing snow over sea-ice is a suitable precondition for bromine activation, but it is still necessary to separate the various factors that co-exist under those conditions. It has been observed that low pH conditions promote halogen recycling but are not an essential component. Overall, abundance of marine salts in a mobile matrix, such as enriched brine channels found in first-year sea-ice, is a strong precondition to bromine activation. These factors promote the importance of first-year sea-ice as a critical substrate for bromine recycling.

The complex conditions of blowing snow do allow for additional processes of bromine recycling. For example, bromine recycling appears to occur between the gas and aerosol phase within the airborne blowing snow. As bromine recycling occurs within a moving airmass, additional factors such as deposition and remobilisation of snow may come into play. Some of these considerations are discussed in sections 3.5 and 3.6.

3.2.2. Iodine

Due to its biological utility, iodine activation is strongly linked to algal communities that inhabit sea-ice. Consequently, organic forms of iodine, such as iodocarbons and methylates, are primarily identified in the vicinity of sea-ice. Biological activity primarily occurs on the underside of the sea-ice, therefore mechanisms for the transfer of iodine through the sea-ice to the upper surface is an essential precondition to activation and atmospheric emission of iodine (Saiz-Lopez et al., 2015). An efficient mechanism for such transport is the formation of liquid brine channels resulting from brine rejection, which is favored in FYSI and in ice that is warmer than -5 °C. It has been proposed that the very low concentrations of iodine in the Arctic are due to the prevalence of thick, older multiyear sea-ice, which inhibits the transmission of light required to sustain photosynthetic organisms in the water column below the ice (Arrigo and van Dijken, 2011). The present trend of thinner and younger Arctic sea-ice (Stroeve et al., 2012b) will be an important test to this proposal, to see if atmospheric iodine levels increase in correspondence with the development of a more seasonal sea-ice environment (Arrigo et al., 2012; Horvat et al., 2017).

3.3. Halogen activation over land-ice

There have been few studies of halogen activation over snowpack from which definitive findings can be concluded. This lack of research is due to the geographical dispersal of the study locations and the low bromine concentrations encountered in polar snow. In some cases, bromine concentrations are at or below detection limits, which places limitations on the study of deposition or emission processes. Two such studies will be described here.

The Greenland Summit Halogen-HO_x Experiment (GSHOX),

conducted in 2007 and 2008 at Summit station in central Greenland, studied surface photochemical processes at the site and considered mechanisms for transport of reactive bromine to central Greenland (Thomas et al., 2012). Samples were collected every 12–24 h: in the gas-phase from the boundary layer and the snowpack (firn-air); in the particulate-phase by ground-based aerosol samplers; and surface snow was also sampled. The bromine results were presented by Dibb et al. (2010): trace levels of bromine were found in boundary layer air (0–1 ppt with a median of 0.3–0.6 ppt) and snowpack (approximately 10 nmol/kg) although bromine/sodium ratios in both matrices were consistently enriched with respect to seasalt. In air, the median bromine concentration was enriched compared to the seawater Br/Na mass ratio by 16 and 8 times (respective results from 2007 to 2008 measurement campaigns) and in snowpack the median enrichments were 33 and 47 times greater (again for the respective 2007 and 2008 measurement campaigns). Bromine enrichment only approached oceanic seasalt values during winter sodium spikes.

The GSHOX experiments were conducted during spring/summer and demonstrated active bromine photochemistry occurring in the snowpack and boundary layer at an altitude of more than 3 km above sea level and hundreds of kilometers from the coast. Importantly, it was observed that surface concentrations of BrO could only be accounted for by emission of bromine from the snowpack. Three mechanisms for transport of reactive bromine to the Summit site were proposed:

- "Rare rapid transport events" were observed during GSHOX. These are analogous to 'atmospheric rivers' in which there is a rapid transport of air masses from the MBL up to the central Greenland ice sheet. These events are not sufficiently frequent to account for the majority of bromine observed at Summit site.
- "Leapfrogging" boundary-layer transport, involving surface deposition and re-emission of reactive bromine, as well as possible reactive halogen chemistry occurring on aerosols during transport. This process was considered to be of particular importance during springtime, when there is a stable boundary layer and bromine photochemistry is particularly active over sea-ice (Fernandez et al., 2019).
- Transport via the free troposphere, with surface-generated bromine lofted into the free troposphere where it is available to be later deposited at distant sites such as Summit.

Importantly, the results revealed that despite diurnal variability, bromine concentrations in the snowpack accurately represented boundary-layer BrO concentrations. Building on the initial findings of Simpson et al. (2007a), the GSHOX study suggests that photochemical bromine recycling processes can occur far from coastal settings and can lead to enhanced bromine concentrations at those sites.

Legrand et al. (2016) investigated sea-salt and bromine content in aerosols and snowpack at Dumont D'Urville (DDU) and Concordia stations in Antarctica. DDU is a coastal station, rich in sea-salt aerosol, whereas Concordia has a weak sea-salt input due to its location approximately 1100 km from the East Antarctic coast and 3233 m in altitude. Combining state-of-the-art chemical models, aerosol and snowpack measurements, they found that bromine was depleted in marine aerosol at DDU, suggesting overall loss of bromine from the aerosol phase to gas phase. The very low concentrations of aerosols at Dome C precluded any interpretation of the bromine content relative to sodium. Based on depletion of sulphate/sodium ratios indicative of mirabilite (i.e., frost flower) production, the sea-ice surface was identified as a dominant source of marine aerosol to DDU (70 %) and a significant source to Dome C (50 %). Similar to the findings of Dibb et al. (2010), concentrations of nitrate and bromide were greatest in snowpack surface layers, indicative of photochemical activation, although photochemical activation of bromine was not found to be sufficient to account for near-surface air concentrations. Instead, Legrand et al. (2016) concluded that marine aerosol sources were the only credible source of bromine found across the Antarctic plateau.

3.4. Seasonality of halogen activation and post-depositional effects

3.4.1. Satellite observations

The spatial and temporal distribution of reactive halogens in the atmosphere is effectively captured by sensors on polar-orbiting satellite platforms. Polar-orbiting satellites typically achieve total coverage of the Earth surface within a 48-h period through overlapping observation swathes. Total atmospheric column concentrations of BrO and IO are currently determined by the GOME-2 and SCIAMACHY sensors, respectively (Burrows et al., 1995, 1999). As these sensors determine BrO and IO column concentrations from sunlight reflecting off the Earth surface, observations are not possible during the polar winter nor from within 5° latitude of the poles. As mentioned, these sensors determine the concentrations of BrO and IO in the total atmospheric column, hence the altitude of any detected halogens must be inferred. Nonetheless the observations derived from these sensors present a clear picture of enhanced atmospheric bromine concentrations above sea-ice, ice shelves and coastal areas during the polar spring and summer. Enhanced IO is only observed in the Antarctic, again over sea-ice, ice shelves and coastal areas. In the Arctic, IO has not been observed above the detection limit of approximately 10^{12} molecules/cm^2.

3.4.2. Bromine

Seasonality of bromine activation has been investigated through a variety of methods, from satellite-based observations to aerosol sampling and snowpack monitoring. Saiz-Lopez et al. (2007) were the first to report seasonal variability of BrO and IO in the boundary layer at Halley station, Antarctica, observing a similar behavior in both molecules – a springtime peak with elevated summer and low winter values (Fig. 4). Schönhardt et al. (2012) produced maps of BrO across Antarctica and the Arctic, identifying enhanced concentrations of BrO over sea-ice throughout the springtime (August to December) and lower concentrations during summer (Fig. 5). This result was confirmed and expanded upon by Bougoudis et al. (2020) who provided a 22-year-long merged time series

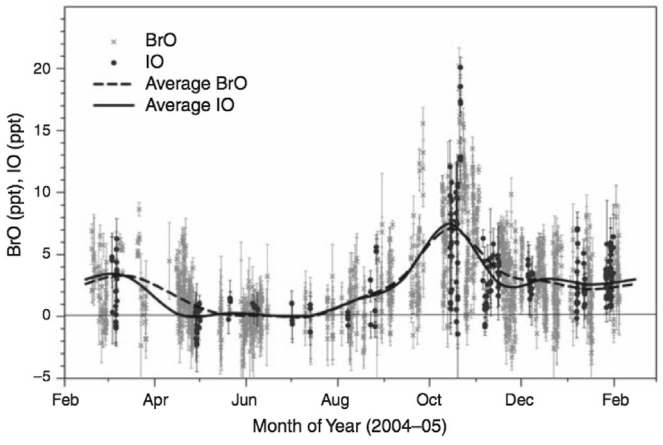

Fig. 4. Annual variation of the halogen oxides measured at Halley Station. Reprinted from Saiz-Lopez et al. (2007).

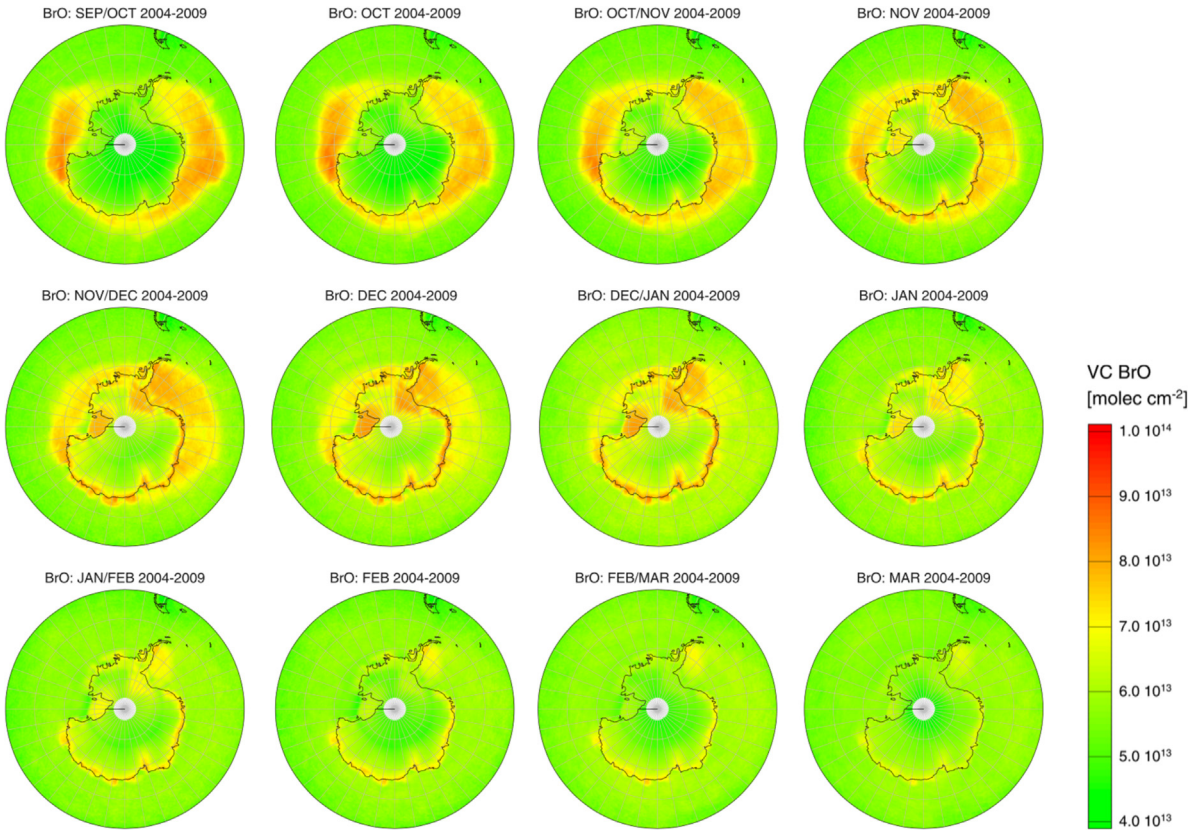

Fig. 5. Monthly maps of BrO vertical column amounts on the Southern Hemisphere (up to 50°S) averaged over six subsequent years each (2004–2009), the individual averaging periods are given in the headers. Reprinted from Schönhardt et al. (2012).

(1996–2017) of Arctic tropospheric BrO vertical column densities (VCDs) derived from four different ultraviolet–visible (UV–VIS) satellite instruments (GOME, SCIAMACHY, GOME-2A and GOME-2B). From this multidecadal dataset, Bougoudis et al. (2020) determined an increasing trend of about 1.5 % per year in the extent and magnitude of tropospheric BrO VCDs during polar springtime, temporally and spatially related to the increase in first-year ice extent in the Arctic north of 70 N (Fig. 6). Similarly, in the Southern Ocean, the highest tropospheric BrO VCDs are observed during austral polar springtime (Sept-Oct-Nov, SON) consistent with the presence of seasonal sea-ice (Fig. 7). During late-spring/summer, maximum BrO concentrations are observed to shift from the sea-ice zone toward ice shelves and the coastal margins of the continent. Validated through a variety of chemical transport models, the importance of bromine activation for ozone depletion events has been demonstrated thoroughly (von Glasow and Crutzen, 2014). Photochemical reactions are critical to bromine explosions; hence they are associated with the polar springtime and arrival of solar activity.

Although the photolysis of bromine compounds has been identified as a critical component to bromine recycling in Polar Regions, a variety of halogen activation processes have been identified that do not require solar radiation and hence may occur through the polar winter (Abrahamsson et al., 2018; Oum et al., 1998). Furthermore, nighttime production of bromine precursors ready for activation in the presence of sunlight is also a topic of consideration. At this stage there are only a few observation campaigns that have attempted to address this issue (Abrahamsson et al., 2018; Foster et al., 2001; Simpson et al., 2018) and a thorough evaluation using a coupled chemistry-general circulation model (GCM) is necessary for greater understanding of these processes.

A number of factors have been suggested to contribute to post-depositional loss or remobilisation of bromine from snowpack. The most thoroughly demonstrated factor is that of photochemical oxidation, as described previously in the studies by Dibb et al. (2010) and Legrand et al. (1997). A recent study indicates that surface reactions may also play a greater role than previously thought – leading to greater oxidation of bromide by ozone at the aqueous solution-vapour interface (Artiglia et al., 2017). Analogous to earlier work conducted on photo-oxidation of nitrate, the snow accumulation rate may be a critical component to limiting the exposure of snow surfaces to sunlight. That is, regions of high snow accumulation should be less sensitive to photo-oxidation of bromine, on account of the relatively shorter time that a deposited snow layer is exposed to sunlight. Coastal regions of Antarctica and Greenland generally feature greater accumulation rates than inland regions, hence this effect should be most apparent on the central Antarctic plateau, and to a lesser extent in central Greenland. The effect of acidity, particularly nitrate, in snowpack has also been considered important to bromine activation (Pratt et al., 2013). Maselli et al. (2017) suggested that increased acidification of Arctic sea-ice may account for increasing bromine concentrations in Greenland surface snow since the 1950s, although it will be interesting to see if this trend follows recent reports of a decrease in acidity of Greenland surface snow layers (Kjær et al., 2016).

3.4.3. Iodine

The seasonality of iodine in Antarctica is distinct from that of bromine, despite early indications of a similar annual profile (Saiz-Lopez et al., 2007). Schönhardt et al. (2012) identified widespread but low concentrations of IO across Antarctica in early spring,

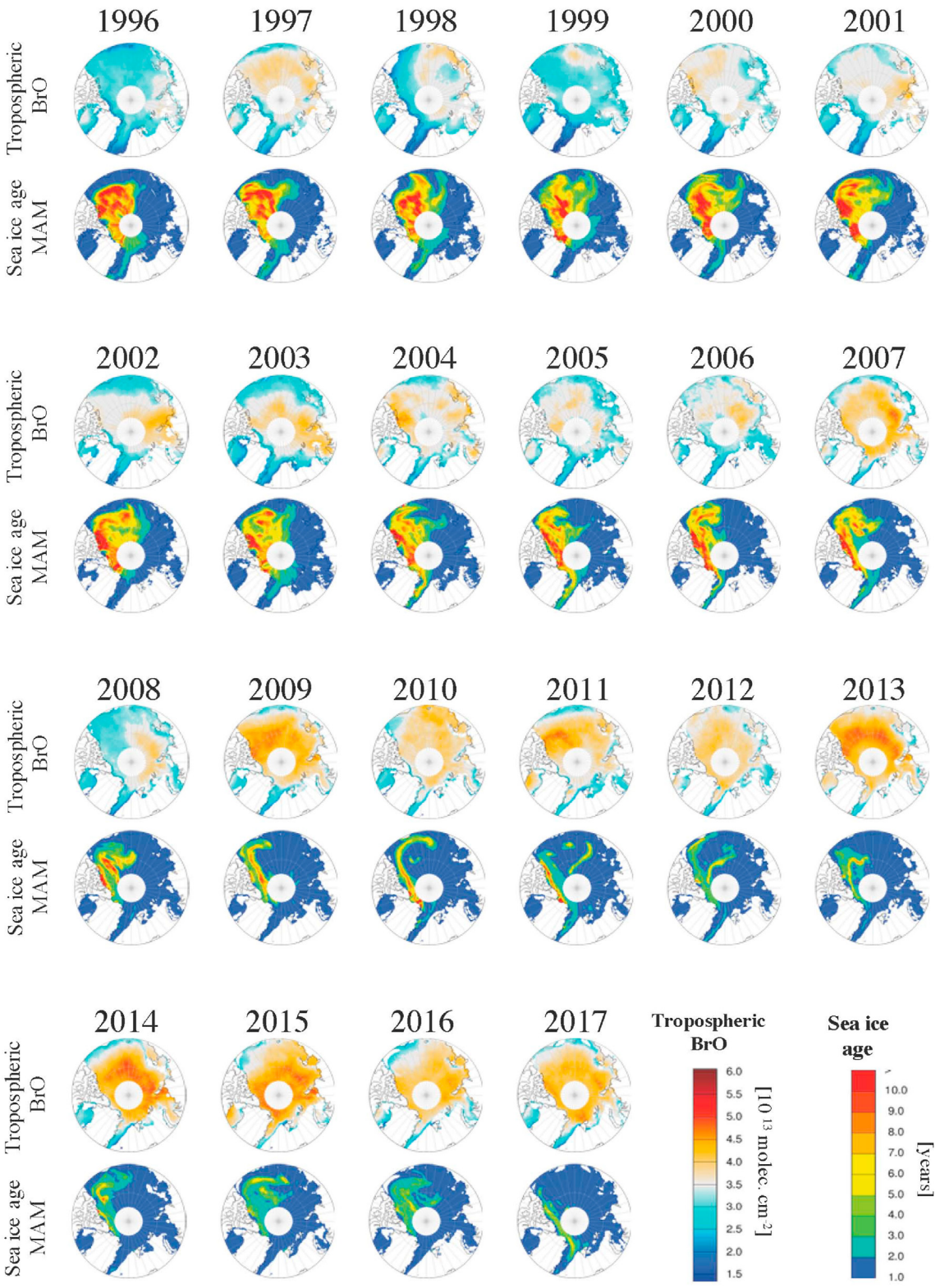

Fig. 6. Averaged tropospheric BrO Vertical Column Densitities (VCDs) and sea-ice age distributions for 22 consecutive Arctic spring seasons (March, April and May, MAM). Redrawn from Bougoudis et al. (2020).

suggesting a possible winter emission mechanism. Annual cycles of Antarctic IO are shown in Fig. 8, indicating strong seasonal and spatial variability. As the atmosphere warmed and spring developed, it was observed that IO would peak above Antarctic sea-ice, later and more briefly than the "bromine explosion" occurring from September to December. IO is produced by algal communities hosted below sea-ice, and it is only when these algal communities have been exposed to light for some time, that the sea-ice warms

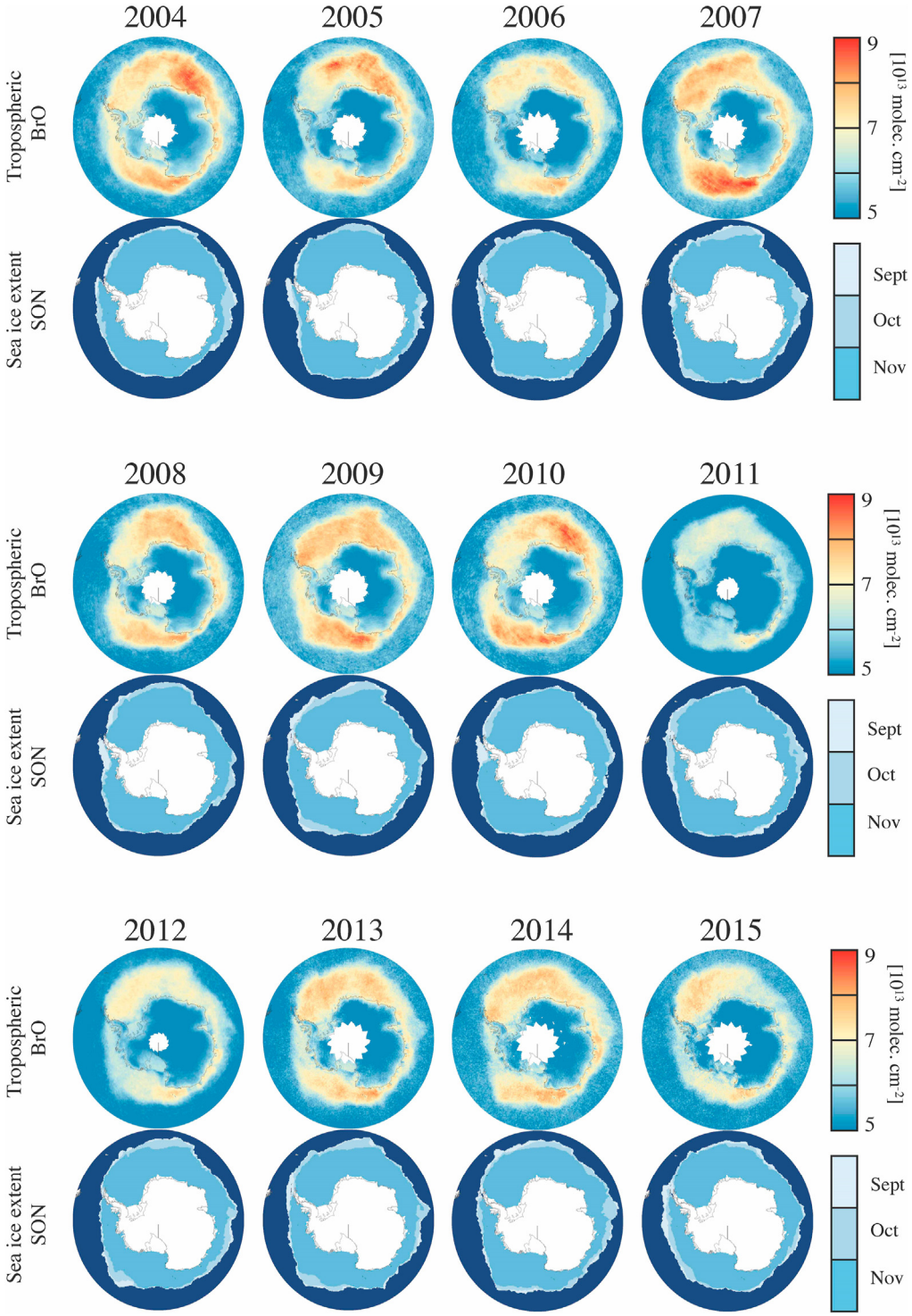

Fig. 7. Averaged tropospheric BrO Vertical Column Densitities (VCDs) and Southern Ocean sea-ice extent distributions for 12 consecutive Antarctic spring seasons (September, October and November, SON). Tropospheric BrO VCDs are from SCIAMACHY (2004–2010) and GOME-2A (2011–2015) sensors courtesy of A. Richter of IUP-Bremen ((Richter, 2020) pers.comm., 2020). Sea-ice extent data are archived at the US National Snow and Ice Data Center in Boulder (http://nsidc.org/data/seaice_index/).

and brine channels develop sufficiently to allow the transmission and release of IO to the atmosphere. Hence, these processes take longer to develop and occur later than the abiotic BrO recycling occurring on the sea-ice surface as soon as sunlight is available. Schönhardt et al. (2012) observed a second zone of IO activation, above Antarctica's ice shelves, occurring later through the summer. Such a process hints at inorganic processes and possibly remobilisation of IO through photochemical processes observed in snowpack by Frieß et al. (2010) and Spolaor et al. (2013a). Recent studies have identified frozen salts of iodate and iodide (Fernandez et al., 2019; Gálvez et al., 2016; Kim et al., 2016) to be potential sources of active iodine in the polar boundary layer.

There is sufficient evidence to conclude that iodine photochemistry is reasonably active in snow, with satellite- and insitu-

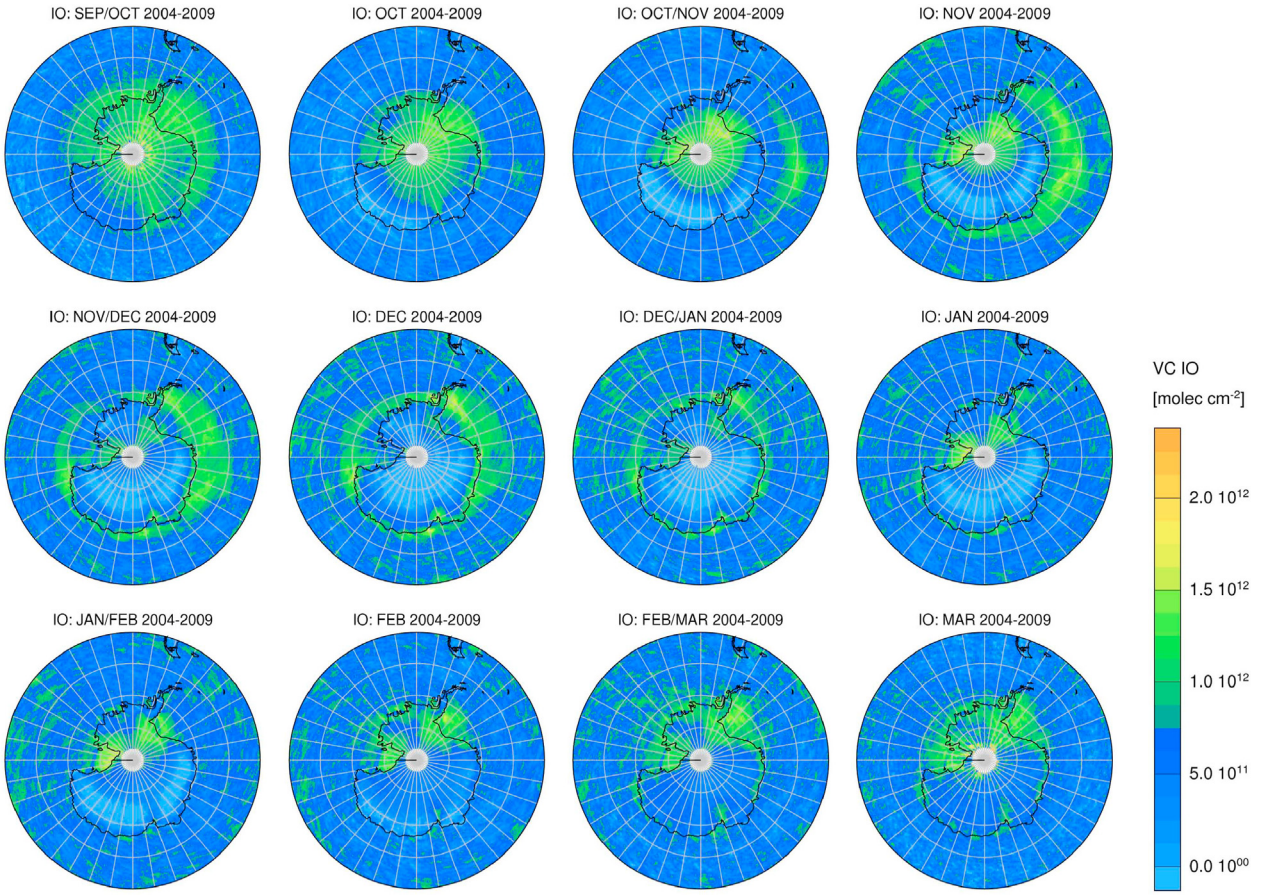

Fig. 8. Monthly maps of IO vertical column amounts on the Southern Hemisphere (up to 50°S) averaged over six subsequent years each (2004–2009), the individual averaging periods are given in the headers. Reprinted from Schönhardt et al. (2012).

based indications of post-depositional remobilisation of iodine in Antarctic surface snow. Consistent with observations of summertime photoactivation (Schönhardt et al., 2012), iodine appears to be depleted from summer strata and retained only in winter strata of Antarctic snowpack. Frieβ et al. (2010) proposed that interstitial air is a mechanism by which iodine can be converted into the gas phase and released from snowpack, as only the upper 10 cm of snowpack receives sufficient sunlight to enable iodine photochemistry. Presenting a four-year time series of sodium, iodine and bromine, Spolaor et al. (2014) showed that iodine was not present in century-old summer snow strata, although concentrations of up to 0.3 ppb of iodine were present in winter strata. In the same work, the authors presented sub-annual iodine records from Greenland and Svalbard although concentrations were lower and seasonal variability was less clear. Such findings are consistent with satellite observations of below-detection-limit-levels of IO in the Arctic (Schönhardt et al., 2012).

Retention of iodine is much more effective on rock and mineral dust surfaces than within the ice matrix. Early studies of Antarctic meteorites identified high concentrations of iodine in surface layers and stability of metallo-iodide molecules has been reported. Spolaor et al. (2013b) found that iodate is only present in the Talos Dome ice core during the dust-rich periods of the last two glacial maxima. Iodine was present throughout the 200 thousand-year record, but iodate was only found during dust-rich periods, implying the formation of stable metallo-iodate complexes on the mineral dust surface.

3.5. Re-emission of halogens from Antarctic surface snow: case studies

As both iodine and bromine are highly reactive and participate readily in oxidation reactions, it is important to consider their behavior in surface snow after deposition. Results obtained from Law Dome ice cores and Neumayer surface snow demonstrate that iodine peaks are found in winter strata whereas bromine peaks are found in spring and summer strata (Frieβ et al., 2010; Spolaor et al., 2014; Vallelonga et al., 2017). With iodine emissions attributed to spring/summer biological activity, winter iodine peaks found in Law Dome ice indicate post depositional mobility of iodine (Fernandez et al., 2019). Evidence of iodine reactivity in the snow pack is also highlighted in more recent work by Spolaor et al. (2018), where the diurnal variation of iodine in surface snow is shown to be driven by changing incoming solar radiation. In contrast, bromine seasonality at the salt-rich, high-accumulation site of Law Dome features higher concentrations in spring and summer, consistent with spring/summer heterogeneous chemical recycling over first-year sea-ice (Spolaor et al., 2014; Vallelonga et al., 2017). The post depositional behaviour of iodine and bromine further inland is a topic of necessary study, particularly considering the high levels of solar irradiance on the dry and elevated East Antarctic plateau. In the following paragraphs we present experiments reporting halogen partitioning in Antarctic snow surface covering a range of geophysical parameters: coastal vs inland, depletion vs deposition zones, and high vs low accumulation.

With an altitude of 3233 m a.s.l., very little snow accumulation (0.03 m ice equivalent/yr, mostly consisting of diamond dust, i.e. "clear sky" precipitation) and located approximately 1100 km from the East Antarctic coast, Dome C may be considered an extreme location for halogen stability in snowpack. In 2015/16, surface snow samples (0–3 cm sampling depth range) were collected with approximately 12-h resolution (10 a.m. and 6 p.m. local time) for more than a month (Spolaor et al., 2018). The results are shown in Fig. 9. Surface snow concentrations of Na, Br and I were observed to vary after a precipitation event, consistent with a change in the wind source: higher concentrations of Na, Br and I between 18 and 25 November 2015 were driven by precipitation from air masses originating from the Ross Sea region; and lower concentrations of the elements from 10 to 29 December 2015 resulted from limited precipitation, primarily diamond dust, of sea-salt-depleted (i.e., non-coastal) air mass origins. Following the precipitation event, iodine concentrations in surface snow declined greatly with a loss close to 80 %. Bromine concentrations decreased by approximately 50 % and sodium decreased about 35 %. The decrease in sodium is most likely due to physical processes such as wind-driven snow remobilisation, whereas iodine (and bromine, to a lesser extent) demonstrate susceptibility to photochemical remobilisation. The findings of this study are consistent with others pointing to remobilisation and loss of bromine from snowpack in low-accumulation zones of central Antarctica (Legrand et al., 2016; McConnell et al., 2017).

The Italian/Korean GV7 ice core drill site is located in North Victoria Land, approximately 200 km from the coast with an elevation of 1950 m a.s.l. and a moderately high snow accumulation. The topmost 3 cm of the snow surface was sampled daily for 38 days (28 November 2013 to 6 January 2014), after which a 2.5 m snow pit was sampled at the same location. No accumulation was observed over the first half of the experiment, followed by 6 cm of steady precipitation from mid-December to early-January (Fig. 10). The left panel of Fig. 10 displays the 3 cm surface sampling, with the 2.5 m snow pit results shown on the right side of the figure. The figure indicates that Br and Na are well preserved after snow deposition at this location, as there is no appreciable difference between the surface snow (left panel) and the snow pit (right panel) concentrations. Iodine concentrations are distinctly lower in the snow pit (45 ppt) compared to surface snow (70 ppt), suggesting an iodine loss of approximately 30 % at this location. These results are consistent with previous observations of iodine loss and/or remobilisation in snowpack at coastal, high-accumulation sites (Frieβ et al., 2010; Spolaor et al., 2014).

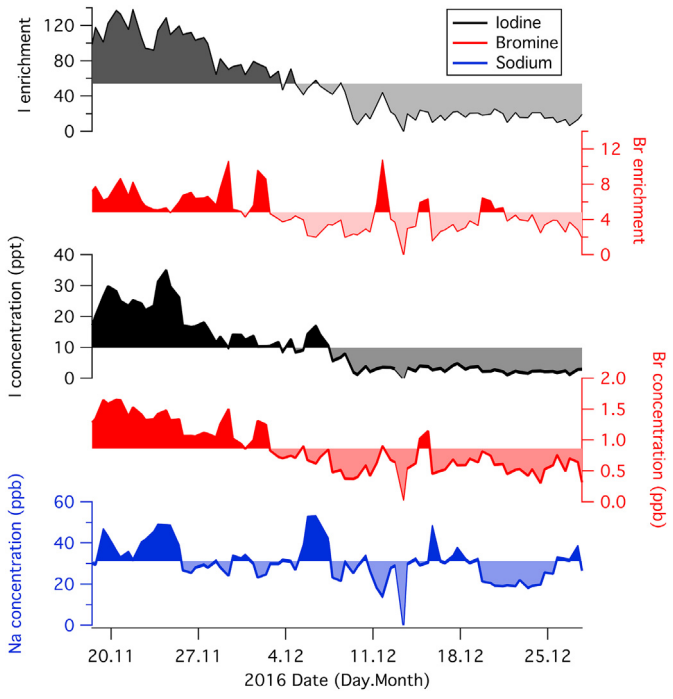

Fig. 9. Bromine, iodine and sodium concentrations and bromine and iodine enrichments in surface snow at Dome C. Each data point represents an individual sample of the upper 3 cm of snowpack at the site. The upper two panels show iodine and bromine enrichments relative to their respective seawater abundances. In all panels, the shading indicates anomalies above or below the mean of the dataset. Iodine and Bromine concentrations decrease following a marine airmass-sourced deposition event occurring 18–25 November 2016. Sporadic precipitation <0.1 mm w.e occurred over the remaining period of the experiment.

Deposition characteristics of sodium and bromine have also been investigated in a compilation of sodium and bromine fluxes reported for 11 ice core drill sites across West Antarctica and Dronning Maud Land (McConnell et al., 2017, Supplementary section 6). The accumulation rates covered by the compilation vary from 0.027 m/yr (NUS7-2) to 0.40 m/yr (DIV), comparable to conditions at Dome C and Talos Dome, respectively. The bromine and sodium flux data for each site are plotted against snowfall (i.e., accumulation) in Fig. 11. As described in section 2.2.3, the arrangement of flux vs accumulation creates a linear array in which the gradient represents the wet-deposition component of flux and the y-intercept represents the dry-deposition component. The authors found sodium fluxes to be almost entirely driven by wet deposition; whereas for bromine dry deposition is comparable to or greater than wet deposition, particularly at low accumulation sites. Furthermore, the study demonstrated a negative y-intercept for bromine, 'indicating substantial release of bromine from the snowpack back to the atmosphere after deposition' (McConnell et al., 2017). It is clear from the compilation that bromine fluxes are consistently and anomalously low at sites with very low accumulation rates less than 0.04 m/y, although the effect is less relevant at higher accumulation sites.

The surface snow experiments described here provide insight into the behaviours of Br and I in different accumulation, irradiation and environmental conditions. We can conclude that halogen postdepositional remobilisation and loss is active on the high Antarctic plateau, with close to 100 % of iodine and at least 50 % of bromine lost from the snowpack at low-accumulation sites. These results are difficult to quantify because confounding processes, such as snow remobilisation, also have a strong influence at low-accumulation sites. At sites with moderate snow accumulation, located nearer to the coast, bromine re-emission appears to be minor although iodine re-emission is still substantial. Additional experiments should be planned with the aim of evaluating the competing influences of solar irradiation and snow burial on the photochemical activation of halogens in snowpack. Further quantification studies should also be carried out in areas with snow accumulation rates between 0.05 and 0.3 m/y. Finally, it is possible that enhanced solar irradiance due to the destruction of stratospheric ozone since the 1970s (the "hole in the ozone layer") could play an important role in halogen photochemical activation. Such questions may be addressed by more widespread sampling of the snowpack on the central Antarctic Plateau.

3.6. Halogen and sea-salt transport from sea-ice to land ice

Considering that seasalt is present in the polar atmosphere only as aerosol, whereas halogens exist in both aerosol and gas phase (as mentioned in sections 2.2.3 and 3.2.1), one would expect *a priori* that seasalts and halogens will respond differently to the various transport and deposition processes present in the polar boundary

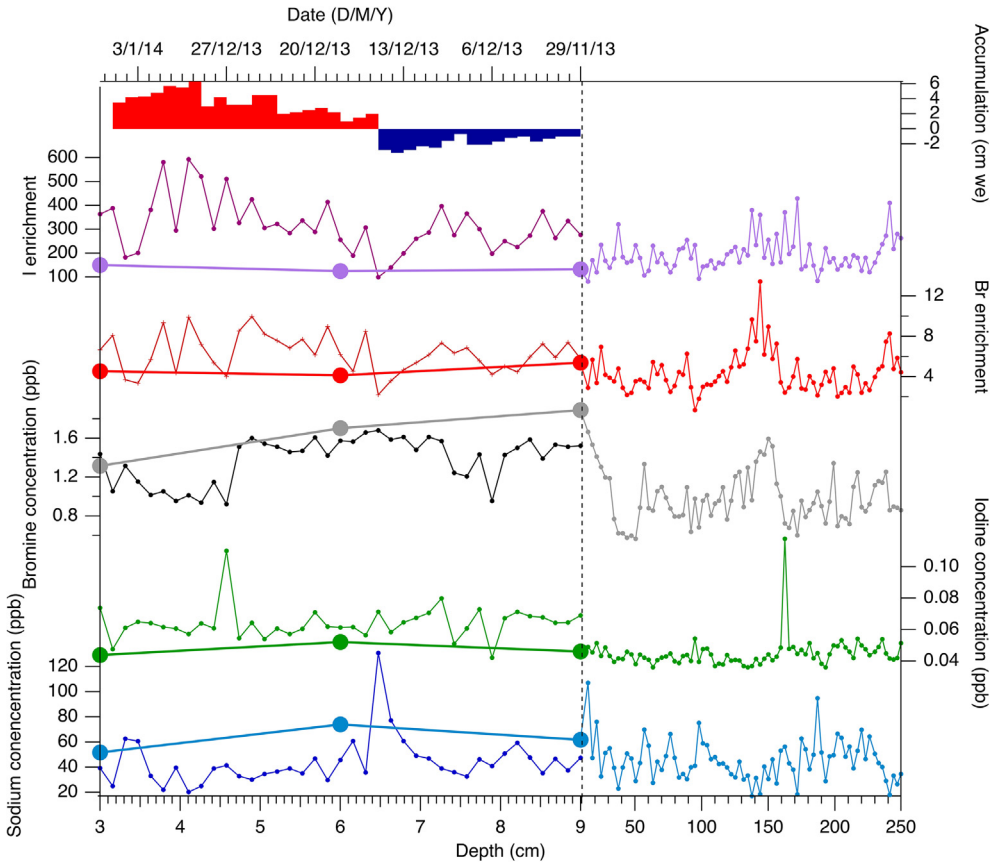

Fig. 10. Bromine, iodine and sodium in surface snow (left panel) and a 2.5 m snow pit (right panel) sampled at the GV7 site in northern Victoria Land. The surface samples (left side of the graph, high resolution data) have been chronologically ordered to fit with the snow pit stratigraphy. The large circles show the concentrations determined in the first three snow pit samples (ie, top 9 cm of the snow pit). Good correspondance is found between the snowpit and surface snow samples for sodium and bromine, whereas iodine concentrations in the snowpit are clearly lower than in the surface snow.

layer. Marine aerosols are micron-scale particles (Legrand et al., 2017; O'Dowd et al., 1997) easily mobilised long distances (several hundreds of kilometres) and subject to wet deposition processes. The atmospheric lifetime of gas-phase halogens (HOBr, BrO and Br_2 for bromine; I_2, IO, OIO and I_2O_2 for iodine) is limited only by its reactivity and is therefore driven primarily by dry deposition processes. Bromine undergoes multiphase (aerosol-gas) chemical exchanges in the course of its transport from the sea-ice surface to a polar ice cap, leading to the photochemically-driven "leapfrogging" proposed by the GSHOX experiment (section 3.3). In this section we revisit two important evaluations of bromine and seasalt transport and critically investigate inconsistencies between the two. We go on to review observational data allowing further evaluation of these studies and propose a framework integrating the two.

3.6.1. Models of halogen and sea-salt transport

Simpson et al. (2005) presented the first evaluation of spatial variability of bromide in snowpack. Snow sampling was conducted in 2004 within a grid pattern consisting of a north-south sampling line from Barrow station to 280 km inland (Douglas and Sturm, 2004). Ion chromatography (Br^-, Cl^-) and Atomic Absorption Spectroscopy (Na^+) were applied to determine bromide, chloride and sodium concentrations, respectively, in three distinct snowpack layers. The main results from the study were: 1) Minimal to no enrichment of Br^- relative to Na^+ in frost flowers; 2) a wide range of Br^-/Na^+ ratios in snowpack from approximately 0.1 to 100 times the ratio found in sea-salt; and 3) Na^+ concentrations decrease strongly with distance from the coast whereas Br^- concentrations decrease gradually or not at all. Fig. 12 displays the primary findings of the study, indicating different coastal concentrations and rates of change for Na^+ and Br^- as snow is sampled at greater distance from the coast. This study demonstrated effective transport of recycled bromine inland, with a clear distinction between the aerosol-phase transport of sodium and the mixed gas/aerosol phase of bromine further complicated by the likelihood of heterogeneous bromine recycling during transport.

Spolaor et al. (2013b) investigated the transport and deposition characteristics of sodium and bromine in East Antarctica, in the first application of halogens data to sea-ice reconstruction (see sections 4.4.1 and 5.1.1). A 1-D chemical transport model was constrained to a small number of surface snow measurements of Br and Na from Talos Dome (assumed 7 h from sea-ice edge) and Dome C (assumed 24 h from the sea-ice edge), based on the transport of an air mass inland at a constant velocity. The model used deposition velocities of 0.2 cm/s for Na and 1 cm/s for HBr, leading to a faster deposition of bromine relative to sodium. These results ran counter to the findings of Simpson et al. (2005) as well as the *a priori* physically-based argument described earlier.

To unravel the contradiction between the schema of bromine transport presented by Simpson et al. (2005) and Spolaor et al. (2013b) we compare representative values of sodium and bromine at the coastal zone (<30 km from the coast), the inland zone (250–300 km from the coast) and a "central ice sheet" zone (>700 km from the coast) from each study, as shown in Table 3. Data equivalent to the "central ice sheet" are not applicable to the

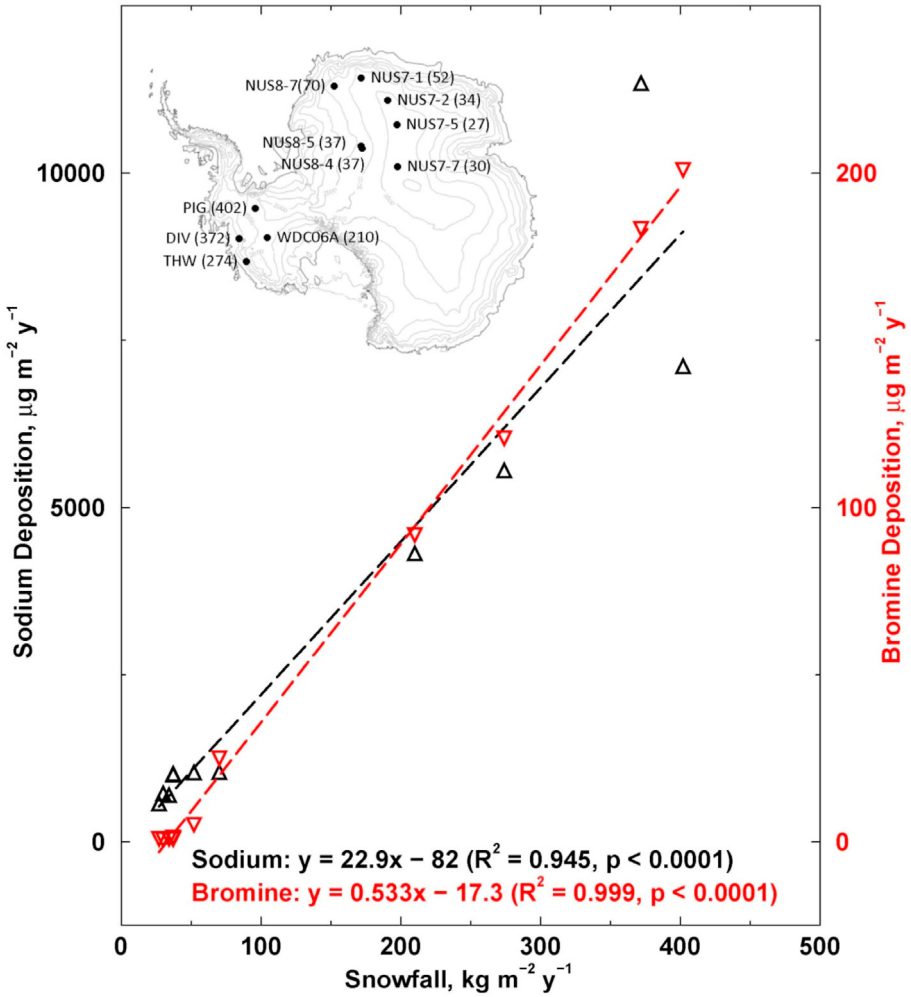

Fig. 11. A compilation of bromine and sodium fluxes from an array of 11 Antarctic ice cores. The inset figure shows the names and locations of the ice cores, with mean snowfall rates (kg m^{-2} y^{-1}) at each site shown in parentheses. The ice core records cover different periods of time, from centuries to millennia. Linear correlations (dashed lines) have been fit to the average net deposition of sodium (black) and bromine (red) for the sites. Reprinted from McConnell et al. (2017, SI Appendix 4). (For interpretation of the references to colour in this figure legend, the reader is referred to the Web version of this article.)

Simpson et al. (2005) model, wherease for the Spolaor et al. (2013b) model we extrapolated the results to the coastal zone.

Table 3 clearly demonstrates that the "coastal zone" sodium concentrations used by Spolaor et al. (2013b) are too low by one to two orders of magnitude. For the inland and central ice sheet zones, sodium values are not unreasonable (e.g.: Bertler et al., 2005; Schüpbach et al., 2013). Bromine concentrations reported by Spolaor et al. (2013b) are consistently lower than those reported by Simpson et al. (2005) but do not seem as strikingly problematic as the sodium concentrations. Although the deposition velocity assigned for HBr (1 cm/s) is consistent with other independent modelling studies (eg. Legrand et al., 2016), the most significant bias in the Spolaor et al. (2013b) study is the inaccurately assigned sodium concentrations. As a result, the model used by Spolaor et al. (2013b) was incorrectly constrained and their findings require re-assessment.

3.6.2. *Compilation of spatial variability: bromine and sodium*

Spatial maps of bromine and sodium concentrations have been compiled for Antarctica and Greenland. All available data are included irrespective of their temporal coverage, varying from days or weeks to millennia of deposition. In all cases, ice core data have been selected to represent Holocene (ie, interglacial) values. Fig. 13 (Antarctica) and 14 (Greenland) show the compiled sodium and bromine concentrations, nssBr and Br_{enr} values. The Br_{enr} values are overlaid on a composite map of BrO total vertical column concentrations for the period 2010–2015 (pers. comm., A. Richter, IUP-Bremen, 2020).

The majority of Antarctic sample data are from transects: Dronning Maud Land (McConnell et al., 2017); Zhongshan station to Dome A (Li et al., 2014); Talos Dome to GV7 (Maffezzoli et al., 2017); and Talos Dome to Dome C (this work). Data are included from individual sites in West Antarctica (McConnell et al., 2017), Roosevelt Island (this work) and Law Dome (Vallelonga et al., 2017). The Roosevelt Island data were obtained from a 35 m deep firn core covering the period 1930–2006 CE (Winstrup et al., 2019). Across Antarctica, bromine concentrations are uniformly low (<0.5 ppb) with the exception of coastal locations where the influence of marine salts is strong (Victoria Land, Roosevelt Island and Law Dome). This pattern is consistent with previous compilations (Bertler et al., 2005). Br_{enr} values are generally low (<2) at coastal locations (Law Dome, Zhongshan, Roosevelt Island) and increase to greater values (>2) on the plateau, as demonstrated on the Zhongshan-Dome A transect. This pattern is less clear across West Antarctica and the Victoria Land/East Antarctic plateau sector, and is actually inverted across Dronning Maud Land (DML).

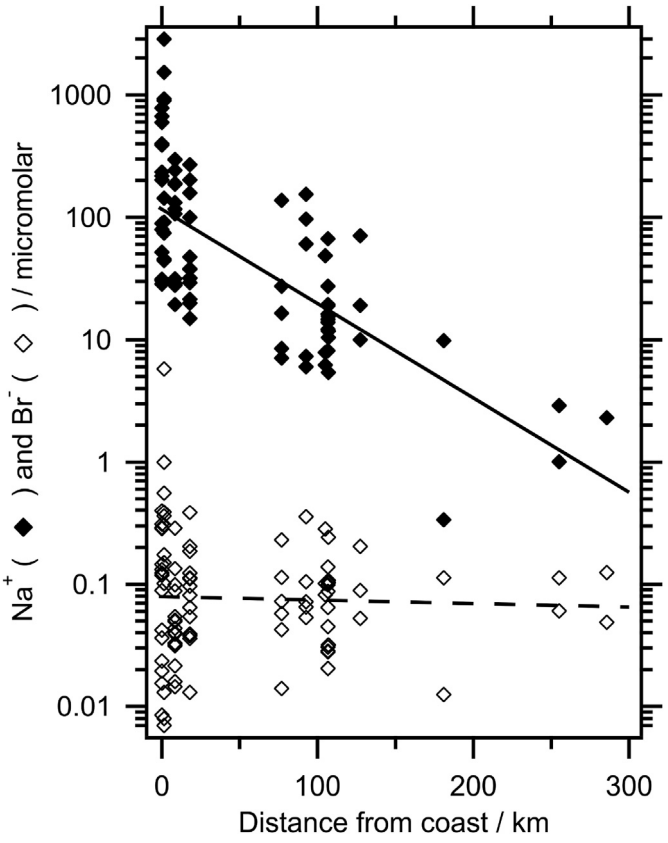

Fig. 12. Sodium and bromide in the springtime snow pack as a function of distance from the Alaskan coast. The lines are trend lines made by linear fits of the logarithm of the concentration versus distance from the coast. Reprinted from Simpson et al. (2005).

Contradictory patterns of bromine and sodium are observed for the Zhongshan-Dome A (Z-DA) transect and the DML dataset: DML data show intermediate sodium (ca. 25 ppb) and very low bromine (ca. 0.03 ppb) concentrations on the plateau; while the Z-DA transect reports lower sodium (ca. 15 ppb) and intermediate bromine (ca. 0.2 ppb) concentrations on the plateau. The differences between these two datasets may be due to the time periods covered (decades vs centuries, respectively) and/or the analytical methods (IC vs ICP-SFMS, respectively). There is not a strong consistency between bromine concentrations and atmospheric BrO concentrations observed by the satellite-based GOME-2 sensor, particularly across the Antarctic plateau.

Fig. 14 shows a composite of bromine data and associated sodium concentrations reported for Greenland. Two transects are included: a 2015 NEEM-EastGRIP traverse and a 2017 Windsled traverse from Kangerlussuaq to EastGRIP, both of which will be discussed in detail in sections 4.1.1 and 4.1.2. Ice core drill sites include TUNU and Summit (Maselli et al., 2017), RECAP (Maffezzoli et al., 2019), NEEM (Spolaor et al., 2016b) and DYE-3 (this work). The DYE-3 data were obtained by resampling archive pieces of the original core drilled in 1981 (Johnsen et al., 1992) corresponding to the period 10–11 ky b2k. The NEEM samples cover the late Holocene period (0.03–3 ky b2k) and the Renland samples cover the period 0–11 ky b2k. Overall patterns of Br, nssBr and sodium are similar in Greenland and Antarctica: higher concentrations of sodium and bromine at the coast and lower concentrations on the inland plateau. Sodium does not show a consistent north-south gradient along the Greenland ice sheet, although there is a dearth of data corresponding to the southern half of the ice sheet. A strong sodium concentration gradient is observed from the northwest toward the central/eastern sector of the ice sheet, consistent with previously reported atmospheric circulation patterns (Fischer and Wagenbach, 1996; Rhodes et al., 2018) and accumulation gradients (Fischer et al., 1998). Bromine enrichment values increase from low values (<6) at sites located nearer the coast to higher values (>15) in the central and northern part of central Greenland. There are large data gaps in coastal and southern Greenland – these could be ideally filled by traverses from the coast to inland stations. Such traverses could include: Thule to NEEM; EastGRIP to station Nord (ideally travelling via the TUNU drill site); and EastGRIP to Zackenberg station. A better understanding of bromine variability across northern Greenland would also be important to the interpretation of existing (Maffezzoli et al., 2019; Spolaor et al., 2016b) and projected (Rhodes et al., 2018) reconstructions of Arctic sea-ice extent.

3.6.3. Synthesis of halogen transport models

Here we combine the spatial data presented in Figs. 13 and 14 into one graph, showing the variability of bromine and sodium as a function of distance from the coast. The data (Fig. 15, Table 4) show that spatial variability of sodium and bromine are consistent across both Antarctica and Greenland, and therefore suitable models should be applicable to both locations. We plot Br and Na concentrations, Br_{enr} and nssBr as a function of the average distance of each site from the sea-ice edge from which airmasses are likely to travel to the site. The calculated distance is an approximation considering the main atmospheric circulation pattern for the area as well as variability in sea-ice extent during the Holocene. In both the Arctic and Antarctic, the sea-ice edge location coincides with the continental coastline since multi-year sea-ice is present mainly in the Canadian Arctic and in only a few sectors of the Antarctic coast. In addition, the average value for Br, Na, Br_{enr} and nssBr for each site is calculated for the entire temporal coverage of the record.

Fig. 15 demonstrates the different behaviours of sodium and bromine concentrations as airmasses travel from the coast to central Greenland and Antarctica. Sodium demonstrates a faster

Table 3
Comparison of Br and Na concentrations and Br_{enr} values for two studies of bromine and seasalt transport from the coast to inland regions of Antarctica and Alaska.

Study name/reference	Parameters of interest	Coastal margin (<30 km from sea ice)	Inland zone (250-300 km from sea ice)	Central ice sheet (>700 km from sea ice edge)
Simpson et al., 2005	Representative Na concentration	2300 ppb (100 uM)	23 ppb (1 uM)	N/A
	Representative Br concentration	8 ppb (0.1 uM)	6 ppb (0.08 uM)	N/A
	Br/Na ratio relative to sea water	0.5	45	N/A
Spolaor et al., 2013(Spolaor et al., 2013b)	Representative Na concentration	3 ppb[a]	15 ppb[b]	45 ppb[b]
	Representative Br concentration	0.2 ppb[a]	0.1 ppb[b]	0.1 ppb[b]
	Br/Na ratio relative to sea water	8[a]	1.3[b]	0.5[b]

[a] Extrapolated data calculated assuming an accumulation rate of 500 mm w.e. at the coast.
[b] Calculated assuming accumulation rates of 25 mm w.e. at Dome C and 80 mm w.e. at Talos Dome

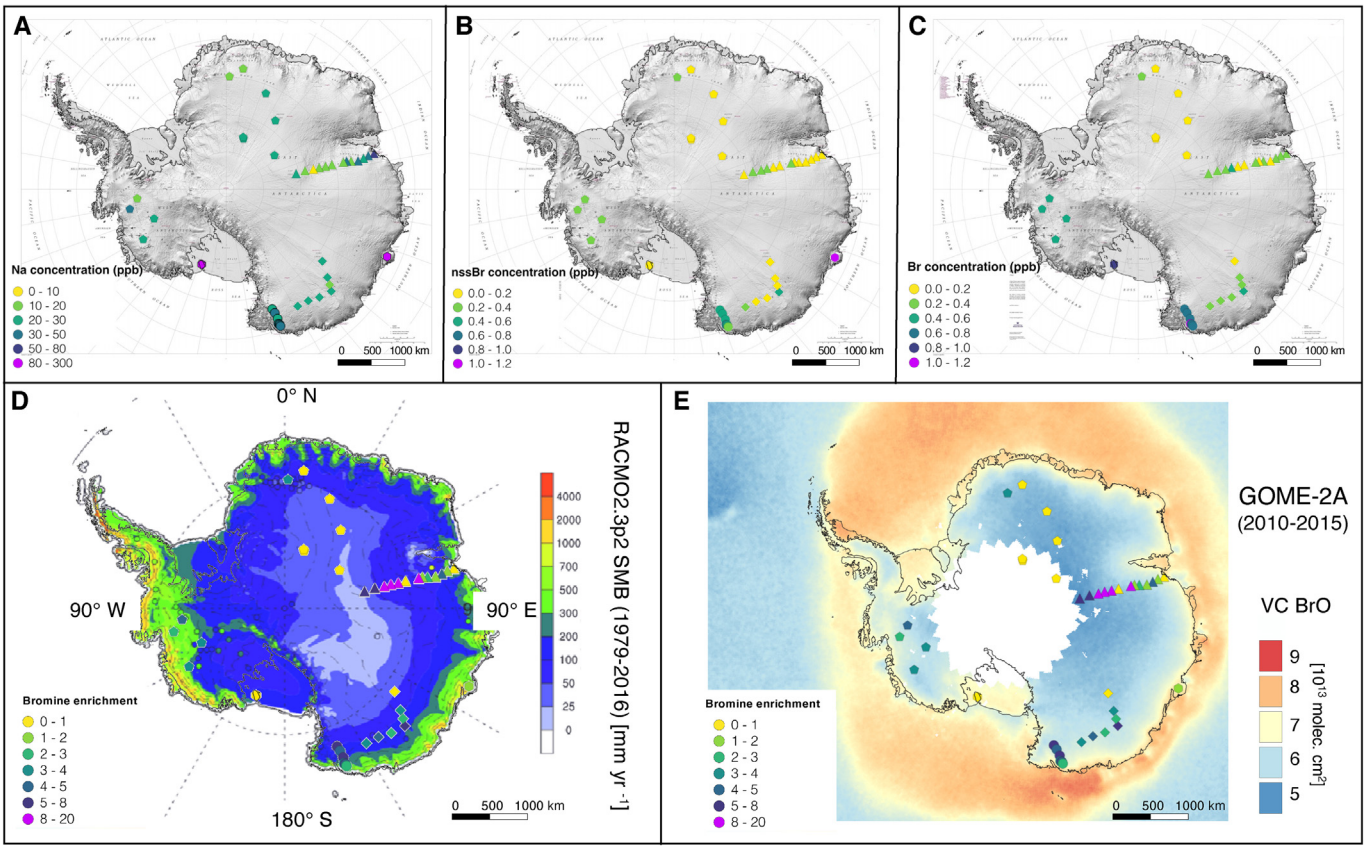

Fig. 13. A compilation of bromine and sodium concentration data indicating spatial variability across Antarctica. Concentrations of sodium (A), non sea-salt bromine (B) and bromine (C) are overlaid on a Digital Elevation Model of Antarctica (Howat et al., 2019). Bromine enrichment is shown overlaid with a RACMO2.3 reconstruction of modern snow accumulation (D, Thomas et al., 2017) and tropospheric BrO vertical column densities from the GOME-2A sensor (E, pers. comm., A. Richter, IUP-Bremen, 2020). Data sources are detailed in the text.

decline than bromine, as it travels from the coast. At approximately 400 km inland, sodium deposition is effectively complete and concentrations remain stable further inland. Bromine shows a quasi-linear decreasing trend from about 100 km inland to about 1000 km inland, after concentrations are extremely low and are very likely present only as a remnant of re-emitted bromine. The different rates of decrease of sodium and bromine suggests different rates of efficiency in the deposition processes moving away from the coast: wet deposition driven by precipitation ensures that sodium deposits faster into the coastal snowpack and then reaches a stable concentration across the very dry central areas of Antarctica. Over the Antarctic plateau, bromine concentrations effectively drop to detection limits of the analytical techniques used. The different Na and Br spatial snowpack concentration patterns are also reflected in the resulting Br_{enr} and nssBr patterns, which are again very similar for the Arctic and Antarctic. Br_{enr} starts with low values near the coast and gradually increases to the highest values approximately 300–600 km inland. Br_{enr} values then quickly decrease further inland and are less than 1 for all sites greater than 800 km from the coast.

The model advanced by Spolaor et al. (2013b) is of use once it is properly located – that is, once the bias caused by inappropriate constraints has been mitigated. The increase of Br_{enr} from the coast to 300–600 km inland is consistent with the findings of Simpson et al. (2005) while the trend determined further inland (>600 km from the coast) aligns with the transport model proposed by Spolaor et al. (2013b). The suitability of these models for interpreting bromine concentrations (and particularly Br_{enr} values) for sea-ice reconstructions will be described in the following section.

3.7. The role of halogen transport models in sea-ice reconstructions

Based on the integration of the Simpson et al. (2005) and Spolaor et al. (2013b) models of halogen transport, we can draw the following initial conclusions regarding the suitability of bromine as a metric for reconstructing sea-ice:

1) The increasing pattern of Br_{enr} vs distance from the coast supports the use of Br as a metric related to sea-ice, specifically the sea salt release from the sea-ice surface, for broad swathes of coastal Antarctica (to approximately 600 km inland) and the majority of the Greenland ice sheet. This band of distance from the coast reflects the zone in which both Br and Na are decreasing with distance.
2) The zone of Antarctica located more than 800 km from the coast – ie, the vast expanse of the Antarctic Plateau – is potentially of limited value for quantitative sea-ice reconstruction. This zone features very low concentrations of bromine, which may be subject to photolytical reactivation and/or snow remobilisation processes. Variability in bromine concentrations and Br_{enr} at such inland sites could reflect changes in solar irradiation, changes in meteorological patterns (influencing deposition of sodium and bromine) and changes in wind fields, influencing both deposition and surface snow remobilisation.
3) During glacial climate periods, the increased extent of Antarctic ice would lead to an outward expansion of the location of the

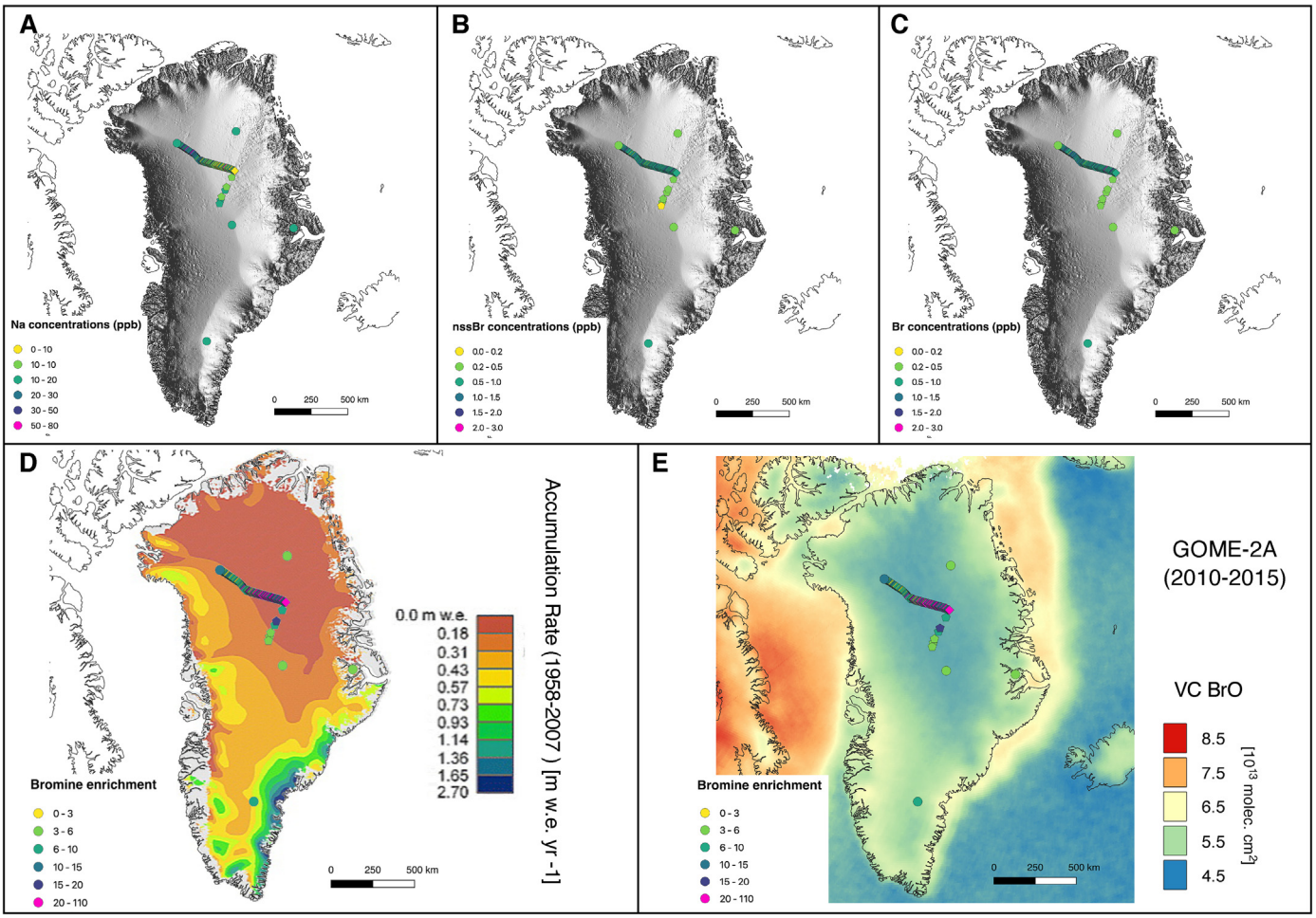

Fig. 14. A compilation of bromine and sodium concentration data indicating spatial variability across Greenland. Concentrations of sodium (A), non sea-salt bromine (B) and bromine (C) are overlaid on a Digital Elevation Model of Greenland (DiMarzio et al., 2007). Bromine enrichment is shown overlaid with a Polar MM5 reconstruction of modern snow accumulation (Burgess et al., 2010) and tropospheric BrO vertical column densities from the GOME-2A sensor (E, pers. comm., A. Richter, IUP-Bremen, 2020). Data sources are detailed in the text.

sea-ice edge, thereby increasing the zone of low-accumulation across central Antarctica. Thus, locations which are currently within 800 km of the Antarctic coast will likely fall outside this zone and therefore cease to be reliable sites for sea-ice proxy reconstruction. This may be the case for Talos Dome, the site for which the Spolaor et al. (2013b) model was first proposed. In such a case, the site may be a qualitative indicator of sea-ice extent – useful for demonstrating the timing of transitions between 'large' and 'small' sea-ice extents rather than continuously quantifying the sea-ice extent over glacial/interglacial cycles.

4) Considering glacial-interglacial transitions, tracts of multi-year sea-ice are likely to form at the coast during glacials which will lead to a displacement of the first-year sea-ice edge away from the coast. For sampling sites located within 100 km of the coast, a relative increase in the Br_{enr} signal is therefore likely occur independent of any change to the first-year sea-ice extension. For ice cores collected further inland (i.e. >300 km inland) the extension of the multi-year sea-ice should cause a decrease of the signal due to the increased distance of the bromine gas phase source.
5) The above considerations have taken into account only the distance from the sea-ice edge to the sampling site. Any potential reconstruction of sea-ice extent will have to take into account two factors: firstly, the distance from the sampling site to the sea-ice edge, and secondly, the area of sea-ice contributing sodium and bromine to the sampling site. Where the general climate conditions have not changed (i.e., during an interstadial), one would expect the first factor (distance) to be approximately constant, and hence bromine variability would primarily reflect changes in the area of FYSI available for photochemical bromine recycling. Where the change in the location of the sea-ice edge is substantial with respect to the distance to the sampling site, the transport models proposed by Simpson et al. (2005) and Spolaor et al. (2013b) will have to be appropriately deployed to accurately interpret the results.
6) The models of Simpson et al. (2005) and Spolaor et al. (2013b) should be further refined by a suitably designed process-study experiment. The experiment design employed by GSHOX should be revisited and ideally applied to East Antarctica, where the full extent of the Simpson et al. (2005) and Spolaor et al. (2013b) models can be tested and an array of monitoring stations can be established – both at the coast and at inland ice core drilling sites.

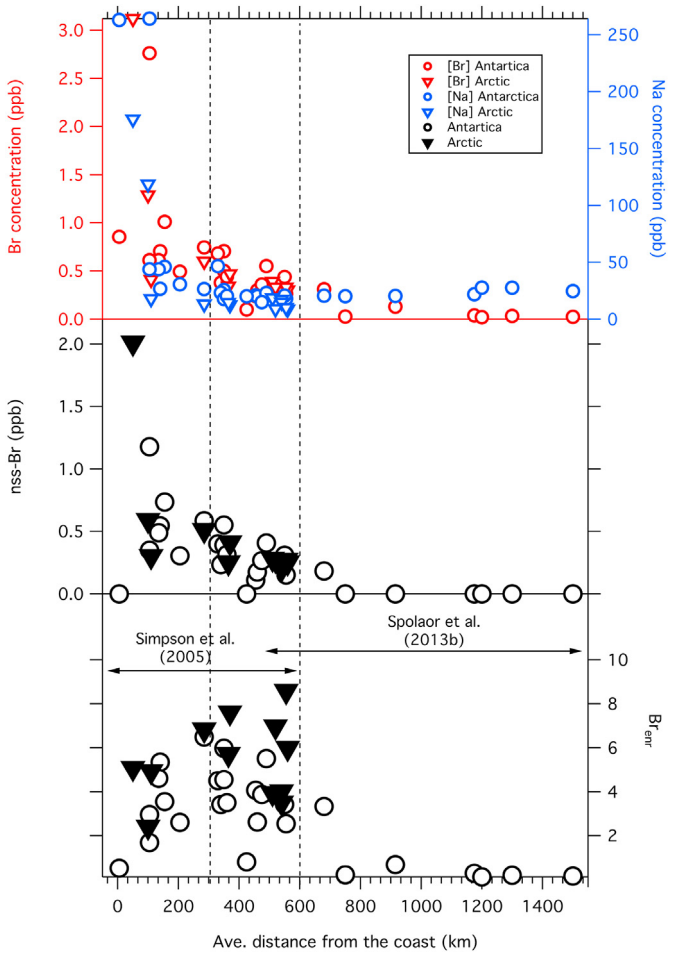

Fig. 15. Compilation of sodium and bromine concentrations from Arctic and Antarctic firn and ice records as a function of distance from the coast. The figure shows the halogen transport range investigated by Simpson et al. (2005) as well as the transport range relevant to the dataset described by Spolaor et al. (2013b) when their transport model is appropriately constrained. See Table 4 for data and references.

4. Snow and ice records of halogens

4.1. Transect data

In this section we consider studies presenting data from surface transects in Antarctica and Greenland. Typically, such data covers a short time period – less than a decade – due to the limited time available at each sampling location. Nonetheless, the spatial coverage offered by such datasets compensate for their potential lack of temporal representativeness. The transects discussed here will be divided into two sub-groups: datasets that were not considered in the previous chapter due to their limited temporal coverage (<3 years); and those with a longer temporal coverage.

4.1.1. Transect data with sample coverage <3 years

Li et al. (2014) reported impurities in surface snow and snow pit samples collected between December 2012 and January 2013 on a transect from Zhongshan Station to Dome A, Antarctica. The character of the sampling sites varied from coastal (40 km inland, altitude 832 m a.s.l., accumulation 260 kg/m^2/yr) to the highest parts of the Antarctic plateau (1250 km inland, altitude 4093 m a.s.l., accumulation 23.5 kg/m^2/yr). Sodium (Na^+) and Br^- were reported for surface snow samples collected every 10 km and 2 m deep snow pits sampled every 100 km along the traverse. The results were consistent with the findings of Simpson et al. (2005), but with a much smoother gradient of sodium decrease. Concerns regarding the representativeness and accuracy of these data, with respect to other measurements available from the Antarctic Plateau, have been discussed in section 3.6.4.

Surface snow was sampled every 10 km during a 120 km transect from Casey station to Law Dome summit in coastal East Antarctica (Vallelonga et al., 2017). This region is strongly influenced by maritime airmasses and features a strong accumulation gradient, from 150 kg/m^2/yr near Casey station to 800 kg/m^2/yr at the summit. Despite a few outliers, sodium concentrations were usually high (average 180 ppb), bromine concentrations were usually low (average 1.3 ppb) and Br_{enr} varied from 0.3 to 1.7. Although little can be concluded with regard to halogen transport due to the short distance covered by the transect, the data from this transect can be taken as indicative of halogen and seasalt concentrations representative of the coastal zone.

In May 2015, scientific sampling and observation programs were conducted in conjunction with a 460 km traverse from northwest (NEEM) to Northeast (EastGRIP) Greenland (Schaller et al., 2016). Surface snow samples were collected every 10 km, in addition to six firn cores drilled to approximately 12 m depth (Kjær et al., 2021). The traverse followed a strong accumulation gradient from 220 kg/m2/y in northwest Greenland (NEEM Community members, 2013) over the central ice divide into northeast Greenland which features accumulation rates of 110 kg/m^2/y (Vallelonga et al., 2014): the lowest reported for the Greenland ice sheet. The results are presented in Fig. 14 and Appendix A.

4.1.2. Transect data with sample coverage >3 years

Maffezzoli et al. (2017) investigated sodium and bromine in snow pits on a 200 km transect in Victoria Land, Antarctica, from Talos Dome (250 km from the Ross Sea) to core site 6 (85 km from the Southern Ocean). The location of the traverse enabled an investigation of the competing influences of seasalt arriving from the Ross Sea and Southern Ocean sectors, but for the purpose of this review we can consider the transect data as representative of the "inland sector" located a few hundred km from the coast. These results indicate the model constraints applied by Spolaor et al. (2013b) (Table 3) for Talos Dome site were accurate for sodium but about an order of magnitude too low for bromine. Extending the Victoria Land transect from Talos Dome to Dome C, seven short (4 m) snow cores were collected in November/December 2016 (this work). The samples were analyzed for sodium and bromine at the University Ca' Foscari of Venice in mid-2017, and the results are included in Fig. 13 and Table 4. There is no clear spatial variability in sodium or bromine concentration over the sampled locations and thus the results may be considered typical for the Antarctic ice sheet plateau.

Bromine and sodium fluxes have been reported for two Norwegian-US collaborative traverses through Dronning Maud Land conducted in 2007/8 and 2008/9 (McConnell et al., 2017). Seven ice cores were collected over the two traverses, which represent high-altitude plateau conditions. Details of the sampling and ice core specifications (McConnell et al., 2014) are reported separately to the halogen data (McConnell et al., 2017).

In May/June 2017, a windsled traverse was conducted from southwest Greenland (inland from Kangerlussuaq) up to the EastGRIP ice core drilling site, along which a number of 2 m deep snow cores were collected. The snow cores each cover the period 2014–2017 CE and were subsampled at the University of Copenhagen with aliquots sent to the University Ca' Foscari of Venice for sodium and bromine determination. We report here the final six cores collected along the traverse, from the central ice divide (north of Summit station) to EastGRIP site (Fig. 13, Table 4). The sampling

Table 4
Compilation of firn and ice core records from the Arctic and Antarctic, characterising variability in Br and Na concentrations with distance from the coast.

Antarctica Study name/location	Site designation	Latitude	Longitude	Distance to coast km	Br ppb	Na ppb	nssBr ppb	Brenr	Time period	Resolution	Reference
TD-GV7 (Traverse)	TD	-72.8	159.1	350	0.70	25	0.55	6.0	2014 - 2010	annual	Maffezzoli et al., 2017
	Site_10	-72.2	158.68	330	0.68	47	0.40	4.5	2014 - 2010		
	Site_9	-71.35	158.38	285	0.74	26	0.59	6.5	2014 - 2009		
	GV7	-70.68	158.85	155	1.01	46	0.73	3.6	2014 - 2009		
	Site_8	-70.6	158.58	140	0.70	27	0.54	5.4	2013 - 2011		
	Site_7	-70.52	158.42	135	0.61	44	0.49	4.6	2013 - 2010		
	Site_6	-70.35	158.4	105	0.61	44	0.35	3.0	2013 - 2010		
TD-Dome C (Traverse)	C1	-71.65	148.67	340	0.38	23	0.23	3.4	2017 -	biannual	Unpublished (This work)
	C2	-71.47	143.64	455	0.24	21	0.11	4.1	2005		
	C3	-70.91	139.18	460	0.30	20	0.17	2.6			
	C4	-70.43	134.15	490	0.55	23	0.41	5.5			
	C5	-71.19	132.76	555	0.26	18	0.15	2.6	2017 - 2000		
	C6	-72.02	131.13	680	0.31	21	0.18	3.3	2017 - 1995		
	C7	-73.89	126.78	915	0.13	20	0.00	0.7	2017 - 1990		
Law Dome		-66.77	112.8	105	2.76	264	1.18	1.7	1989 - 1927	seasonal	Vallelonga et al., 2017
Roosevelt island		-79.36	-161.71	10	0.85	263	0.00	0.5	2004 - 1937	decadal	Unpublished (This work)
Dome C		-75.06	123.2	1100	0.30	40	0.07	1.1	2014 - 1997	biannual	Spolaor et al., 2018
Dronning Maud Land	NUS_7_1	-73.72	7.94	425	0.10	20	0.00	0.8	2005 - 1755	annual	McConnell et al., 2017
	NUS_7_2	-76.07	22.47	750	0.03	20	0.00	0.2	1993 - 337		
	NUS_7_5	-78.65	35.63	1175	0.04	22	0.00	0.3	1989 - (-111)		
	NUS_7_7	-82.07	54.88	1500	0.03	25	0.00	0.2	2005 - 49		
	NUS_8_4	-82.82	18.9	1300	0.03	28	0.00	0.2	2008 - 1622		
	NUS_8_5	-82.63	17.87	1200	0.02	28	0.00	0.1	2008 - 346		
	NUS_8_7	-74.88	1.6	475	0.36	15	0.27	3.9	2008 - 1255		
West Antarctica	DIV	-76.77	-101.74	205	0.49	31	0.30	2.6	2010 - 1786	annual	McConnell et al., 2014 McConnell et al., 2017
	PIG	-77.96	-95.96	350	0.50	18	0.39	4.6	2010 - 1918		
	THW	-76.95	-121.22	360	0.44	20	0.32	3.5	2010 - 1867		
	WDC06A	-79.48	-112.11	550	0.44	21	0.31	3.4	2005 - 1775		
Arctic Study name/location	Site designation	Latitude	Longitude	Distance to coast km	Br ppb	Na ppb	nssBr ppb	Brenr	Time period	Resolution	Reference
Inuit Windsled Greenland (Traverse)	WS2017-5	73.92	-40.15	540	0.32	17	0.21	4	2017-2013	annual	Unpublished (This work)
	WP706	73.73	-40.42	540	0.29	15	0.20	4			
	WP656	74.14	-39.87	560	0.30	9	0.25	6			
	WP606	74.52	-38.92	555	0.33	10	0.27	9			
	WS2017-7	74.71	-38.52	550	0.36	6	0.32	16			
	WP506	75.26	-37.02	520	0.33	9	0.27	7			
DYE-3		65.18	-43.83	285	0.60	13	0.51	7	9900-11000	centennial	Unpublished (This work)
NEEM		77.45	-51.06	370	0.47	13	0.41	8	1975-1000	centennial	Spolaor et al., 2016b
TUNU		78.03	-33.87	365	0.34	15	0.25	6	2010-1750	annual	Maselli et al., 2017
Summit		72.33	-38.29	510	0.39	19	0.28	14			
Renland	RECAP	71.3	-26.72	110	0.41	18	0.30	5	2012-1750	annual	Maffezzoli et al., 2019
Svalbard	Holthedalfonna	79.14	13.39	100	1.29	119	0.59	2	2012-2005	subannual	Spolaor et al., 2013a
Severnaya Zemlya	Akademii Nauk	80.51	94.82	50	3.12	176	2.01	5	1999-1950	subannual	Spolaor et al., 2016a

locations are all far inland and at high altitude (<2900 m a.s.l.) and therefore are important for investigating halogen deposition to the central Greenland ice sheet between EastGRIP and Summit station. There is a strong accumulation gradient also featured along this traverse, essentially halving from the ice sheet divide (accumulation approximately 230 kg/m2/y) to EastGRIP (Karlsson et al., 2020; Nielsen et al., 2015).

4.2. Seasonal timescales

Only a few studies have reported the variability of halogens in ice on seasonal timescales. These include three for Antarctica (Dronning Maud Land, Law Dome, Northern Victoria Land) and four for the Arctic (Severnaya Zemlya, Svalbard and two sites in Greenland). For most of these locations, only bromine seasonality has been reported. The results are summarized in Tables 1, 2 and 4 and also described in the following sections.

4.2.1. Antarctica

Seasonal variability of halogens in Antarctic snow and ice have been reported from coastal locations where snow accumulation is sufficiently high to allow annual cycles in snowpack to be resolved. The first measurements of iodine in Antarctic snowpack were by Frieβ et al. (2010) who reported seasonal strata near Neumayer station, Dronning Maud Land, in a 2 m snowpit covering two annual cycles. High iodine concentrations in winter strata, and low concentrations in summer strata, were interpreted as evidence of photochemical remobilisation of iodine from snowpack during the Antarctic summer. This pattern of low summertime iodine concentrations was confirmed by Spolaor et al. (2014) who reported a four-year sequence (1910–1914 CE) of iodine from a Law Dome ice core. The same article was the first to report the seasonality of bromine in ice in Antarctica, finding a strong summer peak in both nssBr and Br_{enr}. A smaller Br_{enr} peak in late-summer/autumn was also found and tentatively attributed to the deposition of gas-phase boundary-layer bromine reservoir species at the austral dusk. At the same site, the seasonal pattern of Br_{enr} was confirmed and extended by Vallelonga et al. (2017), presenting a high-resolution study of a Law Dome firn core covering the period 1987–2012 CE. For this more detailed study, the summer peak was confirmed but the late-summer/autumn peak was not clearly observed. Maffezzoli et al. (2017) further confirmed the summer peak in Br_{enr}, from a study of six short firn cores collected across Northern Victoria Land in 2015. The highest average Br_{enr} values were found in early summer (October/November). In these samples, iodine concentrations were consistently very low although the few observed concentration peaks corresponded to winter strata. The iodine peaks in Northern Victoria Land (>0.1 ppb) were much lower than those reported for Neumayer (0.6 ppb) and Law Dome (0.3 ppb), consistent with satellite observations of very low atmospheric column amounts IO above Northern Victoria Land, compared to the lower-altitude coastal regions of Antarctica (Spolaor et al., 2014).

4.2.2. Arctic

Arctic iodine concentrations are much lower compared to Antarctica and few measurements are available. Spolaor et al. (2014) reported the first profiles of iodine in the Arctic from a 3-year snow pit from the NEEM ice core drill site in northwest Greenland and from a 5-year snow pit in Holtedahlfonna, Svalbard. In both profiles, surface iodine concentrations (0.2 ppb maximum) quickly decreased to lower values (0.02 ppb for Holthedalfonna and 0.05 ppb for NEEM) within two years of deposition. Only the Severnaya Zemlya ice core (Spolaor et al., 2016a) shows some long-term retention of an iodine signal going back to the 1950s. For the Severnaya Zemlya record, iodine concentrations were highly variable (0.01–3 ppb) but consistent peaks were observed in April (late winter/early spring) and lower concentrations in October. Such behavior is quite different to that observed in Antarctica, perhaps due to the proximity of Severnaya Zemlya to the marginal sea-ice zones of the Laptev and Kara Seas.

Bromine seasonality in the Arctic has been found to be consistent with the behavior shown in Antarctica, with higher concentrations in spring/summer (Fig. 16). Together with iodine, Spolaor et al. (2014) also reported the first Arctic profiles of bromine in snowpack from NEEM and Holtedahlfonna. Despite the short timeseries, consistent summer peaks of bromine and Br_{enr} were observed. These findings have since been confirmed by longer timeseries from Severnaya Zemlya (1950–1999 CE) reported by Spolaor et al. (2016a) and central Greenland Summit2010 ice core (1750–2010 CE) reported by Maselli et al. (2017).

4.3. Decadal-centennial timescales

4.3.1. Antarctica

Only one study of halogen variability over decadal-centennial timescales is available from Antarctica, that being a composite record of bromine, iodine and sodium from Law Dome and covering the period 1927–2016 CE (Vallelonga et al., 2017). The record is a

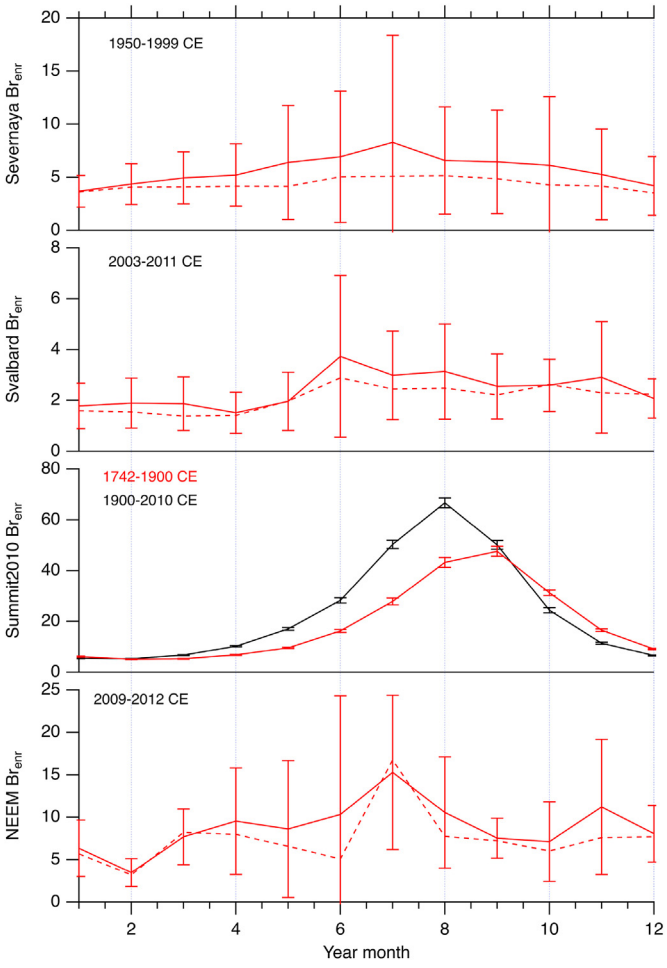

Fig. 16. Seasonal variability of bromine enrichment (Br_{enr}) from Arctic ice cores. The period covered by each record is shown on the figure. The mean of the data is indicated by a solid line with 1σ error bars and the median is indicated by a dashed line. The data are from ice cores drilled at Summit (Maselli et al., 2017) and NEEM (Spolaor et al., 2014) in Greenland, Severnaya Zemlya (Spolaor et al., 2016a) and Svalbard (Spolaor et al., 2013a).

composite of two firn/ice cores and a snowpit, respectively covering the time periods 1927–1986, 1987–2012 and 2015–2016 (Fig. 17). The Law Dome halogen records confirm earlier measurements of median concentrations of sodium (81 ppb), bromine (2.1 ppb) and iodine (0.056 ppb), further finding that these median values were 5–20 % lower than their corresponding arithmetic means due to the 'spiky' nature of the data. No significant trends were identified in the three data series over the sampled time period.

4.3.2. Arctic

A few records have been published reporting halogen variability over decadal-centennial timescales in the Arctic. These range from one decade of iodine and bromine at Svalbard (Spolaor et al., 2013a) to a half-century of iodine from the Alps (Legrand et al., 2018) and nearly three centuries of iodine (Cuevas et al., 2018) and bromine (Maselli et al., 2017) in ice core records from Greenland.

From the Holtedahlfonna glacier (Svalbard), Spolaor et al. (2013a) reported a detailed record of sodium, bromine and iodine covering the period 2003–2012 CE. The samples were obtained from an 11 m hand-auger core drilled at the bottom of a 2 m snowpit. Concentrations of bromine and iodine were within the respective ranges 0.43–7.36 ppb and 0.005–0.249 ppb, where 0.005 ppb was the detection limit for iodine. Despite the ubiquitous presence of melt layers, there was a structured iodine trend, with lower values in 2003/4 and 2007–2010 and higher values in 2005/6 and from 2011 to 2013. Bromine also varied substantially, with lowest values in 2004–2005 and 2011–2012 around a sustained peak from 2006 to 2008.

A longer record of bromine and iodine covering the period 1950–1999 was reported from Severnaya Zemlya (Spolaor et al., 2016a). Bromine and iodine displayed a high level of interannual variability, with mean (1σ) concentration values of 5.2 (6.1) ppb for bromine and 0.23 (0.34) ppb for iodine. Bromine showed an increasing trend from 1950 to the late 1970s, followed by a decreasing to 1999. Iodine showed no apparent trend until the late 1970s, after which concentrations decreased. Sodium variability (mean 187 ppb, standard deviation 197 ppb) was comparable to that of bromine and iodine but no trend was apparent from 1950 to 1999. Variability of bromine and iodine were linked to changes in sea-ice cover in the adjacent Laptev Sea, as discussed further in section 5.2.1.

An iodine concentration record covering the period 1890–1990 CE was reported from ice cores recovered from the Col Du Dome (CDD) saddle in the French Alps, displaying a periodically increasing trend in iodine since 1950 CE (Legrand et al., 2018). Col Du Dome, located at 4250 m asl, is an ideal location for sampling tropospheric air arriving from the North Atlantic Ocean and from western Europe, and anthropogenic pollutant emissions records have been previously reported from the location (Barbante et al., 2011; Preunkert et al., 2000). Combining the ice core record with an iodine emissions inventory and the GEOS-Chem chemical transport model, the authors model a pervasive and steady increase in iodine emissions from the surfaces of the North Atlantic Ocean and Mediterranean Sea. This increase in iodine is due to increasing anthropogenic NOx emissions, which lead to higher atmospheric concentrations of Ozone (O_3), which promotes the emission of iodine from the ocean surface. The authors note also a change in the primary atmospheric species of iodine, from a predominance of HOI in the pre-industrial period to the more-soluble $IONO_2$ after 1950 CE. The higher solubility of $IONO_2$ results in a shorter atmospheric lifetime as well as a greater efficiency of being captured in the snowpack.

The longest iodine record currently available from the northern hemisphere covers the last 250 years and has been extracted from the RECAP ice core in eastern Greenland (Cuevas et al., 2018). The RECAP ice core (Fig. 1) was drilled in 2015 on the Renland ice cap, a coastal ice cap located 2300 m above sea level and isolated from the main Greenland ice sheet. Renland features a relatively high annual snow accumulation rate of approximately 50 cm ice equivalent and receives its precipitation primarily from the North Atlantic Ocean and Nordic Seas. The iodine record shows relatively stable concentrations of 0.02 ppb from 1750 to 1940 CE, then lower values from 1940 to 1970, and a strong increase after 1970 CE. This pattern is also seen in iodine fluxes, but not in sodium concentrations that

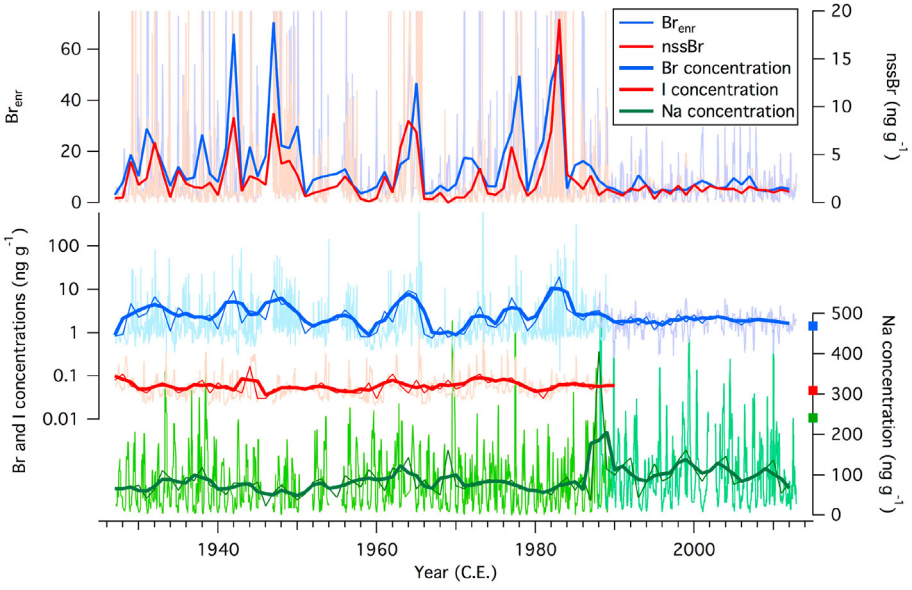

Fig. 17. Time series of sodium, iodine and bromine concentrations as well as nssBr and Br_{enr} at Law Dome. Raw data are shown in pale colours, with annual means shown by a thin line and 3-year running means shown by a thick line. For nssBr and Br_{enr}, only raw data (pale colours) and annual averages (thick line) are shown. Different shades of blue and green are used to distinguish data from DSS0506 (1927–1989) and DSS1213 (1987–2013). The squares indicate average values from the DSS1516 snow pit. Reprinted from Vallelonga et al. (2017). (For interpretation of the references to colour in this figure legend, the reader is referred to the Web version of this article.)

remained stable around 15 ppb for the whole period. The tripling in iodine concentrations observed from 1950 to 2015 CE was attributed to increasing emissions of oceanic inorganic iodine due to anthropogenic ozone increases, as well as increased emissions of oceanic organic iodine from thinning and retreating Arctic sea-ice (Cuevas et al., 2018).

From two sites in Greenland, a well-constrained 250 year high-resolution record of bromine, MSA, sodium and acid species was reported by Maselli et al. (2017). The two core sites investigated were Summit, a medium-accumulation site in central Greenland, and TUNU, a low-accumulation site located in northeast Greenland (Fig. 18). Both records displayed similar trends for MSA and bromine, although concentrations of Br and MSA were consistently lower in TUNU compared to Summit. The authors found a common preindustrial pattern between bromine and MSA, with a stable period of higher values between 1750 CE and 1835 CE and a second stable period of lower values between 1860 CE and 1940 CE. The durations of each stable period varied with respect to the core and analyte considered (MSA or Br). After 1940 CE, bromine and MSA trends diverged, with a sharp decrease in MSA and a sharp increase in bromine leading to a peak in the 1970s. Pre-industrial concentrations of bromine were 0.43 ppb at Summit and 0.34 ppb at TUNU. For the 1970's peak, bromine concentrations were approximately 0.48 ppb at Summit and 0.8 ppb at TUNU. The divergent behaviours of Br and MSA after 1940 CE were thoroughly investigated, as both species displayed similar trends and both have been employed in various manners to reconstruct sea-ice. The decreasing MSA trend was in good agreement with earlier observations of MSA trends in central Greenland (GRIP ice core; Legrand et al., 1997) and Svalbard (Isaksson et al., 2005). A recent study – including the Summit and TUNU MSA records - has proposed that the primary MSA emission source influencing Greenland over the industrial period is North Atlantic Ocean primary productivity rather than sea-ice algae (Osman et al., 2019).

In contrast, the bromine record was strikingly similar to the well-known record of acid deposition to Greenland resulting from anthropogenic emissions of sulfur- and nitrate-acid (NO_X) species associated primarily with the combustion of coal, leaded gasoline and diesel. Through a systematic investigation, Maselli and co-authors identified that sulphate had a negligible covariation with bromine concentrations, whereas nitrate species covaried strongly with bromine (Fig. 19). Other potential bromine sources, such as coal and 1,2-dibromoethane (DBE, used as a scavenging agent to remove lead from engine combustion chambers), were found to be of minor importance. The increased concentrations of bromine in recent Greenland snow strata were thereby attributed to increasing acidity at the sea-ice surface and in Greenland snowpack, enhancing bromine mobility and promoting transport of bromine toward central Greenland. While these results call into question the reliability of using bromine to reconstruct sea-ice since the 1950's, they also confirm the good agreement between bromine and MSA in the two centuries preceding the wide-scale acidification of the Arctic. The reported Summit/TUNU bromine pattern (low values in the 1950's, leading to a 1970's peak and subsequent decline) was similar to that observed in Severnaya Zemlya, even though bromine concentrations in Severnaya Zemlya were ten times greater than those reported for Greenland. The application of this data to sea-ice reconstructions in the North Atlantic Ocean and Nordic Seas is discussed further in section 5.2.3.1.

4.4. Millennial timescales

4.4.1. Antarctica

Only one record of bromine and iodine, covering millennial timescales, has been reported from the TALDICE ice core recovered from Talos Dome in northern Victoria Land (Spolaor et al., 2013b) and is shown in Fig. 20. The TALDICE ice core was drilled between 2005 and 2007, covering the past 220 kyr of climate and covering the last two full glacial-interglacial cycles (Buiron et al., 2011). Concentrations of bromide (Br^-), iodide (I^-) and iodate (IO_3^-) were determined using a coupled HPLC-IC-ICPMS technique, which split the elements into their major species using HPLC-IC and then detected them using ICPMS. Similar to the concerns raised in section 3.6.4, the reported TALDICE Br concentrations were conspicuously low compared to total Br concentrations later reported by ICP-SFMS for comparable sites in Victoria Land (e.g., Maffezzoli et al., 2017). Although the reported concentration of bromine may be incorrect – and these samples should be remeasured as a matter of priority – it is likely that the qualitative pattern of $Br_{fi\%}$ (and Br_{enr}) over time is correct even though the quantitative values may be incorrect.

This study presented the first evidence of long-term (multi-millennial) stability of halogens species in polar ice. The highest bromide concentrations corresponded to interglacial periods 0–12 kyr, 120–130 kyr and 210–220 kyr ago. Bromine/sodium ratios were found to be enriched during interglacials and depleted during the glacials. A rather unwieldly bromine fractionation metric was used, bromine fractionation index ($Br_{fi\%}$), although this is shown in section 2.2.2 to be equivalent to the more commonly-used Br_{enr} metric. Both bromine metrics are shown in Fig. 20. Regarding the iodine species, iodide was found throughout the record with lower values during interglacials and higher values during the glacials – a pattern matching that of sodium – while IO_3^- was only present during the coldest climate periods with high dust fluxes (17–34 kyr and 134–143 kyr ago). The findings reported by Spolaor et al. (2013b) and their applicability to Antarctic sea-ice

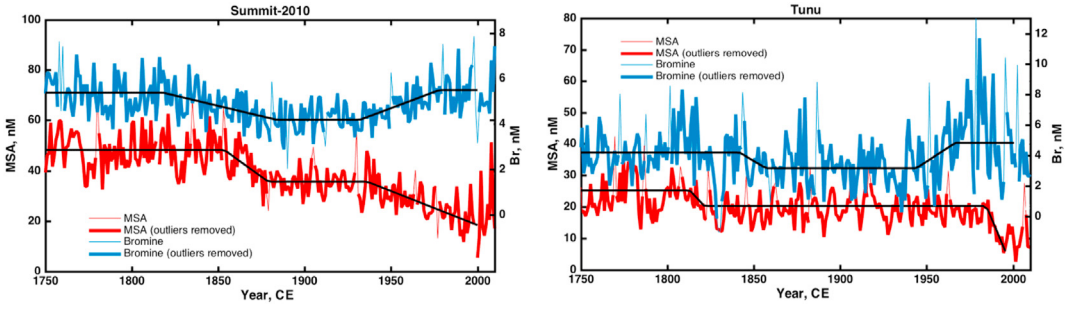

Fig. 18. Annual record of bromine (thin blue) and MSA (thin red). Annual record of bromine (thick blue) and MSA (thick red) with outlying spikes removed using a 25-year running average filter described by Sigl et al. (2013). All records were fit with a three-step linear regression (black) and the results of the fits which identify the timing of inflection points are summarized in Maselli et al. (2017, Table S1). The time series have been plotted to match the signal variability in the pre-industrial era (1750–1850 CE). Reprinted from (Maselli et al., 2017). (For interpretation of the references to colour in this figure legend, the reader is referred to the Web version of this article.)

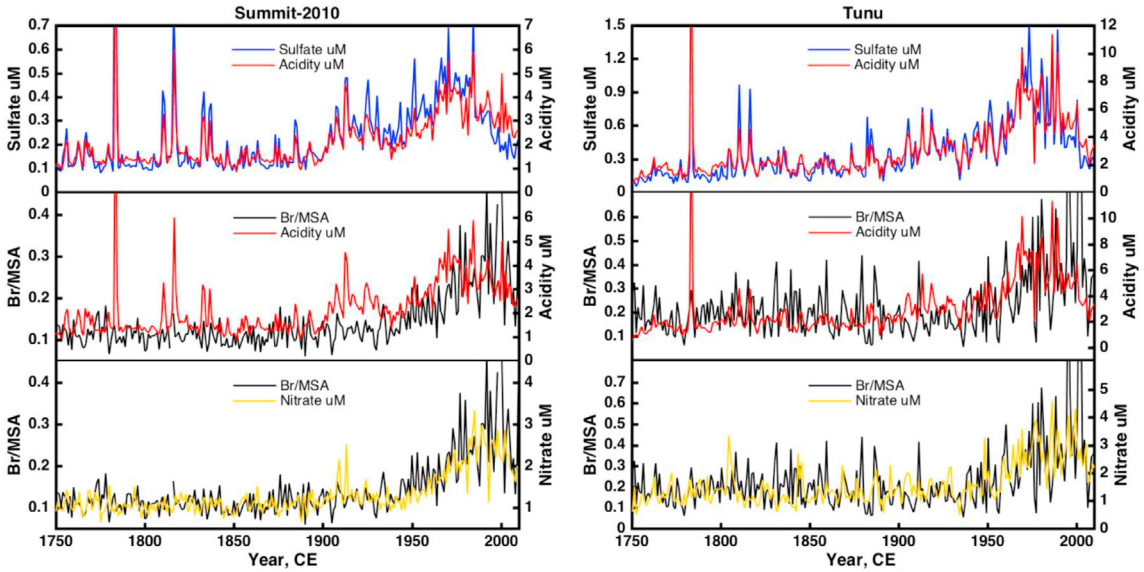

Fig. 19. Comparison between the measured total sulfur (shown as sulphate) and acidity records from each ice core (top panels). The acidity record is dominated by the influence of the sulfur species until the early 21st century when the NOx pollution remains elevated whilst anthropogenic sulfur sources are depleted resulting in a slight relative elevation of the total acidity relative to total sulfur concentrations. The large spikes in the acidity and sulfur records are identified as volcanic events. The ice core records cover the period of the 1783 Laki eruption as well as the unknown 1909 eruption and Tambora eruption (Indonesia) in 1815 (Sigl et al., 2013). Comparison between Br/MSA and total acidity (centre panels) and nitrate (NO_3^-, bottom panels) measured in the ice cores. The Br/MSA ratio follows the total acidity record closely except where the record is dominated by the sulfur component (e.g. early 1900s). Of the two major acidic species the Br/MSA follows the nitrate most closely at both ice core sites. Reprinted from (Maselli et al., 2017).

reconstructions are discussed further in section 5.1.1.

4.4.2. Arctic

From the Arctic, two millennial-scale bromine records have been reported from ice cores: NEEM (Spolaor et al., 2016b) in northwest Greenland and RECAP (Maffezzoli et al., 2019) in central eastern Greenland.

The NEEM ice core (drilled within the Northwest Greenland Eemian Ice Coring project) covers the past 130 ky and contains the first complete Eemian interglacial climate record from a Greenland ice core (NEEM Community members, 2013). The location of NEEM is favourable to aerosol transport from the west and southwest, with atmospheric transport models indicating North America as a primary source of terrestrial aerosols (Schüpbach et al., 2018) and the Canadian Arctic, including the Baffin and Hudson Bays, as a primary source of marine aerosols (Barrie et al., 1992). Samples for halogen analysis were obtained discretely from the CFA system used to determine chemical impurities, with each sample integrating a 1.1 m length of ice (Schüpbach et al., 2018). The NEEM brittle zone was unsuitable for CFA analysis, thus approximately 400 m of ice was not measured, corresponding to the period 3–9 ky b2k. The bromine record from NEEM was measured at University Ca' Foscari of Venice by ICP-SFMS, with particularly dense sampling from the present back to 50 ky b2k (Spolaor et al., 2016b).

Bromine concentrations in the NEEM ice core generally varied in a similar manner to those of sodium, but with relatively more bromine during interglacials (Fig. 21). It should be noted that in this study the authors assumed that sodium was purely of marine origin without any crustal contribution: nssNa = 0. Bromine concentrations ranged from Holocene values of 0.45 ± 0.15 (1σ) ppb to glacial values of 1.45 ± 0.07 (1σ) ppb. The sampling density was sufficient to observe bromine variability through the deglaciation and glacial interstadials (GIs) including the Younger Dryas/Bølling-Allerød and GIs 3–13. Bromine enrichment values varied from approximately 16 during the early Holocene to approximately 2.5 during the glacial stadials. A strong positive correlation was observed between oxygen isotope temperature proxy ($\delta^{18}O$) and Br_{enr} ($r^2 = 0.68$), providing a basis for linking sea-ice extent to Br_{enr} and Greenland temperature (Section 5.2.2).

The bromine record from RECAP (Maffezzoli et al., 2019) is shown in Fig. 22. RECAP bromine concentrations are low in the Holocene 0.3 ± 0.1 (1σ) ppb, higher in the glacial 0.7 ± 0.3 (1σ) ppb and slightly higher than Holocene during the late Eemian 0.4 ± 0.2 (1σ) ppb. The RECAP record sodium crustal contribution was deeply investigated and was found to be negligible during the Holocene and up to 20–30 % the glacial period. Such sodium crustal contribution was subtracted to the total sodium concentrations to calculate the bromine enrichment values. Br_{enr} values are highly variable, with Holocene values ranging from 2 to 6. Glacial values of Br_{enr} vary from 2 to 10, with values weakly correlating with broad variations in Greenland temperature, and late-Eemian average 5. The sampling resolution of the bromine record (integrating 55 cm depth in the Holocene and 18 cm in the glacial) provided annual to centennial resolution during the Holocene, but centennial-millennial resolution in the glacial. This was a result of the extreme glaciological thinning of the Renland glacial section – 100 thousand years of climate was archived in less than 50 m of ice. The interpretation of RECAP Br_{enr} as a sea-ice proxy is discussed in section 5.2.3.2.

5. Sea-ice reconstructions

5.1. Antarctica

Only two halogen-based sea-ice reconstructions (SIRs) have been reported from Antarctica, both from East Antarctica. The first, from Talos Dome in Northern Victoria Land, covers the last two glacial cycles (Spolaor et al., 2013b). The second, from Law Dome, covers the past century (Vallelonga et al., 2017). One other SIR is available for comparison, that being an MSA record reported for Law Dome (Curran et al., 2003) covering the period 1841–1995 CE. For the 220 ky Talos Dome reconstruction, the EPILOG compilation

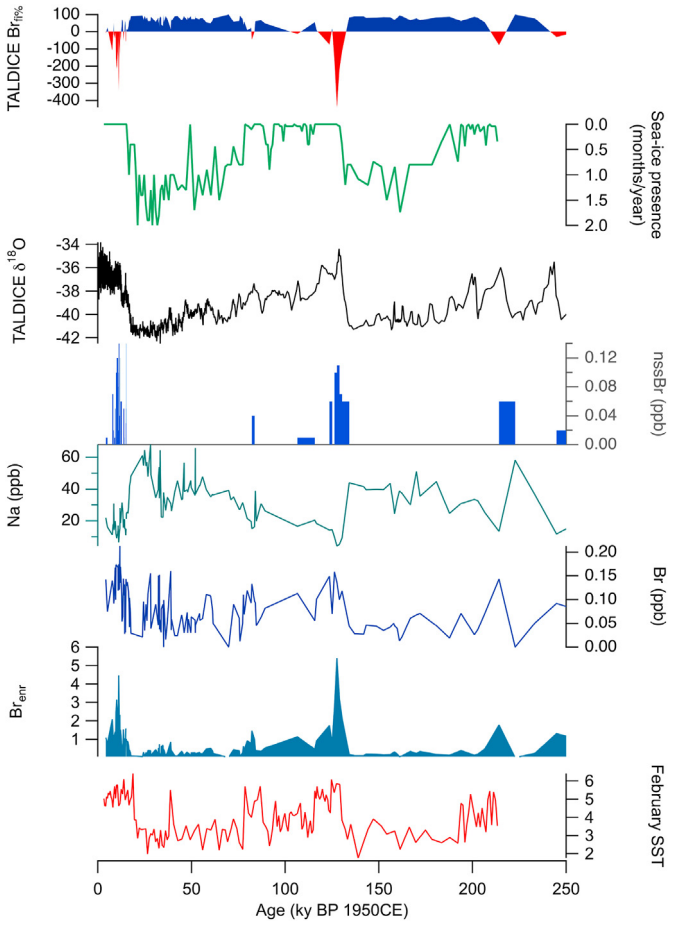

Fig. 20. Bromine and sodium in the TALDICE ice core from Talos Dome, Antarctica. Bromine fractionation index ($Br_{fi\%}$) is plotted with sea ice presence and February sea-surface temperature (SST) (Crosta et al., 2004). Talos Dome $\delta^{18}O$ is also shown. The red areas indicate Br^- enrichment (i.e. negative $Br_{fi\%}$) while blue areas indicate bromide depletion. The figure has been modified from the original (Spolaor et al., 2013b). (For interpretation of the references to colour in this figure legend, the reader is referred to the Web version of this article.)

of marine-sediment-based SIRs provides an essential data set for comparison (Gersonde et al., 2005).

5.1.1. Victoria Land

The Talos Dome SIR (Spolaor et al., 2013b) was based on bromine fractionation relative to sodium ($Br_{fi\%}$, see sections 2.2.2 and 4.4.1 and Fig. 20) and employed a novel but poorly constrained transport model to evaluate glacial/interglacial movement of the marginal sea-ice zone (see section 3.6). The synthesis of bromine and sodium transport mechanisms presented in section 3.7 will be applied here to critically re-evaluate the findings of the Talos Dome SIR.

In summary, Spolaor et al. (2013b) reported low Br_{enr} values (or positive $Br_{fi\%}$) during the glacial periods from 16 to 80 ky BP and 134–205 ky BP and interpreted this as indicative of increased MYSI. The few data points corresponding to the last interglacial featured higher Br_{enr} values (or negative $Br_{fi\%}$) compared to the Holocene, interpreted as a sign of reduced FYSI extent during the last interglacial. The findings were comparable in timing and variability to an SIR based on fossil diatom assemblages in marine sediments (Crosta et al., 2004). In particular, the sea ice record indicated relatively little sea-ice expansion during the period 80–125 ky BP, but a rapid increase in sea-ice through the later part of the glacial, 16–80 ky BP. Perhaps the most salient point regarding the interpretation applied by Spolaor and coworkers, in contrast to later studies, was that there was no attempt to characterise the area of sea-ice expansion, only the radial distance of the extension. Such an approach is apposite for East Antarctica, where there are no barriers to sea-ice expansion. This approach is not possible in the Arctic, where sea-ice expansion in the numerous ocean basins is substantially constrained by continental barriers.

Following critical reappraisal of the analysis technique (section 4.4.1) and interpretive model (section 3.6) reported in the original work, it is not possible to draw any definite conclusions from the dataset in its current form. Primarily, the samples will need to be remeasured with a more sensitive and reliable analytical method, such as ICP-SFMS. Once a quantitatively reliable dataset is available, it will be possible to determine the extent to which variations in Br_{enr} reported at the site are linked to variability in sea ice extent, as opposed to other factors such as transport distance/efficiency or surface remobilisation/re-emisson effects.

5.1.2. Wilkes land

Law Dome is a coastal ice rise approximately 1200 m in thickness which features regular annual snow accumulation of 0.7 m/yr ice equivalent at the summit (Roberts et al., 2015), making it an ideal location for investigation of the past marine environment with sub-annual resolution. With respect to SIRs, the Wilkes coast is also favourable because there is almost no MYSI, ensuring that any detected sea-ice signal may be attributed to FYSI only. Curran et al. (2003) reported the first SIR for the region, covering the period 1841–1995 CE, based on the then-novel sea-ice proxy MSA. MSA results from the oxidation of DMS, which is produced by phytoplankton and in the sub-Antarctic Ocean algal communities hosted by sea-ice dominated the production of DMS. Hence, a link may be established between FYSI, which hosts DMS-producing algae, and the MSA deposited at Law Dome when the sea-ice melts and DMS is released to the local marine atmosphere. Several MSA records have subsequently been reported from Antarctica, with each site requiring a critical evaluation of the link between MSA and local/regional sea-ice conditions (Abram et al., 2013). Curran et al. (2003) employed the available satellite observation record (1974–1995 CE) as a calibration dataset, finding a correlation of $r = 0.6$ ($p < 0.002$) between Law Dome MSA concentrations (annual mean) and the northernmost latitude of FYSI extent in the 80°E-140°E sector during the preceding winter (August–October). Applying this calibration to the full MSA record, a 20 % decline in sea-ice extent since 1950 CE was predicted, with no discernible trend for the preceding period of 1841–1950 CE. High decadal variability was observed, with an 11-year cycle discernible from 1950 to 1995 CE. The source of such variability was not established, although cyclicity of similar duration was also proposed following sea-ice observations by satellite (10 years, Zwally et al., 2002) and recordings of fast-ice extent (9 years, Murphy et al., 1995).

The availability of an existing multi-centennial SIR at Law Dome makes it an ideal location for evaluating new proxies for sea-ice extent, even though some level of discrepancy is to be expected when comparing proxies. Extending a preliminary dataset covering the period 1910–1914 CE (Spolaor et al., 2014), Vallelonga et al. (2017) reported a SIR from Law Dome covering the period 1927–2012 CE (Fig. 23). The SIR was a composite from two firn/ice cores analyzed using different methods in two laboratories (see section 4.2.1), with bromine reported for the period 1927–2012 CE and iodine for 1927–1989 CE. Hence, the satellite-calibration periods were different for bromine (35 years) and iodine (12 years). A significant correlation was found between annually-averaged (January–December) $\ln(Br_{enr})$ and FYSI area in the 90°E-110°E

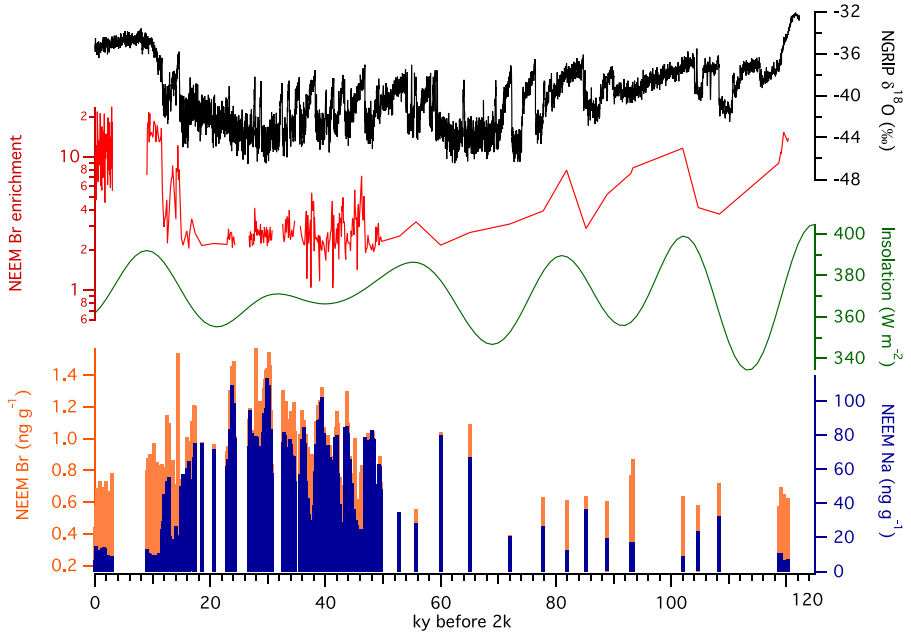

Fig. 21. Bromine and sodium in the NEEM ice core over the past glacial cycle. Bromine and sodium concentrations are decoupled from interglacial to glacial climates. The enrichment of bromine relative to sodium (Br enrichment) more closely follows the NGRIP $\delta^{18}O$ temperature proxy rather than 65°N summer solstice insolation. Minimum Br_{enr} values are observed during the coldest phases of the glacial, while the maximum is observed during the Holocene climatic optimum. Reprinted from Spolaor et al. (2016b).

sector, with $r^2 = 0.357$ and $p < 0.001$. Such a correlation is surprisingly similar to that found for MSA (the r = 0.6 coefficient of correlation quoted above equates a coefficient of determination $r^2 = 0.36$), albeit with a slightly smaller dataset for MSA (22 years), which may suggest a common level of noise due to meteorological effects, transport variability and uncertainties associated with the satellite data. Similar to MSA, high decadal variability was observed in the I_{enr} and Br_{enr} records, with higher values observed in the 1940s and 1970s. Br_{enr} shows a decreasing trend over the period 1927–2012 CE, consistent with that reported for MSA, but there are differences in the decadal patterns of the two proxies. Both records suggest a maximum of sea-ice extent over the periods 1940–1950 CE and 1975–1985 CE, although there is apparent disagreement over the relative extent during these two maxima: MSA suggests 12 % lower sea-ice extent in the latter period, whereas Br_{enr} suggests similar sea-ice extent for both periods. It is worthy of note that Maselli et al. (2017) also observe a discrepancy between MSA and Br_{enr} in the period 1950–2000 CE, which they attribute to the increasing influence of anthropogenic NO_x, leading to enhanced emissions of bromine from the FYSI. This process is not apparent at Law Dome, where no increases in NO_x or $nssSO_4$ have been observed in recent decades (pers. comm., Mark Curran) with sources of anthropogenic emissions in the southern hemisphere being fewer, less active and more distant. The dataset reported by Vallelonga et al. (2017) provides a preliminary comparison of SIRs based on MSA and halogens, but for a more thorough evaluation the halogen record should be extended back to at least 1841 CE (the start of the MSA record) and ideally to the onset of the Holocene, to allow comparisons with available SIRs from high-resolution marine sediment records (Denis et al., 2010; Hodell et al., 2001; Nielsen et al., 2004)

5.2. Arctic

5.2.1. Laptev Sea

Although they did not quantitatively reconstruct SIE, Spolaor et al. (2016a) did link Br_{exc} values and iodine concentrations in the Akademii Nauk (Severnaya Zemlya) ice core to Laptev Sea sea-ice variability and report a dataset covering the period 1950–1999 CE. The authors reported iodine, bromine and sodium concentrations, determining both Br_{exc} and Br_{enr} (described in section 4.3.2) which showed similar trends - but different patterns of decadal variability - over the 50-year record. This preliminary study, in which only the upper 29 m of the 724 m core was presented, employed the HYSPLIT model to calculate seasonal airmass back trajectories for the period 1976–2000 CE and therefore identify FYSI areas over which sea-salt aerosols were arriving. The model identified the Laptev sea as the dominant and most consistent airmass source in springtime, although for some periods the Kara sea was an important summertime airmass source. Therefore Spolaor et al. (2016a) investigated correlations between Br and I in the ice core to satellite observations of FYSI extent in both the Kara and Laptev seas. They found Laptev sea FYSI area was significantly correlated with both Br_{exc} ($r = 0.44$, $p < 0.02$) and iodine concentrations ($r = 0.50$, $p < 0.009$); and Laptev sea summer FYSI area also correlated with iodine concentrations ($r = 0.49$, $p < 0.011$). Such correlations were consistent with the current understanding of reactive halogen chemistry as well as satellite observations of halogens in the Arctic: spring is the peak season for bromine explosions – heterogeneous recycling of bromine above FYSI – while summer coincides with the peak extent of iodine-emitting algal blooms. As the algal community is hosted below FYSI, the extent of springtime FYSI may be related to the size of the summertime algal population.

The halogen record was also compared to an Arctic SIR by Polyakov et al. (2003), for which SIE in both the Kara and Laptev seas was resolved. Significant correlations are found between Laptev sea summer sea-ice anomalies and Br_{exc} ($r = 0.31$, $p < 0.009$) as well as I ($r = 0.32$, $p < 0.002$). Although inconsistent with airmass back trajectory reconstructions, significant correlation was also determined between Br_{exc} and reconstructed summer SIE anomalies for the Kara sea ($r = 0.34$, $p < 0.015$). The relatively brief

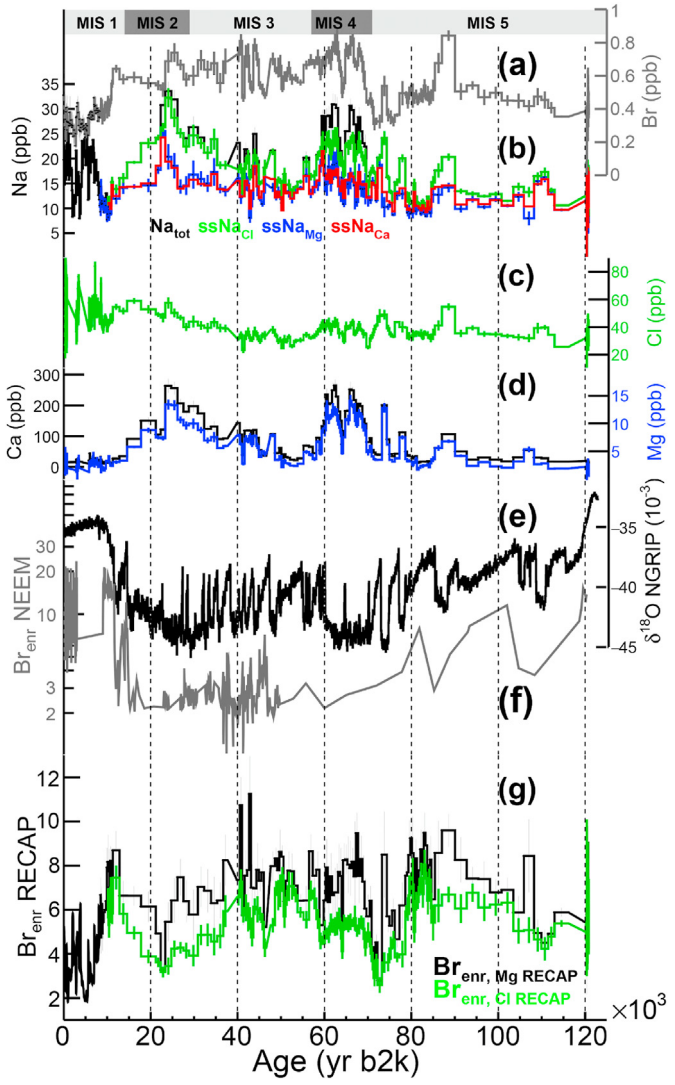

Fig. 22. The 120 kyr time series of analyte concentrations in the RECAP ice core. The last 8 kyr are 100-year averages. (a) bromine; (b) total sodium and sea-salt sodium (ssNa) series calculated using chlorine (green), magnesium (blue) and calcium (red); (c) chlorine; (d) calcium (black) and magnesium (blue); (e) NEEM δ^{18}O from (North Greenland Ice Core Project members, 2004) (f) NEEM Br$_{enr}$from (Spolaor et al., 2016b)); (g) RECAP Br$_{enr}$ series (Br$_{enr,Cl}$, green and Br$_{enr,Mg}$, black) calculated using chlorine and magnesium respectively. Reprinted from Maffezzoli et al. (2019). (For interpretation of the references to colour in this figure legend, the reader is referred to the Web version of this article.)

timeseries presented by Spolaor et al. (2016a) is insufficient to critically evaluate the suitability of either bromine or iodine for quantitative SIR for Laptev Sea but offers a basis for further study. An important test case would be during the Medieval warm period, approximately 800–1000 CE, when warm climate conditions occurred through much of the northern hemisphere. During this period, it would be expected that a quantitative sea-ice proxy would show a noticeable reduction in SIE.

5.3. Canadian Arctic

From measurements of the northwest Greenland NEEM ice core, Spolaor et al. (2016b) reported the first multi-millennial halogen-based SIR for the Arctic (Fig. 24). The halogen record covered the past 120 ky but with low sampling resolution for the period prior to 50 ky ago. The sampling was sufficient to establish estimates of sea-ice extent at important climate extrema: the late Holocene (last 3 ky), the Holocene Climatic Optimum (HCO, 6–9 ky ago), and the Last Glacial Maximum (LGM, 20–30 ky ago). Note that with respect to the HCO, samples from the period 9–11.5 ky ago were used for comparison, as poor ice quality prohibited sampling of ice corresponding to the period 3–9 ky ago. Based on aerosol source evaluations, the reconstruction was applied to the marine sector to the west and northwest of NEEM: the Canadian Arctic, Baffin Bay and Hudson Bay. The source of aerosols to NEEM was evaluated from both atmospheric modeling work and satellite observations of bromine explosion events. Based on the results of a 1-D chemical transport model run, greater values of Br$_{enr}$ at NEEM were interpreted as a greater extent of FYSI. In contrast, the model indicated that both MYSI and Greenland surface snow were zones of deposition of Br. FYSI is considered the predominantly gas phase bromine source (Bougoudis et al., 2020; Saiz-Lopez et al., 2012; Simpson et al., 2007a) mainly because the recycling over MYSI occurs on salts deposited becoming halide depleted in much shorter time periods compared FYSI. In FYSI the halide content is in excess with respect to the gaseous halogen recycling, able to sustain the bromine recycling process longer. Bromine recycling over MYSI could occur but is limited compared to the recycling occurring over FYSI. Ice core observations suggest significant correlation only with FYSI and not when considering MYSI extension supporting the hypothesis that FYSI extension is the main driver for gas phase bromine in the polar spring. Satellite measurements also support that bromine explosions are less frequent over the central Arctic where the multiyear sea-ice is mainly present.

The hypothesis proposed by Spolaor et al. (2016b) to reconstruct sea-ice extent from the NEEM Br$_{enr}$ record was based on the model results showing FYSI being a source of bromine species, as also supported by several experimental campaigns and satellite sensing over the Arctic. In contrast, the same model suggests that both MYSI and Greenland surface snow are zones of deposition of bromine. We point out, however, that the FYSI-Br$_{enr}$ apportionment made by Spolaor et al. (2013b) in the Antarctic TALDICE record was originally based on different fractionations of bromine and sodium, hence on a transport mechanism, leading to increased bromine enrichment further inland (Fig. 20), rather than on a source effect. The differences in the interpretation of sea-ice extent in the two studies are based on the differing geographical settings between the Canadian Arctic and East Antarctica: Arctic sea-ice is strongly constrained by continents (even more so considering the lowered sea level during the glacial) and therefore the transport effect was assumed of secondary importance, Antarctic sea-ice grows radially with no continental constraints. Although the overall glacial/interglacial variability is comparable between TALDICE and NEEM Br$_{enr}$ records, the absolute values likely reflect the different geographical settings of the two sites and their respective bromine source regions. Well-constrained chemical transport models are required to disentangle the influences of sea-ice source area changes and transport fractionation effects, if accurate interpretations are to be applied to ice core records of Bromine enrichment.

Following the assumptions made in Spolaor et al. (2016b) of higher Br$_{enr}$ indicating greater FYSI surfaces, the NEEM Br$_{enr}$ SIR indicates extensive FYSI in the Canadian Arctic during the Holocene and glacial interstadials, interspersed with periods of extensive MYSI cover during the LGM and glacial stadials. The data suggested reduced FYSI during the HCO, with respect to the last 3 ky, and also that MYSI during the Younger Dryas was less extensive than the preceding LGM period. For the first time, an ice core-based SIR indicated repeated and extensive sea-ice changes over stadial/interstadial cycles. Although the NEEM results relate to the Canadian Arctic, not the Nordic Seas, the finding of repeated and rapid

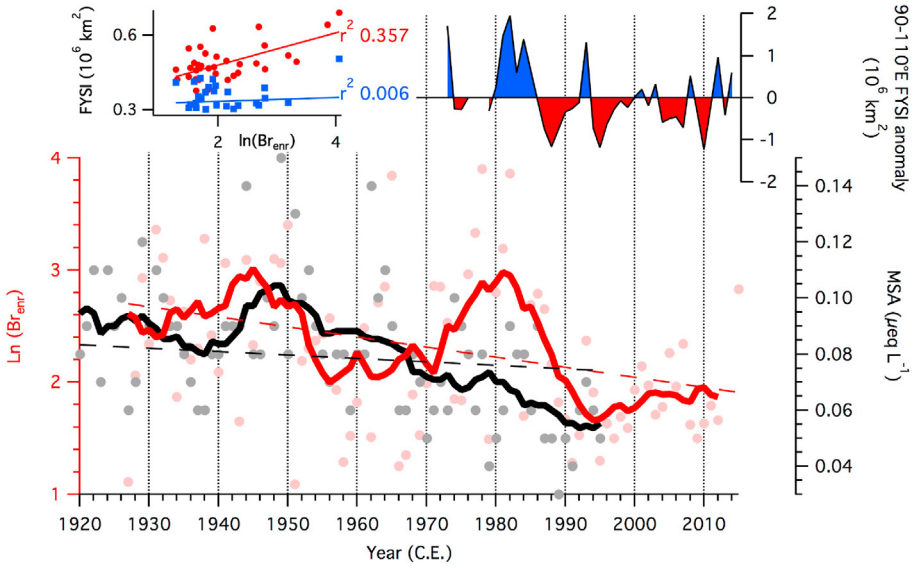

Fig. 23. Bromine enrichment (Br_{enr}, red), MSA (black) and first-year sea ice (FYSI) at Law Dome. Bromine enrichment and MSA data are shown as annual averages (circles) as well as 11-year (thick lines) running means. Linear regression trends are shown as dotted lines. FYSI areas in the 90–110° E sector (top right) are shown as annual anomalies from the 1973–2014 average. Shown in the top left panel are correlations between Br_{enr} and FYSI areas in the 90–110° E (red) and 110–130° E (blue) sector. Reprinted from Vallelonga et al. (2017). (For interpretation of the references to colour in this figure legend, the reader is referred to the Web version of this article.)

stadial/interstadial sea-ice change supports studies arguing that sea-ice is a key component to understanding the mechanisms of rapid climate change in the Arctic (Dokken et al., 2013). Despite the relatively low sampling resolution, there was also some indication that FYSI extent was less during the "cooler, shorter" glacial interstadials (GI-3, -4 and -6) in comparison to the "warmer, longer" interstadials (GI-8 and -12).

Spolaor et al. (2016b) also provided a quantitative estimate of past sea-ice extent by combining satellite observations of sea-ice variability and physical constraints on glacial sea-ice extent imposed by lowered sea levels and the Laurentide ice sheet. The reconstruction was based on some key assumptions:

1. That the linear relationship observed between temperature proxy $\delta^{18}O$ and $\ln(Br_{enr})$ may be similarly applied to FYSI extent and $\ln(Br_{enr})$.
2. That the range of variability in FYSI area observed by satellites over the period 1979–2013 CE may be taken as representative of the range of FYSI area incorporated in the early Holocene (0–3 ky b2k) Br_{enr} data.
3. That there was complete MYSI coverage (that is, no FYSI) in the Canadian Arctic during the LGM.

Considering these assumptions, perhaps the most critical is the second one – that the 30-year satellite data set may be used to represent 3000 years of climate variability – including such events as the little ice age and medieval climatic optimum. Considering the extreme reduction of Arctic MYSI (and corresponding increase in FYSI) in recent decades, the satellite data set may be biased toward greater values of FYSI. Kinnard et al. (2011) evaluated the Arctic MYSI reduction of the past decades as being anomalous with respect to the last 2000 years, which suggests that in the context of assumption 2 the high end of satellite FYSI observations should be treated with caution. In comparison, assumption 1 is reasonably tentative – a linear model is the simplest possible and the logarithmic scaling of Br_{enr} reduces the relative effect of extremely high Br_{enr} values. Of the three assumptions, the third is the most reliable: the exposure of continental shelves due to lowered sea levels at the LGM, and the presence of the Laurentide ice sheet, would have massively reduced the presence of FYSI in the Canadian Arctic during the late glacial, even before considering the influence of ice shelves on MYSI extent.

Even though the NEEM halogen SIR was the longest and most detailed available at the time, many questions remain unanswered. The NEEM halogen SIR implies that Arctic summer sea-ice extent was approximately 30 % lower in the Canadian sector of the Arctic Ocean during the HCO, relative to present values. But the last interglacial, the Eemian, was not sampled even though this period corresponds to approximately 6–10 m higher sea level and 5 °C warmer global temperatures (NEEM Community members, 2013). Br_{enr} values corresponding to the Eemian would have provided an extremely valuable context for evaluating the two Holocene time slices presented. In the context of a growing anticipation that Arctic summer sea-ice will disappear within the next decades, it would be extremely valuable to determine the upper limit of corresponding Br_{enr} values for the NEEM site.

5.3.1. North Atlantic Ocean/Nordic Seas

5.3.1.1. Decadal-centennial time scales. Only in a few cases have multiple sea-ice proxies been directly compared within the same sample set or location. We discussed in section 5.1.2 the Antarctic Law Dome halogen record (Vallelonga et al., 2017) and here we discuss the bromine and MSA records reported from Greenland Summit and TUNU ice cores (Maselli et al., 2017). The two Greenland ice cores were measured on the same analytical system, with both bromine and MSA determined continuously. Bromine was determined by ICP-SFMS using the same system as for the Severnaya Zemlya halogens record (Spolaor et al., 2016a). MSA was determined using a novel electrospray triple-quadrupole mass spectrometer (ESI-MS-MS) technique, with discrete samples collected for verification of the accuracy of the continuous method. The two ice cores covered the period 1750–2010 CE, with the Summit 2010 core analyzed with seasonal resolution. The low snow accumulation rate at TUNU prohibited sub-annual data resolution. The Hysplit4 atmospheric circulation model was used to determine airmass back trajectories for the two ice core sites. On this basis, the

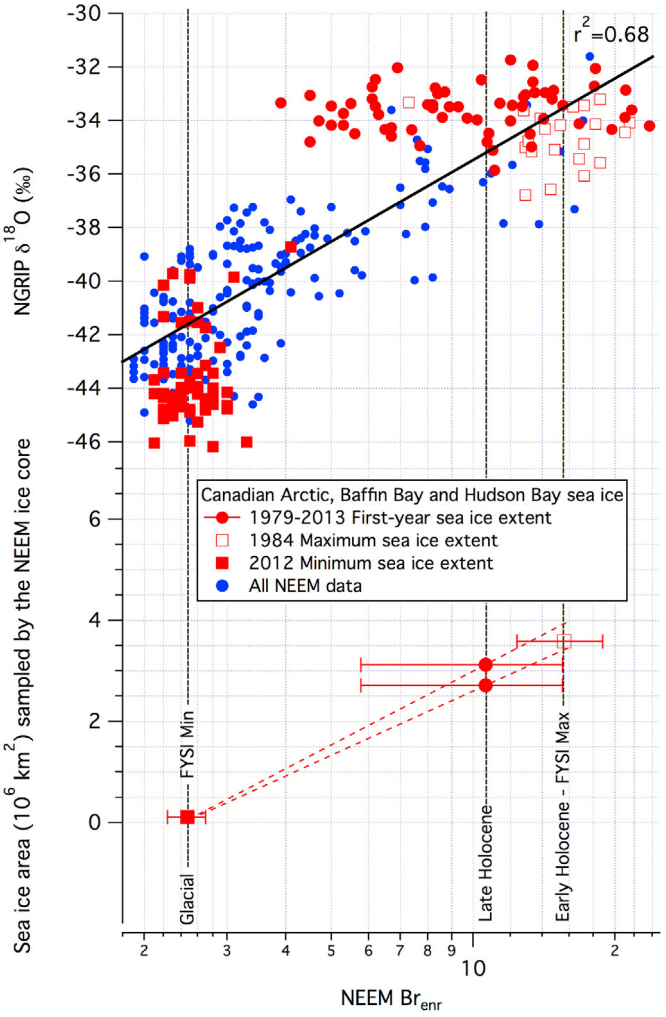

Fig. 24. Calibration of the NEEM Br enrichment (Br_{enr}) signal to current and past sea ice extent in the NEEM aerosol entrainment area (Canadian Archipelago, Hudson Bay, Baffin Bay). Three climate scenarios are evaluated, full glacial (Br_{enr} = 2.5, 20.6–30.7 ky b2k, solid red squares), late Holocene (Br_{enr} = 10.6, 0.03–3.03 ky b2k, solid red circles) and early Holocene (Br_{enr} = 15.6, 9.0–11.5 ky b2k, hollow red squares). The remainder of the NEEM Br_{enr} dataset consists of glacial samples with intermediate $\delta^{18}O$ values (11.5–20.6 ky b2k and 30.7–120.3 ky b2k) represented by solid blue circles. The average Br_{enr} value corresponding to each climate scenario is then applied (vertical dotted lines) to the calibration scheme in the lower panel. For the calibration scheme, we employ the maxima and minima of sea ice extent observed between 1979 and 2013, and range of first-year sea ice variability, for calibration. Bromine enrichment is plotted on a logarithmic scale to provide the best linear fit of Arctic temperature variability represented by the NGRIP $\delta^{18}O$ profile. 1σ error bars represent the variability observed for the three climate intervals evaluated. (For interpretation of the references to colour in this figure legend, the reader is referred to the Web version of this article.)

representative origin of marine aerosols arriving to Summit core site was determined to be southeast Greenland, comprising Denmark Strait and the southern Nordic seas. The origin of marine aerosol to TUNU site was similarly evaluated as west Greenland, essentially Baffin Bay. In this manner, two complementary sea-ice records were produced, covering different ocean sectors. Correlations were also determined: MSA and Br_{enr} were compared to the HadSST1 ICE dataset (1900–2012 CE) which incorporates satellite observations for the period 1979–2012 CE and uses this information to correct for potential bias in the pre-satellite data, primarily composed of ship-based observations. Both sea-ice concentration (SIC) and Open Water in Ice Pack (OWIP) were considered, where OWIP is the difference between sea-ice area and sea-ice extent. Both of these metrics indicate the absence of sea-ice within the zone of study, but they do not distinguish between MYSI and FYSI.

The sea-ice reconstruction by Maselli et al. (2017) proposes gradually declining sea-ice over the period 1750–1900 CE, followed by a more pronounced decline in the late 20th century (Fig. 18). The reconstruction is also shown in Fig. 25, with other relevant metrics for Arctic sea-ice. The step-change model identified an initial "high" state for Br and MSA at Summit, from approximately 1750 to 1830 CE, after which a second, lower state occurred from 1879 to 1931 CE. From 1931 CE, the two Summit datasets diverge, with Br increasing and MSA decreasing. For TUNU, the initial state is from 1750 to 1830 CE, the second state from 1840 to 1960 CE, and the divergence in Br and MSA is not synchronous (Br rises from 1944 CE, MSA decreases from 1984 CE). Overall, the 1854–1878 CE step change in Summit Br is the most clearly identified by the statistical model, as is the increase of Br after 1932 CE. In TUNU, the clearest step change is the decrease in MSA after 1984 CE. These changes are interpreted as indicative of a gradual decrease in sea-ice extent in the Nordic seas commensurate with the end of the little ice age, followed by a more rapid decrease in the late 20th century: earlier in southern Greenland, later in northern Greenland.

As described in section 4.3.2, different trends are reported for MSA and Br variability in the Summit2010 and TUNU cores (Maselli et al., 2017). Potential explanations are presented for these divergent behaviours, although a detailed modelling study is likely required to distinguish between the various possible sources of influence. Increased bromine concentrations observed in the cores after 1950 were attributed to the influence of anthropogenic emissions of acids, particularly nitric and sulfuric acid, causing sea-ice acidity to increase (see section 5.2.3.1). In contrast, the increasing emission of bromine may also be due to the steady decline in Arctic MYSI and its replacement by FYSI (Fig. 24). A recent study also calls into question the reliability of the Greenland MSA record as a proxy for sea-ice extent: Osman et al. (2019) extract a common trend from MSA records in 12 Greenland ice cores - including those reported by Maselli et al. (2017) – and attribute this trend to changes in North Atlantic Ocean primary productivity over the recent centuries. The Greenland composite MSA record is correlated with North Atlantic Ocean sea surface temperature and Atlantic meridional overturning circulation, which play a strong influence on the sustenance of primary producers in the North Atlantic Ocean.

Ultimately, to better understand the behaviour of sodium, MSA and bromine – the leading proxies for sea-ice extent – a combination of ice core records and chemical transport models will be required. The availability of a more extensive array of ice cores, from locations other than central Greenland, will provide a richer dataset for validating the behaviour of sodium, MSA and bromine over recent centuries. Comprehensive chemical transport modelling should then be applied to such a dataset to accurately apportion the relative influences of sea-ice and oceanic circulation on the ice core MSA record, as well as the relative influences of sea-ice extent and anthropogenic acid emissions, on the ice core Br record.

5.3.1.2. Millennial time scales. For the North Atlantic Ocean, the only halogen-based sea-ice reconstruction available is from Maffezzoli et al. (2019), reporting a 120 ky record of Br_{enr} from the RECAP ice core recovered from the Renland ice cap located in coastal East Greenland. The RECAP ice core was drilled in 2015, updating and improving the climate record produced from an earlier Renland ice core drilled in 1989 (Hansson, 1994). The RECAP ice core is 584 m long, with a complete Holocene profile within the upper 530 m and a complete glacial profile within 30 m of ice. The extreme thinning of the glacial section limits the resolution of Br_{enr} variability over stadial/interstadial timescales, although the

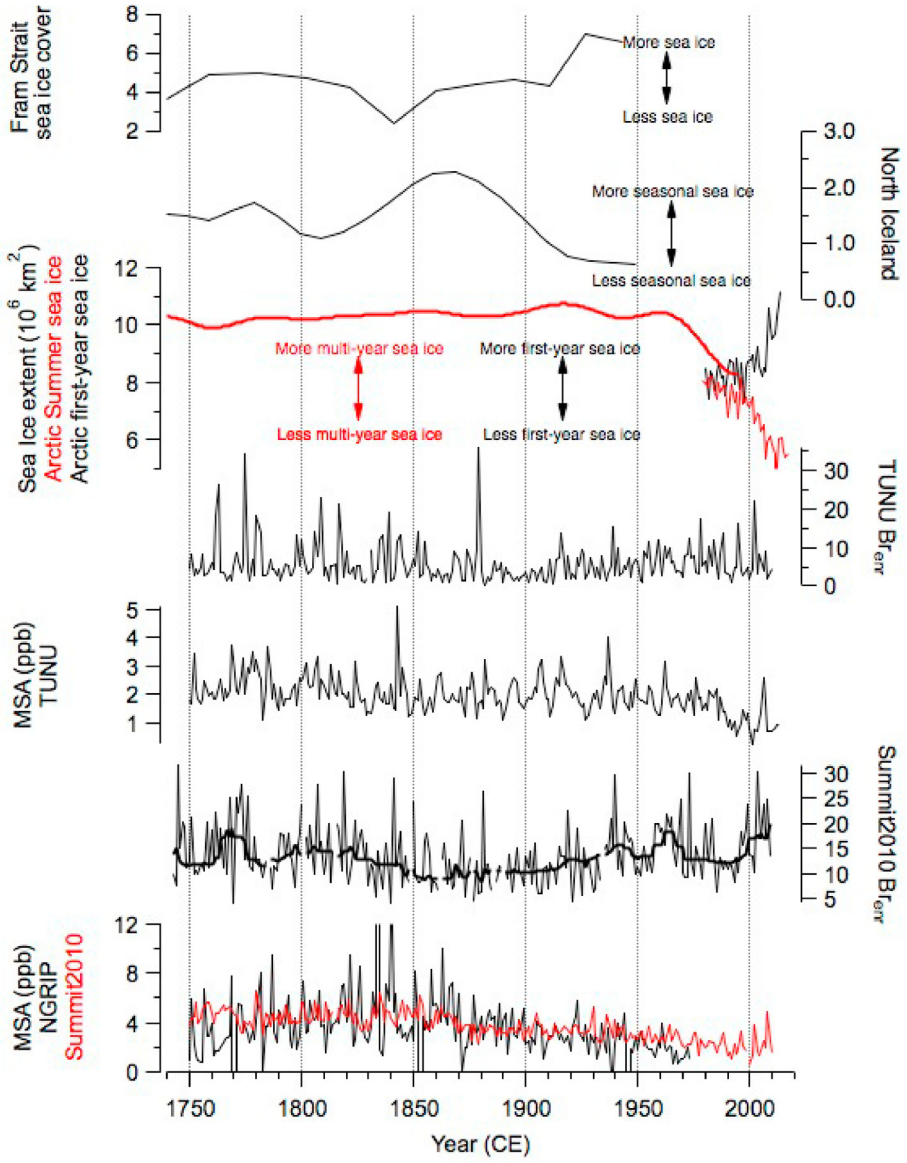

Fig. 25. Comparison of Arctic sea-ice reconstructions with MSA and Bromine enrichment (Br_{enr}) records from Greenland ice cores. Data are replotted from the following sources: Northern Iceland coast IP25 (Massé et al., 2008), Fram Strait sea-ice (Bonnet et al., 2010), Arctic summer (Kinnard et al., 2011) and first-year (Stroeve et al., 2012a) sea-ice extents, ice core data from TUNU and Summit2010 (Maselli et al., 2017) and NGRIP (Legrand et al., 1997b) Greenland ice cores.

Younger Dryas/Bølling-Allerød transition is clearly defined in the data (Fig. 22). Similar to the technique employed by (Maselli et al., 2017), the sources of marine airmasses arriving to the Renland ice cap were identified using the Hysplit4 model. In this case, the authors studied the origins of 72 h-long back trajectories arriving at Renland every hour for the period 2000–2016 CE. In order to isolate the airmasses likely transporting marine aerosols, only the airmasses that were located within the MBL (defined as the 900 hPa isosurface, approximately 1000 m asl) for longer than 10 h were considered. From this analysis, 75 % of the marine trajectory endpoint distribution contours a portion of the North Atlantic Ocean extending from ca. 50 °N to 85°N, thus including the Greenland Sea and the Denmark Strait region, the Icelandic Sea and the Norwegian Seas. Hence the RECAP Br_{enr} record was interpreted as primarily representing changing marine conditions within the Nordic seas as north as the Fram Strait, although the ocean regions closer to Renland are expected to carry a more significant marine contribution.

The RECAP Br_{enr} record shows low values during the Holocene and coldest periods of the glacial (MIS 2 and MIS 4), with intermediate/high values during the deglaciation and during the warmest periods of the last glacial period, MIS 3 and late MIS 5 (Fig. 22). Contrasting with the NEEM results, where the highest Br_{enr} values were found during the Holocene and the lowest Br_{enr} values during the cold glacial stadials, the RECAP Br_{enr} record features low values during both the Holocene and cold stadials. This asymmetry was interpreted as a dual behavior of the Br_{enr} indicator at Renland. Specifically, since reduced bromine explosions occur in the absence of seasonal sea-ice, a low Br_{enr} value can indicate either open water conditions or multi-year sea-ice. Therefore, the authors suggested that RECAP low Br_{enr} values during the Holocene indicated open water conditions, while the low values during cold glacial periods were indicative of extended multi-year sea-ice in the Nordic Seas. Their results are qualitatively consistent with the

only existing sea-ice record extracted from a sediment core in the Norwegian Sea and covering the last 90,000 years (Hoff et al., 2016).

6. Recommendations and conclusions

6.1. Conclusions

We have described the chemical and physical basis for the application of halogens, particularly bromine, in polar snow and ice as a proxy for sea-ice reconstruction. While the state of understanding of polar halogen chemistry has advanced to a sufficient stage that heterogeneous halogen recycling may be modeled effectively, there remain gaps in the understanding and accurate description of mixed-phase transport and deposition of bromine over the polar ice sheets. Retention of halogens in snowpack is an important consideration to the reliability of any proxy records: it has been consistently shown that iodine is poorly retained in the snowpack of high-accumulation sites, whereas bromine is retained reliably in sites with moderate levels of snow accumulation rates (greater than approximately 20 cm ice equivalent per year). For the purposes of reconstructing sea-ice extent over multiple glacial/interglacial cycles, the reliability of bromine records from central Antarctica is still to be established.

Regarding the application of halogen proxy records to sea-ice reconstructions, caution must be applied in the interpretation of bromine enrichment records. The different deposition velocities of sodium and bromine, and particularly the mixed-phase nature of bromine transport, require a careful effort to accurately translate ice core bromine records to variability in sea-ice parameters. We demonstrate a method of: 1) collecting available spatial distributions of bromine and sodium concentrations, 2) developing appropriate transport models for describing the disparate transport of halogens and sea-salts, and 3) applying these models to distinguish between the competing influences of transport distance, sea-ice source area, and MYSI/FYSI variability. Published halogen-based sea-ice reconstructions for the northern and southern polar regions have been presented and critically assessed. Where possible, halogen-based SIRs have been compared to other available sea-ice proxy records. The halogen elements, particularly bromine, offer great potential for unlocking a wealth of knowledge regarding sea-ice variability during the late Quaternary period. It is vital that the available ice core records are accurately measured and appropriate chemical transport modeling is applied to the resulting records, to unlock the full potential of these valuable and rapidly diminishing climate treasures.

6.2. Recommendations

With regard the future development of halogens in ice cores as a quantitative proxy for sea-ice extent, we submit the following recommendations for future work:

- Surface sampling of snow should be conducted during Arctic and Antarctic traverses, with the aim of increasing the spatial coverage of Na and Br data presented in Figs. 13 and 14. This data will improve and inform models of halogen transport and retention in polar snowpack. Where possible, the sampling should be conducted along traverse routes where inland ice core drilling sites are supplied from coastal stations.
- Bromine data should be consistently measured by ICP-SFMS techniques, with a NH_4OH washing step included between samples. Caution should be applied to Br records produced by a combination of Continuous Flow Analysis sampling and online ICPMS determination. Where possible, discrete samples should be collected and measured by ICP-SFMS. Where possible, previously reported studies employing Ion Chromatography should be repeated using ICP-SFMS. Interlaboratory comparisons will be of benefit in standardizing analytical setups and avoiding bias due to instrumentation or sampling techniques.
- A more complete understanding is required of halogen emission from FYSI and potentially MYSI. While it is known that MYSI is depleted in halides compared to FYSI, it is still necessary to characterise the extent to which MYSI may participate in heterogeneous recycling of bromine and otherwise augment or retard the enrichment of boundary-layer bromine with respect to sodium.
- An intercomparison project should be applied to the available chemical transport models incorporating halogen chemistry modules. There are currently a few halogen chemical transport models and these should be benchmarked for consistency. Particular attention should be placed on the deposition velocities used and the characterisation of mixed-phase transport over long distances. Ideally, the intercomparison project would include glacial and interglacial transport scenarios.
- Where possible, bromine, sodium and MSA should be consistently measured in ice core records, particularly those located 300–600 km from the present coastline. This is the zone offering elevated Br_{enr} as well as being relatively close to the coast, with moderate snow accumulation and potential for multi-centennial record duration.
- The record of multi-millennial Br records in Antarctica should be expanded from Talos Dome to other suitable ice core sites, such as WAIS Divide in West Antarctica, EDML in Dronning Maud Land, DSS/Law Dome in East Antarctica, and potentially the SPICE ice core from the South Pole. For ice cores located on the Antarctic plateau with very low snow accumulation, such as EPICA Dome C, Vostok, Dome Fuji and Dome A, preliminary sampling should be conducted on strata containing interglacial ice and glacial maxima ice, to determine representative glacial and interglacial values of bromine and iodine and investigate the potential for semi-quantitative evaluations of past sea-ice extent.
- More extensive ice core records of sodium and bromine are required across the Arctic. Two zones of immediate interest are 1) the available small ice caps circling the Arctic Sea, including northern Greenland, northeast Canada, Alaska, Siberia and Svalbard; and 2) Central and Southern Greenland. The circum-Arctic records should elucidate a record of Arctic sea-ice variability over the last millennia and possibly as far back as the Holocene Climatic Optimum approximately 8 ky ago. The

records from Central and Southern Greenland should extend well into the last glacial period, providing a detailed record of sea-ice variability and timing related to Atlantic Meridional Ocean Circulation and other important mid-latitudinal climate forcings.

- An indication of Arctic sea-ice extent during the Eemian, the last interglacial, may possibly be obtained by sampling the ice strata close to the base of Greenland deep ice drilling sites including DYE-3, GISP2, GRIP, NGRIP and NEEM. A compilation of Br_{enr} values from the Eemian sections of these ice cores would provide an important timeslice of Br_{enr} variability across Greenland, relevant to future warming Arctic climate scenarios.

The consistent application of these recommendations will contribute to a successful and thorough development of the full potential for halogen-based proxy reconstruction of past sea-ice changes. The foundation for this development is ongoing discussion, communication and collaboration within the ice core and associated paleoclimate research communities.

Author contributions

All authors contributed to writing and editing the paper.

All authors should have made substantial contributions to a submission. PV wrote the manuscript, with assistance from NM, ASL, FS, HAK and AS. All authors have approved the final version of the manuscript.

Declaration of competing interest

The authors declare that they have no known competing financial interests or personal relationships that could have appeared to influence the work reported in this paper

Acknowledgements

This research has received funding from the European Research Council under the European Community's Seventh Framework Programme (FP7/2007–2013)/ERC grant agreement 610055 as part of the ice2ice project. We thank the following for providing polar ice and snow data: Olivia Maselli (Summit), Joe McConnell (Antarctic array), Chuanjin Li and Shichang Kang (Dome A traverse), Mark Curran (Law Dome) and Mirko Severi (TALDICE). We thank Andreas Richter (IUP-Bremen) for providing BrO and IO satellite data product. We also thank colleagues Carlo Barbante, Sarah Berben, Pablo Corella, Giulio Cozzi, Carlos A. Cuevas, Tobias Erhardt, Peter Neff, Jason Roberts, Anders Svensson, Marius Simonsen and Clara Turetta. We would like to acknowledge the essential contribution of the Inuit Windsled Project, consisting of Ross Edwards, Hermenegildo Moreno, Jens Jacob Simonsen and Ramon Larramendi, in providing snow samples collecting during the 2017 Kangerlussuaq-EGRIP traverse.

The GV7 surface sampling was support by the MIUR (Italian Ministry of University and Research) - PNRA (Italian Antarctic Research Programme) program through the IPICS-2kyr-It project (International Partnership for Ice Core Science, reconstructing the climate variability for the last 2kyr, the Italian contribution). The IPICS-2kyr-It project is carried out in cooperation with KOPRI (Korea Polar Research Institute, grant No. PE15010). The Dome C surface snow sampling was supported by the Programma Nazionale per la Ricerca in Antartide (PNRA, project 650 number 2013/AC3.03 PEA 2013–2015, PI Warren Cairns). The Talos Dome-Dome C traverse and associated analyses was supported by the Programma Nazionale per la Ricerca in Antartide (PNRA), project A2 number PNRA0016_295 “Bromine and mercury, cycles and transport processes on the Antarctic plateau”. We thank the CNR Dirigibile Italia Arctic station and the Department of Earth systems science and environmental technologies for logistical support in Svalbard.

Abbreviations

asl	above sea level
b2k	before 2000 CE
BP	Before Present (1950 CE),
Br_{dep}	Bromine deposition
Br_{enr}	Bromine enrichment
Br_{exc}	Bromine excess
Br_{fi}	Bromine fractionation index
BrO	Bromine monoxide
CE	Common Era
CFA	Continuous Flow Analysis
DMS	Dimethylsulphide
DOAS	Differential optical absorption spectroscopy
FYSI	First-year Sea-ice
GCM	General Circulation Model
HCO	Holocene Climatic Optimum
Hysplit	Hybrid Single-Particle Lagrangian Integrated Trajectory
IC	Ion Chromatography
ICPMS	Inductively Coupled Plasma Mass Spectrometer
ICP-QMS	Inductively Coupled Plasma – Quadrupole Mass Spectrometer
ICP-SFMS	Inductively Coupled Plasma –Sector Field Mass Spectrometer
LGM	Last Glacial Maximum
MIS	Marine Isotope Stage
MSA	Methanesulphonic Acid
MYSI	Multi-year Sea-ice
NEEM	Northwest Greenland Eemian ice core
nss	non-sea-salt
OWIP	Open Water Ice Presence
ppb	part per billion (here used as equivalent to ppb)
ppt	part per trillion (here used as equivalent to ppt)
RECAP	Renland Ice Core Project
SIC	Sea-ice Concentration
SIE	Sea-ice Extent
SIR	Sea-ice Reconstruction
ss	sea-salt
SSA	sea-salt aerosol
SST	Sea Surface Temperature

Appendix A. Sample data for surface snow collected along scientific traverse from NEEM ice core drill site to EastGRIP ice core drill site

Sample designation	Latitude (degreesN)	Longitude (degreesE)	Na concentration (ppb)	Br concentration (ppb)	nssBr (ppb)	Brenr	Air temperature (degreesC)	Snow temperature (degrees C)
N2E_5	77.430	50.885	46.4	1.39	1.10	4.8		
N2E_22	77.414	50.695	55.7	0.79	0.45	2.3		
N2E_6	77.397	50.502	28.1	0.83	0.66	4.8		
N2E_21	77.382	50.306	30.1	1.17	0.99	6.3		
N2E_23	77.367	50.114	39.9	0.84	0.60	3.4		
N2E_16	77.345	49.937	20.4	1.13	1.00	8.9	−21.1	−22
N2E_17	77.323	49.763	29.4	1.25	1.07	6.9	−21.2	−22.6
N2E_12	77.300	49.583	25.0	0.72	0.56	4.6	−22	−21.4
N2E_10	77.277	49.405	13.1	0.73	0.65	9.0	−20.9	−21.3
N2E_20	77.254	49.230	15.8	0.94	0.84	9.6	−20.2	−22.4
N2E_13	77.232	49.048	19.9	1.20	1.08	9.7	−20	−21.4
N2E_1	77.210	48.876	49.6	0.86	0.56	2.8	−20.4	−21.3
N2E_19	77.187	48.700	35.4	1.27	1.05	5.8	−20.5	−20.9
N2E_8	77.164	48.523	19.6	1.39	1.26	11.4	−20.6	−21.4
N2E_2	77.142	48.348	22.5	1.65	1.51	11.9	−21.3	−21.3
N2E_25	77.119	48.174	14.8	0.88	0.79	9.6	−21.6	−21.4
N2E_4	77.098	47.998	20.2	1.19	1.06	9.5	−21.6	−24.3
N2E_11	77.076	47.823	54.3	0.91	0.57	2.7	−21.4	−24.1
N2E_9	77.053	47.648	23.1	0.94	0.79	6.6	−21.2	−24.5
N2E_15	77.005	47.303	29.6	1.28	1.10	7.0	−16.5	−20.8
N2E_18	76.981	47.133	19.8	0.44	0.31	3.5	−16.5	−19.2
N2E_7	76.950	46.950	20.5	1.05	0.92	8.2	−16.2	−19.4
N2E_3	76.912	46.621	20.7	1.53	1.41	12.0	−15.1	−21.8
N2E_50	76.889	46.454	46.5	0.75	0.46	2.6	−15.5	−21
N2E_44	76.866	46.287	59.6	1.27	0.90	3.4	−16	−21.2
N2E_41	76.843	46.112	25.7	1.33	1.17	8.3	−15.6	−21.6
N2E_46	76.782	45.818	38.3	1.10	0.86	4.6	−22.9	−24.7
N2E_47	76.749	45.711	26.7	1.17	1.00	7.0		−24.4
N2E_42	76.711	45.584	24.1	0.98	0.83	6.5		−24.6
N2E_35	76.677	45.480	24.0	1.02	0.87	6.8		−24
N2E_43	76.638	45.358	20.1	0.71	0.59	5.7		−24.1
N2E_29	76.601	45.245	21.1	0.96	0.83	7.3		−25.2
N2E_34	76.565	45.133	13.3	1.11	1.02	13.4		−24.8
N2E_31	76.528	45.022	14.4	0.99	0.90	11.1		−25.2
N2E_40	76.491	44.908	7.4	1.03	0.98	22.5		−25.2
N2E_33	76.460	44.592	52.0	1.17	0.85	3.6		−26.9
N2E_37	76.455	44.795	29.3	1.32	1.14	7.3		−23
N2E_45	76.437	44.408	16.2	0.84	0.74	8.4		−26.3
N2E_38	76.435	44.225	20.5	1.03	0.90	8.1		−26.5
N2E_39	76.421	44.043	32.9	0.96	0.76	4.7		−26
N2E_27	76.408	43.861	8.5	0.88	0.83	16.7		−26.1
N2E_48	76.383	43.821	13.5	1.32	1.24	15.9		−25
N2E_30	76.372	43.671	4.4	1.28	1.25	46.8		−23.5
N2E_32	76.357	43.490	11.5	0.71	0.64	10.0		−23.3
N2E_36	76.344	43.309	28.8	0.95	0.78	5.4		−22.8
N2E_26	76.331	43.128	16.9	0.40	0.30	3.9		−21.8
N2E_28	76.318	42.938	6.9	0.86	0.82	20.3		−22
N2E_74	76.305	42.765	18.4	0.83	0.71	7.2		−25.6
N2E_71	76.292	42.585	8.8	0.96	0.91	17.7		−25.2
N2E_69	76.277	42.406	33.1	0.67	0.46	3.3		−23.5
N2E_66	76.264	42.227	6.9	0.83	0.79	19.4		−24.5
N2E_63	76.249	42.052	6.5	1.06	1.02	26.3		−22.6
N2E_65	76.236	41.869	15.8	0.91	0.81	9.3		−21.8
N2E_56	76.222	41.692	7.9	0.90	0.85	18.3		−21.9
N2E_64	76.207	41.514	6.4	0.78	0.74	19.7		−22.8
N2E_62	76.192	41.335	13.0	1.32	1.24	16.3		−21.7
N2E_52	76.178	41.156	31.1	1.04	0.84	5.4		−22.2
N2E_70	76.163	40.983	6.9	0.74	0.70	17.3		−23.3
N2E_67	76.148	40.972	6.4	0.93	0.89	23.5		−22
N2E_68	76.133	40.631	14.7	1.23	1.14	13.5		−22.8
N2E_51	76.118	40.452	1.7	1.10	1.09	103.9		−22.9
N2E_54	76.103	40.280	7.8	0.65	0.60	13.4		−26.3
N2E_55	76.088	40.106	5.4	0.90	0.87	26.9		−26.2

(*continued on next page*)

(*continued*)

Sample designation	Latitude (degreesN)	Longitude (degreesE)	Na concentration (ppb)	Br concentration (ppb)	nssBr (ppb)	Brenr	Air temperature (degreesC)	Snow temperature (degrees C)
N2E_61	76.073	39.930	2.8	1.23	1.21	69.9		−25.5
N2E_73	76.057	39.755	14.2	1.04	0.96	11.9		−25.3
N2E_53	76.041	39.583	4.5	0.93	0.90	33.2		−24.5
N2E_57	76.025	39.408	2.1	0.74	0.73	57.3		−24.1
N2E_58	76.009	39.234	17.4	0.91	0.80	8.5		−22.1
N2E_59	75.993	39.063	11.5	0.85	0.78	11.9	−13.1	−23.3
N2E_60	75.977	38.892	7.0	0.75	0.71	17.3		−23.4
N2E_72	75.960	38.720	2.1	0.81	0.80	62.5		−22.3
N2E_75	75.943	38.549	6.3	1.39	1.35	35.3		−22.2
N2E_123	75.926	38.380	7.4	0.68	0.63	14.8		−21.5
N2E_91	75.910	38.207	10.1	1.10	1.04	17.7		−21.3
N2E_80G	75.893	38.038	57.1	2.28	1.93	6.4		−21.2
N2E_297	75.876	37.867	4.7	0.77	0.74	26.6		−21.3
N2E_283	75.859	37.696	14.9	0.99	0.90	10.7		−21
N2E_90	75.838	37.507	8.6	0.64	0.58	12.0		−24
N2E_83	75.820	37.340	10.3	0.63	0.57	9.9		−24
N2E_97	75.802	37.175	2.9	0.81	0.79	44.6	−19.4	−23.5
N2E_98	75.783	37.009	13.6	0.95	0.86	11.3		−23
N2E_95	75.764	36.842	10.5	0.85	0.79	13.1		−23
N2E_93	75.745	36.677	4.0	1.09	1.07	44.1		−23.4
N2E_89	75.733	36.579	3.2	1.71	1.69	84.9	−18	−23.4
N2E_84	75.689	36.482	22.7	1.10	0.96	7.8		−23
N2E_81	75.675	36.307	9.2	0.88	0.83	15.5		−20.3
N2E_80	75.652	36.146	13.2	0.77	0.69	9.5		−20.1
N2E_88	75.638	36.045	4.2	0.93	0.90	35.6		−19.7

References

Abbatt, J.P.D., Thomas, J.L., Abrahamsson, K., Boxe, C., Granfors, A., Jones, A.E., King, M.D., Saiz-Lopez, A., Shepson, P.B., Sodeau, J., Toohey, D.W., Toubin, C., von Glasow, R., Wren, S.N., Yang, X., 2012. Halogen activation via interactions with environmental ice and snow in the polar lower troposphere and other regions. Atmos. Chem. Phys. 12, 6237–6271.

Abrahamsson, K., Granfors, A., Ahnoff, M., Cuevas, C.A., Saiz-Lopez, A., 2018. Organic bromine compounds produced in sea ice in Antarctic winter. Nat. Commun. 9, 1–8.

Abram, N.J., Wolff, E.W., Curran, M.A.J., 2013. A review of sea ice proxy information from polar ice cores. Quat. Sci. Rev. 79, 168–183.

Alley, R., Finkel, R.C., Nishiizumi, K., Anandakrishnan, S., Shuman, C.A., Mershon, G.R., Zielinski, G.A., Mayewski, P.A., 1995. Changes in continental and sea-salt atmospheric loadings in central Greenland during the most recent deglaciation: model-based estimates. J. Glaciol. 41, 503–514.

Anderson, P.S., Neff, W.D., 2008. Boundary layer physics over snow and ice. Atmos. Chem. Phys. 8, 3563–3582.

Arrigo, K.R., van Dijken, G.L., 2011. Secular trends in Arctic Ocean net primary production. J. Geophys. Res.: Oceans 116.

Arrigo, K.R., Perovich, D.K., Pickart, R.S., Brown, Z.W., van Dijken, G.L., Lowry, K.E., Mills, M.M., Palmer, M.A., Balch, W.M., Bahr, F., Bates, N.R., Benitez-Nelson, C., Bowler, B., Brownlee, E., Ehn, J.K., Frey, K.E., Garley, R., Laney, S.R., Lubelczyk, L., Mathis, J., Matsuoka, A., Mitchell, B.G., Moore, G.W.K., Ortega-Retuerta, E., Pal, S., Polashenski, C.M., Reynolds, R.A., Schieber, B., Sosik, H.M., Stephens, M., Swift, J.H., 2012. Massive phytoplankton blooms under arctic sea ice. Science 336, 1408.

Artiglia, L., Edebeli, J., Orlando, F., Chen, S., Lee, M.-T., Corral Arroyo, P., Gilgen, A., Bartels-Rausch, T., Kleibert, A., Vazdar, M., Andres Carignano, M., Francisco, J.S., Shepson, P.B., Gladich, I., Ammann, M., 2017. A surface-stabilized ozonide triggers bromide oxidation at the aqueous solution-vapour interface. Nat. Commun. 8, 700.

Barbante, C., Gabrieli, J., Gabrielli, P., Vallelonga, P., Cozzi, G., Turetta, C., Hong, S., Rosman, K.J.R., Boutron, C., Cescon, P., 2011. A historical record of heavy metal pollution in Alpine snow and ice. In: Quante, M., Ebinghaus, R., Flöser, G. (Eds.), Persistent Pollution - Past, Present and Future, 1 ed. Springer Verlag, Berlin.

Barrie, L.A., 1986. Arctic air pollution : an overview of current knowledge. Atmos. Environ. 20, 643–663.

Barrie A, L, Gregor, D, Hargrave, B, Lake, R, Muir, D, Shearer, R, Tracy, B, Bidleman, T, 1992. Arctic contaminants: sources, occurrence and pathways. Sci. Total Env. 122, 1–74.

Belt, S.T., Massé, G., Rowland, S.J., Poulin, M., Michel, C., LeBlanc, B., 2007. A novel chemical fossil of palaeo sea ice: IP25. Org. Geochem. 38, 16–27.

Bertler, N., Mayewski, P.A., Aristarain, A., Barrett, P., Becagli, S., Bernardo, R., Bo, S., Xiao, C., Curran, M., Qin, D., Dixon, D., Ferron, F., Fischer, H., Frey, M., Frezzotti, M., Fundel, F., Genthon, C., Gragnani, R., Hamilton, G., Handley, M., Hong, S., Isaksson, E., Kang, J., Ren, J., Kamiyama, K., Kanamori, S., Kärkäs, E., Karlöf, L., Kaspari, S., Kreutz, K., Kurbatov, A., Meyerson, E., Ming, Y., Zhang, M., Motoyama, H., Mulvaney, R., Oerter, H., Osterberg, E., Proposito, M., Pyne, A., Ruth, U., Simões, J., Smith, B., Sneed, S., Teinilä, K., Traufetter, F., Udisti, R., Virkkula, A., Watanabe, O., Williamson, B., Winther, J.G., Li, Y., Wolff, E., Li, Z., Zielinski, A., 2005. Snow chemistry across Antarctica. Ann. Glaciol. 41, 167–179.

Bertler, N.A.N., Conway, H., Dahl-Jensen, D., Emanuelsson, D.B., Winstrup, M., Vallelonga, P.T., Lee, J.E., Brook, E.J., Severinghaus, J.P., Fudge, T.J., Keller, E.D., Baisden, W.T., Hindmarsh, R.C.A., Neff, P.D., Blunier, T., Edwards, R., Mayewski, P.A., Kipfstuhl, S., Buizert, C., Canessa, S., Dadic, R., Kjær, H.A., Kurbatov, A., Zhang, D., Waddington, E.D., Baccolo, G., Beers, T., Brightley, H.J., Carter, L., Clemens-Sewall, D., Ciobanu, V.G., Delmonte, B., Eling, L., Ellis, A., Ganesh, S., Golledge, N.R., Haines, S., Handley, M., Hawley, R.L., Hogan, C.M., Johnson, K.M., Korotkikh, E., Lowry, D.P., Mandeno, D., McKay, R.M., Menking, J.A., Naish, T.R., Noerling, C., Ollive, A., Orsi, A., Proemse, B.C., Pyne, A.R., Pyne, R.L., Renwick, J., Scherer, R.P., Semper, S., Simonsen, M., Sneed, S.B., Steig, E.J., Tuohy, A., Venugopal, A.U., Valero-Delgado, F., Venkatesh, J., Wang, F., Wang, S., Winski, D.A., Winton, V.H.L., Whiteford, A., Xiao, C., Yang, J., Zhang, X., 2018. The Ross Sea Dipole – temperature, snow accumulation and sea ice variability in the Ross Sea region, Antarctica, over the past 2700 years. Clim. Past 14, 193–214.

Bonne, J.-L., Steen-Larsen, H.C., Risi, C., Werner, M., Sodemann, H., Lacour, J.-L., Fettweis, X., Cesana, G., Delmotte, M., Cattani, O., Vallelonga, P., Kjær, H.A., Clerbaux, C., Sveinbjörnsdóttir, Á.E., Masson-Delmotte, V., 2015. The summer 2012 Greenland heat wave: in situ and remote sensing observations of water vapor isotopic composition during an atmospheric river event. J. Geophys. Res.: Atmosphere 120, 2970–2989.

Bonnet, S., de Vernal, A., Hillaire-Marcel, C., Radi, T., Husum, K., 2010. Variability of sea-surface temperature and sea-ice cover in the Fram Strait over the last two millennia. Mar. Micropaleontol. 74, 59–74.

Bougoudis, I., Blechschmidt, A.-M., Richter, A., Seo, S., Burrows, J.P., Theys, N., Rinke, A., 2020. Long-term time series of Arctic tropospheric BrO derived from UV–VIS satellite remote sensing and its relation to first-year sea-ice. Atmos. Chem. Phys. 20, 11869–11892.

Boutron, C.F., Görlach, U., Candelone, J.-P., Bolshov, M.A., Delmas, R.J., 1991. Decrease in anthropogenic lead, cadmium and zinc in Greenland snows since the late 1960's. Nature 353, 153–156.

Bradley, R.S., 2015. Chapter 5 - ice cores. In: Bradley, R.S. (Ed.), Paleoclimatology, third ed. Academic Press, San Diego, pp. 137–194.

Buiron, D., Chappellaz, J., Stenni, B., Frezzotti, M., Baumgartner, M., Capron, E., Landais, A., Lemieux-Dudon, B., Masson-Delmotte, V., Montagnat, M., Parrenin, F., Schilt, A., 2011. TALDICE-1 age scale of the Talos Dome deep ice core, East Antarctica. Clim. Past 7, 1–16.

Burgess, E.W., Forster, R.R., Box, J.E., Mosley-Thompson, E., Bromwich, D.H., Bales, R.C., Smith, L.C., 2010. A spatially calibrated model of annual accumulation rate on the Greenland Ice Sheet (1958–2007). J. Geophys. Res. 115.

Burrows, J.P., Hölzle, E., Goede, A.P.H., Visser, H., Fricke, W., 1995. Sciamachy - scanning imaging absorption spectrometer for atmospheric chartography. Acta Astronom. 35, 445–451.

Burrows, J.P., Weber, M., Buchwitz, M., Rozanov, V.V., Ladstätter, A., Weißenmayer, A., Richter, A., DeBeek, R., Hoogen, R., Bramstedt, K., Eichmann, K.U., 1999. The global ozone monitoring experiment (GOME): mission concept and first scientific results. J. Atmos. Sci. 56, 151–175.

Carpenter, L.J., MacDonald, S.M., Shaw, M.D., Kumar, R., Saunders, R.W., Parthipan, R., Wilson, J., Plane, J.M.C., 2013. Atmospheric iodine levels influenced by sea surface emissions of inorganic iodine. Nat. Geosci. 6, 108–111.

Community, S.I.M.I.P., 2020. Arctic sea ice in CMIP6. Geophys. Res. Lett. 47 e2019GL086749.
Crosta, X., Sturm, A., Armand, L., Pichon, J.-J., 2004. Late Quaternary sea ice history in the Indian sector of the Southern Ocean as recorded by diatom assemblages. Mar. Micropaleontol. 50, 209–223.
Cuevas, C.A., Maffezzoli, N., Corella, J.P., Spolaor, A., Vallelonga, P., Kjær, H.A., Simonsen, M., Winstrup, M., Vinther, B., Horvat, C., Fernandez, R.P., Kinnison, D., Lamarque, J.-F., Barbante, C., Saiz-Lopez, A., 2018. Rapid increase in atmospheric iodine levels in the North Atlantic since the mid-20th century. Nat. Commun. 9, 1452.
Curran, M.A.J., Jones, G.B., Burton, H., 1998. Spatial distribution of dimethylsulfide and dimethylsulfoniopropionate in the Australasian sector of the Southern Ocean. J. Geophys. Res.: Atmosphere 103, 16677–16689.
Curran, M.A.J., Palmer, A.S., Van Ommen, T.D., Morgan, V.I., Phillips, K.L., McMorrow, A.J., Mayewski, P.A., 2002. Post-depositional movement of methanesulphonic acid at Law Dome, Antarctica, and the influence of accumulation rate. Ann. Glaciol. 35, 333–339.
Curran, M.A.J., van Ommen, Tas D., Morgan, V.I., Phillips, K.L., Palmer, A.S., 2003. Ice core evidence for Antarctic sea ice decline since the 1950s. Science 302, 1203–1206.
Denis, D, Crosta, X, Barbara, L, Massé, G, Renssen, H, Ther, O, Giraudeau, J, 2010. Sea ice and wind variability during the Holocene in East Antarctica: insight on middle–high latitude coupling. Quat. Sci. Rev. 29, 3709–3719.
Dibb, J.E., Ziemba, L.D., Luxford, J., Beckman, P., 2010. Bromide and other ions in the snow, firn air, and atmospheric boundary layer at Summit during GSHOX. Atmos. Chem. Phys. 10, 9931–9942.
DiMarzio, J., Brenner, A., Schutz, R., Shuman, C.A., Zwally, H.J., 2007. In: Center, N.S.a.I.D. (Ed.), GLAS/ICESat 1 Km Laser Altimetry Digital Elevation Model of Greenland. Boulder, Colorado, USA.
Dokken, T.M., Nisancioglu, K.H., Li, C., Battisti, D.S., Kissel, C., 2013. Dansgaard-Oeschger cycles: interactions between ocean and sea ice intrinsic to the Nordic seas. Paleoceanography 28, 491–502.
Douglas A, T, Sturm, M, 2004. Arctic haze, mercury and the chemical composition of snow across northwestern Alaska. Atmos. Environ. 38, 805–820.
Eicken, H., 2003. From the microscopic to the macroscopic to the regional scale: growth, microstructure and properties of sea ice. In: Thomas, D.N., Dieckmann, G.S. (Eds.), Sea Ice – an Introduction to its Physics, Biology, Chemistry and Geology. Blackwells Scientific Ltd., Oxford, pp. 22–81.
EPICA community members, 2006. One-to-one coupling of glacial climate variability in Greenland and Antarctica. Nature 444, 195–198.
Fernandez, R.P., Carmona-Balea, A., Cuevas, C.A., Barrera, J.A., Kinnison, D.E., Lamarque, J.F., Blaszczak-Boxe, C., Kim, K., Choi, W., Hay, T., Blechschmidt, A.M., Schönhardt, A., Burrows, J.P., Saiz-Lopez, A., 2019. Modeling the sources and chemistry of polar tropospheric halogens (Cl, Br, and I) using the CAM-Chem Global Chemistry-Climate Model. J. Adv. Model. Earth Syst. 11, 2259–2289.
Fischer, H., Wagenbach, D., 1996. Large-scale spatial trends in recent firn chemistry along an east-west transect through central Greenland. Atmos. Environ. 30, 3227–3238.
Fischer, H., Wagenbach, D., Kipfstuhl, J., 1998. Sulfate and nitrate firn concentrations on the Greenland ice sheet 1. Large-scale geographical deposition changes. J. Geophys. Res. 103, 21927–21934.
Foster, K.L., Plastridge, R.A., Bottenheim, J.W., Shepson, P.B., Finlayson-Pitts, B.J., Spicer, C.W., 2001. The role of Br_2 and BrCl in surface ozone destruction at polar sunrise. Science 291, 471.
Frey, M.M., Norris, S.J., Brooks, I.M., Anderson, P.S., Nishimura, K., Yang, X., Jones, A.E., Nerentorp Mastromonaco, M.G., Jones, D.H., Wolff, E.W., 2020. First direct observation of sea salt aerosol production from blowing snow above sea ice. Atmos. Chem. Phys. 20, 2549–2578.
Frieß, U., Deutschmann, T., Gilfedder, B.S., Weller, R., Platt, U., 2010. Iodine monoxide in the Antarctic snowpack. Atmos. Chem. Phys. 10, 2439–2456.
Gálvez, Ó., Baeza-Romero, M.T., Sanz, M., Saiz-Lopez, A., 2016. Photolysis of frozen iodate salts as a source of active iodine in the polar environment. Atmos. Chem. Phys. 16, 12703–12713.
Gersonde, R., Crosta, X., Abelmann, A., Armand, L., 2005. Sea-surface temperature and sea ice distribution of the Southern Ocean at the EPILOG Last Glacial Maximum—a circum-Antarctic view based on siliceous microfossil records. Quat. Sci. Rev. 24, 869–896.
Hansson, M.E., 1994. The Renland ice core. A Northern Hemisphere record of aerosol composition over 120,000 years. Tellus B 46, 390–418.
Hezel, P.J., Alexander, B., Bitz, C.M., Steig, E.J., Holmes, C.D., Yang, X., Sciare, J., 2011. Modeled methanesulfonic acid (MSA) deposition in Antarctica and its relationship to sea ice. J. Geophys. Res.: Atmosphere 116.
Hodell A, D, Kanfoush L, S, Shemesh, A, Crosta, X, Charles D, C, Guilderson P, T, 2001. Abrupt cooling of Antarctic surface waters and sea ice expansion in the South Atlantic sector of the Southern Ocean at 5000 cal yr B.P. Quat. Res. 56, 191–198.
Hoff, U., Rasmussen, T.L., Stein, R., Ezat, M.M., Fahl, K., 2016. Sea ice and millennial-scale climate variability in the Nordic seas 90 kyr ago to present. Nat. Commun. 7.
Horvat, C., Jones, D.R., Iams, S., Schroeder, D., Flocco, D., Feltham, D., 2017. The frequency and extent of sub-ice phytoplankton blooms in the Arctic Ocean. Science Advances 3.
Howat, I.M., Porter, C., Smith, B.E., Noh, M.-J., Morin, P., 2019. The reference elevation model of Antarctica (REMA). The Cryosphere 13, 665–674.
Isaksson, E., Kekonen, T., Moore, J., Mulvaney, R., 2005. The methanesulfonic acid (MSA) record in a Svalbard ice core. Ann. Glaciol. 42, 345–351.
Johnsen, S.J., Clausen, H.B., Dansgaard, W., Fuhrer, K., Gundestrup, N., Hammer, C.U., Iversen, P., Steffensen, J.P., Jouzel, J., Stauffer, B., 1992. Irregular glacial interstadials recorded in a new Greenland ice core. Nature 359, 311–313.
Johnsen, S.J., Hansen, S.B., Sheldon, S.G., Dahl-Jensen, D., Steffensen, J.P., Augustin, L., Journé, P., Alemany, O., Rufli, H., Schwander, J., Azuma, N., Motoyama, H., Popp, T., Talalay, P., Thorsteinsson, T., Wilhelms, F., Zagorodnov, V., 2007. The Hans Tausen drill: design, performance, further developments and some lessons learned Ann. Glaciol 47 (10), 89–98.
Karlsson, N.B., Razik, S., Hörhold, M., Winter, A., Steinhage, D., Binder, T., Eisen, O., 2020. Surface accumulation in Northern Central Greenland during the last 300 years. Ann. Glaciol. 61, 214–224.
Kaufmann, P., Federer, U., Hutterli, M.A., Bigler, M., Schüpbach, S., Ruth, U., Schmitt, J., Stocker, T.F., 2008. An improved continuous flow analysis system for high-resolution field measurements on ice cores. Environ. Sci. Technol. 42, 8044–8050.
Kelly, P.J., Kern, C., Roberts, T.J., Lopez, T., Werner, C., Aiuppa, A., 2013. Rapid chemical evolution of tropospheric volcanic emissions from Redoubt Volcano, Alaska, based on observations of ozone and halogen-containing gases. J. Volcanol. Geoth. Res. 259, 317–333.
Kim, K., Yabushita, A., Okumura, M., Saiz-Lopez, A., Cuevas, C.A., Blaszczak-Boxe, C.S., Min, D.W., Yoon, H.-I., Choi, W., 2016. Production of molecular iodine and tri-iodide in the frozen solution of iodide: implication for polar atmosphere. Environ. Sci. Technol. 50, 1280–1287.
Kinnard, C., Zdanowicz, C.M., Fisher, D.A., Isaksson, E., de Vernal, A., Thompson, L.G., 2011. Reconstructed changes in Arctic sea ice over the past 1,450 years. Nature 479, 509–512.
Kjær, H.A., Vallelonga, P., Svensson, A., Elleskov, L., Kristensen, M., Tibuleac, C., Winstrup, M., Kipfstuhl, S., 2016. An optical dye method for continuous determination of acidity in ice cores. Environ. Sci. Technol. 50 (19), 10485–10493.
Kjær, H.A., Zens, P., Edwards, R., Olesen, M., Mottram, R., Lewis, G., Terkelsen Holme, C., Black, S., Holst Lund, K., Schmidt, M., Dahl-Jensen, D., Vinther, B., Svensson, A., Karlsson, N., Box, J.E., Kipfstuhl, S., Vallelonga, P., 2021. Recent North Greenland temperature warming and accumulation. Cryosphere Discuss. submitted for publication.
Legrand, M., 1987. Chemistry of antarctic snow and ice. J. Phys. Colloq. 48, 77–86.
Legrand, M., Mayewski, P., 1997. Glaciochemistry of Polar ice cores: a review. Rev. Geophys. 35, 219–243.
Legrand, M., Hammer, C., De Angelis, M., Savarino, J., Delmas, R., Clausen, H., Johnsen, S.J., 1997. Sulfur-containing species (methanesulfonate and SO4) over the last climatic cycle in the Greenland Ice Core Project (central Greenland) ice core. J. Geophys. Res.: Oceans 102, 26663–26679.
Legrand, M., Yang, X., Preunkert, S., Theys, N., 2016. Year-round records of sea salt, gaseous, and particulate inorganic bromine in the atmospheric boundary layer at coastal (Dumont d'Urville) and central (Concordia) East Antarctic sites. J. Geophys. Res.: Atmosphere 121, 997–1023.
Legrand, M., Preunkert, S., Wolff, E., Weller, R., Jourdain, B., Wagenbach, D., 2017. Year-round records of bulk and size-segregated aerosol composition in central Antarctica (Concordia site) – Part 1: fractionation of sea-salt particles. Atmos. Chem. Phys. 17, 14039–14054.
Legrand, M., McConnell, J.R., Preunkert, S., Arienzo, M., Chellman, N., Gleason, K., Sherwen, T., Evans, M.J., Carpenter, L.J., 2018. Alpine ice evidence of a three-fold increase in atmospheric iodine deposition since 1950 in Europe due to increasing oceanic emissions. Proc. U.S. Nat. Acad. Sci. 115, 12136.
Levine, J.G., Yang, X., Jones, A.E., Wolff, E.W., 2014. Sea salt as an ice core proxy for past sea ice extent: a process-based model study. J. Geophys. Res. Atmos. 119, 5737–5756.
Li, C., Kang, S., Shi, G., Huang, J., Ding, M., Zhang, Q., Zhang, L., Guo, J., Xiao, C., Hou, S., Sun, B., Qin, D., Ren, J., 2014. Spatial and temporal variations of total mercury in Antarctic snow along the transect from Zhongshan Station to Dome A. Tellus B 66, 25152.
Maffezzoli, N., Spolaor, A., Barbante, C., Bertò, M., Frezzotti, M., Vallelonga, P., 2017. Bromine, iodine and sodium in surface snow along the 2013 Talos Dome–GV7 traverse (northern Victoria Land, East Antarctica). Cryosphere 11, 693–705.
Maffezzoli, N., Vallelonga, P., Edwards, R., Saiz-Lopez, A., Turetta, C., Kjær, H.A., Barbante, C., Vinther, B., Spolaor, A., 2019. A 120,000-year record of sea ice in the North Atlantic? Clim. Past 15, 2031–2051.
Maselli, O.J., Chellman, N.J., Grieman, M., Layman, L., McConnell, J.R., Pasteris, D., Rhodes, R.H., Saltzman, E., Sigl, M., 2017. Sea ice and pollution-modulated changes in Greenland ice core methanesulfonate and bromine. Clim. Past 13, 39–59.
Massé, G., Rowland, S.J., Sicre, M.-A., Jacob, J., Jansen, E., Belt, S.T., 2008. Abrupt climate changes for Iceland during the last millennium: Evidence from high resolution sea ice reconstructions. Earth Planet. Sci. Lett. 269, 565–569.
McConnell, J.R., Maselli, O.J., Sigl, M., Vallelonga, P., Neumann, T., Anschütz, H., Bales, R.C., Curran, M.A.J., Das, S.B., Edwards, R., Kipfstuhl, S., Layman, L., Thomas, E.R., 2014. Antarctic-wide array of high-resolution ice core records reveals pervasive lead pollution began in 1889 and persists today. Nature Scientific Reports 4.
McConnell, J.R., Burke, A., Dunbar, N.W., Köhler, P., Thomas, J.L., Arienzo, M.M., Chellman, N.J., Maselli, O.J., Sigl, M., Adkins, J.F., Baggenstos, D., Burkhart, J.F., Brook, E.J., Buizert, C., Cole-Dai, J., Fudge, T.J., Knorr, G., Graf, H.-F., Grieman, M.M., Iverson, N., McGwire, K.C., Mulvaney, R., Paris, G., Rhodes, R.H., Saltzman, E.S., Severinghaus, J.P., Steffensen, J.P., Taylor, K.C., Winckler, G., 2017. Synchronous volcanic eruptions and abrupt climate change ~17.7 ka plausibly linked by stratospheric ozone depletion. Proc. U.S. Nat. Acad. Sci. 114, 10035.

Mezgec, K., Stenni, B., Crosta, X., Masson-Delmotte, V., Baroni, C., Braida, M., Ciardini, V., Colizza, E., Melis, R., Salvatore, M.C., Severi, M., Scarchilli, C., Traversi, R., Udisti, R., Frezzotti, M., 2017. Holocene sea ice variability driven by wind and polynya efficiency in the Ross Sea. Nat. Commun. 8, 1334.
Millero, F.J., 1974. The physical chemistry of seawater. Annu. Rev. Earth Planet Sci. 2, 101–150.
Millero, F.J., Feistel, R., Wright, D.G., McDougall, T.J., 2008. The composition of standard seawater and the definition of the reference-composition salinity scale. Deep-Sea Res. Part I Oceanogr. Res. Pap. 55, 50–72.
Murphy, E.J., Clarke, A., Symon, C., Priddle, J., 1995. Temporal variation in Antarctic sea-ice: analysis of a long term fast-ice record from the South Orkney Islands. Deep-Sea Res. Part I Oceanogr. Res. Pap. 42, 1045–1062.
Murphy, E.J., Clarke, A., Abram, N.J., Turner, J., 2014. Variability of sea-ice in the northern Weddell Sea during the 20th century. J. Geophys. Res.: Oceans 119, 4549–4572.
NEEM Community members, 2013. Eemian interglacial reconstructed from a Greenland folded ice core. Nature 493, 489–494.
Nghiem, S.V., Hall, D.K., Mote, T.L., Tedesco, M., Albert, M.R., Keegan, K., Shuman, C.A., DiGirolamo, N.E., Neumann, G., 2012. The extreme melt across the Greenland ice sheet in 2012. Geophys. Res. Lett. 39, L20502.
Nielsen, L.T., Karlsson, N.B., Hvidberg, C.S., 2015. Large-scale reconstruction of accumulation rates in northern Greenland from radar data. Ann. Glaciol. 56, 70–78.
Nielsen H.H, S, Koç, N, Crosta, X, 2004. Holocene climate in the Atlantic sector of the Southern Ocean: Controlled by insolation or oceanic circulation? Geology 32, 317–320.
Nilsson, J., Vallelonga, P., Simonsen, S.B., Sørensen, L.S., Forsberg, R., Dahl-Jensen, D., Hirabayashi, M., Goto-Azuma, K., Hvidberg, C.S., Kjær, H.A., Satow, K., 2015. Greenland 2012 melt event effects on CryoSat-2 radar altimetry. Geophys. Res. Lett. 42, 3919–3926.
O'Dowd, C.D., Smith, M.H., Consterdine, I.E., Lowe, J.A., 1997. Marine aerosol, sea-salt, and the marine sulphur cycle: a short review. Atmos. Environ. 31, 73–80.
Ogilvie, A.E.J., 1984. The past climate and sea-ice record from Iceland. I. Data to AD 1780. Climatic Change 6, 131–152.
Osman, M., Das, S.B., Marchal, O., Evans, M.J., 2017. Methanesulfonic acid (MSA) migration in polar ice: data synthesis and theory. Cryosphere 11, 2439–2462.
Osman, M.B., Das, S., Trusel, L.D., Evans, M.J., Fischer, H., Grieman, M., Kipfstuhl, S., McConnell, J.R., Saltzman, E.S., 2019. Industrial-era decline in subarctic Atlantic productivity. Nature 569, 551–555.
Oum, K.W., Lakin, M.J., Finlayson-Pitts, B.J., 1998. Bromine activation in the troposphere by the dark reaction of O3 with seawater ice. Geophys. Res. Lett. 25, 3923–3926.
Parrenin, F., Barnola, J.-M., Beer, J., Blunier, T., Castellano, E., Chappellaz, J., Dreyfus, G., Fischer, H., Fujita, S., Jouzel, J., Kawamura, K., Lemieux-Dudon, B., Loulergue, L., Masson-Delmotte, V., Narcisi, B., Petit, J.-R., Raisbeck, G., Raynaud, D., Ruth, U., Schwander, J., Severi, M., Spahni, R., Steffensen, J.P., Svensson, A., Udisti, R., Waelbroeck, C., Wolff, E., 2007. The EDC3 chronology for the EPICA Dome C ice core. Clim. Past 3, 485–497.
Peterson, P.K., Hartwig, M., May, N.W., Schwartz, E., Rigor, I., Ermold, W., et al., 2019. Snowpack measurements suggest role for multi-year sea-ice regions in Arctic atmospheric bromine and chlorine chemistry. Elementa 7 (14), 2019. Snowpack measurements suggest role for multi-year sea-ice regions in Arctic atmospheric bromine and chlorine chemistry. Elementa 7, 14.
Pohjola, V.A., Moore, J.C., Isaksson, E., Jauhiainen, T., van de Wal, R.S.W., Martma, T., Meijer, H.A.J., Vaikmäe, R., 2002. Effect of periodic melting on geochemical and isotopic signals in an ice core from Lomonosovfonna. Svalbard. J. Geophys. Res. 107, 4036.
Polyakov, I.V., Alekseev, G.V., Bekryaev, R.V., Bhatt, U.S., Colony, R., Johnson, M.A., Karklin, V.P., Walsh, D., Yulin, A.V., 2003. Long-term ice variability in Arctic marginal seas. J. Clim. 16, 2078–2085.
Popp, T.J., Hansen, S.B., Sheldon, S.G., Panton, C., 2014. Deep ice-core drilling performance and experience at NEEM, Greenland. Ann. Glaciol. 55, 53–64.
Prados-Roman, C., Cuevas, C.A., Fernandez, R.P., Kinnison, D.E., Lamarque, J.F., Saiz-Lopez, A., 2015. A negative feedback between anthropogenic ozone pollution and enhanced ocean emissions of iodine. Atmos. Chem. Phys. 15, 2215–2224.
Pratt, K.A., Custard, K.D., Shepson, P.B., Douglas, T.A., Pohler, D., General, S., Zielcke, J., Simpson, W.R., Platt, U., Tanner, D.J., Gregory Huey, L., Carlsen, M., Stirm, B.H., 2013. Photochemical production of molecular bromine in Arctic surface snowpacks. Nat. Geosci. 6, 351–356.
Preunkert, S., Wagenbach, D., Legrand, M., Vincent, C., 2000. Col du Dôme (Mt Blanc Massif, French Alps) suitability for ice-core studies in relation with past atmospheric chemistry over Europe. Tellus B 52, 993–1012.
Raisbeck, G.M., Cauquoin, A., Jouzel, J., Landais, A., Petit, J.-R., Lipenkov, V.Y., Beer, J., Synal, H.-A., Oerter, H., Johnsen, S.J., Steffensen, J.P., Svensson, A., Yiou, F., 2017. An improved north–south synchronization of ice core records around the 41 kyr 10Be peak. Clim. Past 13, 217–229.
Rankin, A.M., Wolff, E.W., Martin, S., 2002. Frost flowers: implications for tropospheric chemistry and ice core interpretation. J. Geophys. Res. 107, 4683, 4610.1029/2002JD002492.
Rhodes, R.H., Yang, X., Wolff, E.W., 2018. sea ice versus storms: what controls sea salt in arctic ice cores? Geophys. Res. Lett. 45, 5572–5580.
Richter, A., 2020. Pers. Comm. IUP-Bremen Email: richter@iup.Physik. uni-bremen.de.
Roberts, J., Plummer, C., Vance, T., van Ommen, T., Moy, A., Poynter, S., Treverrow, A., Curran, M., George, S., 2015. A 2000-year annual record of snow accumulation rates for Law Dome, East Antarctica. Clim. Past 11, 697–707.
Röthlisberger, R., Mulvaney, R., Wolff, E.W., Hutterli, M.A., Bigler, M., Angelis, M.d., Hansson, M.E., Steffensen, J.P., Udisti, R., 2003. Limited dechlorination of sea-salt aerosols during the last glacial period: evidence from the European Project for Ice Coring in Antarctica (EPICA) Dome C ice core. J. Geophys. Res. 108, 4526, 4510.1029/2003JD003604.
Saiz-Lopez, A., Blaszczak-Boxe, C.S., 2016. The polar iodine paradox. Atmos. Environ. 145, 72–73.
Saiz-Lopez, A., von Glasow, R., 2012. Reactive halogen chemistry in the troposphere. Chem. Soc. Rev. 41, 6448–6472.
Saiz-Lopez, A., Mahajan, A.S., Salmon, R.A., Bauguitte, S.J.B., Jones, A.E., Roscoe, H.K., Plane, J.M.C., 2007. Boundary layer halogens in coastal Antarctica. Science 317, 348–351.
Saiz-Lopez, A., Plane, J.M.C., Baker, A.R., Carpenter, L.J., von Glasow, R., Gomez Martin, J.C., McFiggans, G., Saunders, R.W., 2012. Atmospheric chemistry of iodine. Chem. Rev. 112, 1773–1804.
Saiz-Lopez, A., Blaszczak-Boxe, C.S., Carpenter, L.J., 2015. A mechanism for biologically induced iodine emissions from sea ice. Atmos. Chem. Phys. 15, 9731–9746.
Schaller, C.F., Freitag, J., Kipfstuhl, S., Laepple, T., Steen-Larsen, H.C., Eisen, O., 2016. A representative density profile of the North Greenland snowpack. Cryosphere 10, 1991–2002.
Schönhardt, A., Begoin, M., Richter, A., Wittrock, F., Kaleschke, L., Gómez Martín, J.C., Burrows, J.P., 2012. Simultaneous satellite observations of IO and BrO over Antarctica. Atmos. Chem. Phys. 12, 6565–6580.
Schüpbach, S., Federer, U., Kaufmann, P.R., Albani, S., Barbante, C., Stocker, T.F., Fischer, H., 2013. High-resolution mineral dust and sea ice proxy records from the Talos Dome ice core. Clim. Past 9, 2789–2807.
Schüpbach, S., Fischer, H., Bigler, M., Erhardt, T., Gfeller, G., Leuenberger, D., Mini, O., Mulvaney, R., Abram, N.J., Fleet, L., Frey, M.M., Thomas, E., Svensson, A., Dahl-Jensen, D., Kettner, E., Kjaer, H., Seierstad, I., Steffensen, J.P., Rasmussen, S.O., Vallelonga, P., Winstrup, M., Wegner, A., Twarloh, B., Wolff, K., Schmidt, K., Goto-Azuma, K., Kuramoto, T., Hirabayashi, M., Uetake, J., Zheng, J., Bourgeois, J., Fisher, D., Zhiheng, D., Xiao, C., Legrand, M., Spolaor, A., Gabrieli, J., Barbante, C., Kang, J.H., Hur, S.D., Hong, S.B., Hwang, H.J., Hong, S., Hansson, M., Iizuka, Y., Oyabu, I., Muscheler, R., Adolphi, F., Maselli, O., McConnell, J., Wolff, E.W., 2018. Greenland records of aerosol source and atmospheric lifetime changes from the Eemian to the Holocene. Nat. Commun. 9, 1476.
Sheldon, S.G., Popp, T.J., Hansen, S.B., Hedegaard, T.M., Mortensen, C., 2014. A new intermediate-depth ice-core drilling system. Ann. Glaciol. 55, 271–284.
Sigl, M., McConnell, J.R., Layman, L., Maselli, O., McGwire, K., Pasteris, D., Dahl-Jensen, D., Steffensen, J.r.P., Vinther, B., Edwards, R., Mulvaney, R., Kipfstuhl, S., 2013. A new bipolar ice core record of volcanism from WAIS Divide and NEEM and implications for climate forcing of the last 2000 years. J. Geophys. Res.-Atmos. 118, 1151–1169.
Sigl, M., Winstrup, M., McConnell, J.R., Welten, K.C., Plunkett, G., Ludlow, F., Buntgen, U., Caffee, M., Chellman, N., Dahl-Jensen, D., Fischer, H., Kipfstuhl, S., Kostick, C., Maselli, O.J., Mekhaldi, F., Mulvaney, R., Muscheler, R., Pasteris, D.R., Pilcher, J.R., Salzer, M., Schupbach, S., Steffensen, J.P., Vinther, B.M., Woodruff, T.E., 2015. Timing and climate forcing of volcanic eruptions for the past 2,500 years. Nature 523, 543–549.
Sigl, M., Fudge, T.J., Winstrup, M., Cole-Dai, J., Ferris, D., McConnell, J.R., Taylor, K.C., Welten, K.C., Woodruff, T.E., Adolphi, F., Bisiaux, M., Brook, E.J., Buizert, C., Caffee, M.W., Dunbar, N.W., Edwards, R., Geng, L., Iverson, N., Koffman, B., Layman, L., Maselli, O.J., McGwire, K., Muscheler, R., Nishiizumi, K., Pasteris, D.R., Rhodes, R.H., Sowers, T.A., 2016. The WAIS Divide deep ice core WD2014 chronology - Part 2: annual-layer counting (0-31 ka BP). Clim. Past 12, 769–786.
Simpson, W.R., Alvareaz-Aviles, L., Douglas, T.A., Sturm, M., Domine, F., 2005. Halogens in the coastal snow pack near Barrow, Alaska: evidence for active bromine air-snow chemistry during springtime. Geophys. Res. Lett. 32, 4.
Simpson, W.R., Carlson, D., Honninger, G., Douglas, T.A., Sturm, M., Perovich, D., Platt, U., 2007a. First-year sea-ice contact predicts bromine monoxide (BrO) levels at Barrow, Alaska better than potential frost flower contact. Atmos. Chem. Phys. 7, 621–627.
Simpson, W.R., von Glasow, R., Riedel, K., Anderson, P., Ariya, P., Bottenheim, J., Burrows, J., Carpenter, L.J., Frie√ü, U., Goodsite, M.E., Heard, D., Hutterli, M., Jacobi, H.W., Kaleschke, L., Neff, B., Plane, J., Platt, U., Richter, A., Roscoe, H., Sander, R., Shepson, P., Sodeau, J., Steffen, A., Wagner, T., Wolff, E., 2007b. Halogens and their role in polar boundary-layer ozone depletion. Atmos. Chem. Phys. 7, 4375–4418.
Simpson, W.R., Brown, S.S., Saiz-Lopez, A., Thornton, J.A., Glasow, R.v., 2015. Tropospheric halogen chemistry: sources, cycling, and impacts. Chem. Rev. 115, 4035–4062.
Simpson, W.R., Frieß, U., Thomas, J.L., Lampel, J., Platt, U., 2018. Polar nighttime chemistry produces intense reactive bromine events. Geophys. Res. Lett. 45 (18), 9987–9994.
Spolaor, A., Vallelonga, P., Gabrieli, J., Kehrwald, N., Turetta, C., Cozzi, G., Plane, J.M.C., Boutron, C., Barbante, C., 2012. Speciation analysis of iodine and bromine at picogram-per-gram levels in Polar Ice. Anal. Bioanal. Chem. 405, 647–654.
Spolaor, A., Gabrieli, J., Martma, T., Kohler, J., Björkmann, M., Isaksson, E., Varin, C., Vallelonga, P., Plane, J.M.C., Barbante, C., 2013a. Sea ice dynamics influence halogen deposition to Svalbard. Cryosphere 7, 1645–1658.
Spolaor, A., Vallelonga, P., Plane, J.M.C., Kehrwald, N., Gabrieli, J., Varin, C., Turetta, C., Cozzi, G., Kumar, R., Boutron, C., Barbante, C., 2013b. Halogen species record Antarctic sea ice extent over glacial-interglacial periods. Atmos. Chem.

Phys. 13, 6623–6635.
Spolaor, A., Vallelonga, P., Gabrieli, J., Martma, T., Björkman, M.P., Isaksson, E., Cozzi, G., Turetta, C., Kjær, H.A., Curran, M.A.J., Moy, A.D., Schönhardt, A., Blechschmidt, A.M., Burrows, J.P., Plane, J.M.C., Barbante, C., 2014. Seasonality of halogen deposition in polar snow and ice. Atmos. Chem. Phys. 14, 9613–9622.
Spolaor, A., Opel, T., McConnell, J.R., Maselli, O.J., Spreen, G., Varin, C., Kirchgeorg, T., Fritzsche, D., Saiz-Lopez, A., Vallelonga, P., 2016a. Halogen-based reconstruction of Russian Arctic sea ice area from the Akademii Nauk ice core (Severnaya Zemlya). Cryosphere 10, 245–256.
Spolaor, A., Vallelonga, P., Turetta, C., Maffezzoli, N., Cozzi, G., Gabrieli, J., Barbante, C., Goto-Azuma, K., Saiz-Lopez, A., Cuevas, C.A., Dahl-Jensen, D., 2016b. Canadian Arctic sea ice reconstructed from bromine in the Greenland NEEM ice core. Sci. Rep. 6, 33925.
Spolaor, A., Angot, H., Roman, M., Dommergue, A., Scarchilli, C., Vardè, M., Del Guasta, M., Pedeli, X., Varin, C., Sprovieri, F., Magand, O., Legrand, M., Barbante, C., Cairns, W.R.L., 2018. Feedback mechanisms between snow and atmospheric mercury: results and observations from field campaigns on the Antarctic plateau. Chemosphere 197, 306–317.
Stroeve, J., Notz, D., 2015. Insights on past and future sea-ice evolution from combining observations and models. Global Planet. Change 135, 119–132.
Stroeve, J.C., Kattsov, V., Barrett, A., Serreze, M., Pavlova, T., Holland, M., Meier, W.N., 2012a. Trends in Arctic sea ice extent from CMIP5, CMIP3 and observations. Geophys. Res. Lett. 39, L16502.
Stroeve, J.C., Serreze, M.C., Holland, M.M., Kay, J.E., Malanik, J., Barrett, A.P., 2012b. The Arctic's rapidly shrinking sea ice cover: a research synthesis. Climatic Change 110, 1005–1027.
Svensson, A., Dahl-Jensen, D., Steffensen, J.P., Blunier, T., Rasmussen, S.O., Vinther, B.M., Vallelonga, P., Capron, E., Gkinis, V., Cook, E., Kjær, H.A., Muscheler, R., Kipfstuhl, S., Wilhelms, F., Stocker, T.F., Fischer, H., Adolphi, F., Erhardt, T., Sigl, M., Landais, A., Parrenin, F., Buizert, C., McConnell, J.R., Severi, M., Mulvaney, R., Bigler, M., 2020. Bipolar volcanic synchronization of abrupt climate change in Greenland and Antarctic ice cores during the last glacial period. Clim. Past 16, 1565–1580.
Thomas, E.R., Abram, N.J., 2016. Ice core reconstruction of sea ice change in the Amundsen-Ross Seas since 1702 A. D. Geophys. Res. Lett. 43, 5309–5317.
Thomas, D.N., Dieckmann, G.S., 2003. Sea Ice – an Introduction to its Physics, Biology, Chemistry and Geology. Blackwell Scientific Ltd., Oxford.
Thomas, J.L., Dibb, J.E., Stutz, J., von Glasow, R., Brooks, S., Huey, L.G., Lefer, B., 2012. Overview of the 2007 and 2008 campaigns conducted as part of the Greenland summit halogen-HOx experiment (GSHOX). Atmos. Chem. Phys. 12, 10833–10839.
Thomas, E.R., van Wessem, J.M., Roberts, J., Isaksson, E., Schlosser, E., Fudge, T.J., Vallelonga, P., Medley, B., Lenaerts, J., Bertler, N., van den Broeke, M.R., Dixon, D.A., Frezzotti, M., Stenni, B., Curran, M., Ekaykin, A.A., 2017. Regional Antarctic snow accumulation over the past 1000 years. Clim. Past 13, 1491–1513.
Turekian, K.K., 1968. Oceans. Prentice-Hall, New Jersey.
Vallelonga, P., Barbante, C., Cozzi, G., Gaspari, V., Candelone, J.-P., van de Velde, K., Morgan, V.I., Rosman, K.J.R., Boutron, C.F., Cescon, P., 2004. Elemental indicators of natural and anthropogenic aerosol inputs to Law Dome, Antarctica. Ann. Glaciol. 39, 169–174.
Vallelonga, P., Barbante, C., Cozzi, G., Gabrieli, J., Schüpbach, S., Spolaor, A., Turetta, C., 2013. Iron fluxes to Talos Dome, Antarctica, over the past 200 kyr. Clim. Past 9, 597–604.
Vallelonga, P., Christianson, K., Alley, R.B., Anandakrishnan, S., Christian, J.E.M., Dahl-Jensen, D., Gkinis, V., Holme, C., Jacobel, R.W., Karlsson, N., Keisling, B.A., Kipfstuhl, S., Kjær, H.A., Kristensen, M.E.L., Muto, A., Peters, L.E., Popp, T., Riverman, K.L., Svensson, A.M., Tibuleac, C., Vinther, B.M., Weng, Y., Winstrup, M., 2014. Initial results from geophysical surveys and shallow coring of the Northeast Greenland Ice Stream (NEGIS). Cryosphere 8, 1275–1287.
Vallelonga, P., Maffezzoli, N., Moy, A.D., Curran, M.A.J., Vance, T.R., Edwards, R., Hughes, G., Barker, E., Spreen, G., Saiz-Lopez, A., Corella, J.P., Cuevas, C.A., Spolaor, A., 2017. sea-ice-related halogen enrichment at Law Dome, coastal East Antarctica. Clim. Past 13, 171–184.
Vallelonga, P., de Gois, J.S., Borges, D.L.G., Costas-Rodríguez, M., Gkinis, V., Lannuzel, D., Spolaor, A., Vanhaecke, F., 2020. Concentration and isotopic composition of bromine and chlorine in Antarctic sea ice. Geochem. Cosmochim. Acta 293, 18–27.
Vancoppenolle, M., Meiners, K.M., Michel, C., Bopp, L., Brabant, F., Carnat, G., Delille, B., Lannuzel, D., Madec, G., Moreau, S., Tison, J.-L., van der Merwe, P., 2013. Role of sea ice in global biogeochemical cycles: emerging views and challenges. Quat. Sci. Rev. 79, 207–230.
von Glasow, R., Crutzen, P.J., 2014. 5.2 - tropospheric halogen chemistry. In: Holland, H.D., Turekian, K.K. (Eds.), Treatise on Geochemistry, second ed. Elsevier, Oxford, pp. 19–69.
Wagenbach, D., Ducroz, F., Mulvaney, R., Keck, L., Minikin, A., Legrand, M., Hall, J.S., Wolff, E.W., 1998. Sea-salt aerosol in coastal Antarctic regions. J. Geophys. Res. 103, 10961–10974.
Winstrup, M., Vallelonga, P., Kjær, H.A., Fudge, T.J., Lee, J.E., Riis, M.H., Edwards, R., Bertler, N.A.N., Blunier, T., Brook, E.J., Buizert, C., Ciobanu, G., Conway, H., Dahl-Jensen, D., Ellis, A., Emanuelsson, B.D., Hindmarsh, R.C.A., Keller, E.D., Kurbatov, A.V., Mayewski, P.A., Neff, P.D., Pyne, R.L., Simonsen, M.F., Svensson, A., Tuohy, A., Waddington, E.D., Wheatley, S., 2019. A 2700-year annual timescale and accumulation history for an ice core from Roosevelt Island, West Antarctica. Clim. Past 15, 751–779.
Wolff, E.W., Fischer, H., Fundel, F., Ruth, U., Twarloh, B., Littot, G.C., Mulvaney, R., Röthlisberger, R., de Angelis, M., Boutron, C.F., Hansson, M., Jonsell, U., Hutterli, M.A., Lambert, F., Kaufmann, P., Stauffer, B., Stocker, T.F., Steffensen, J.P., Bigler, M., Siggaard-Andersen, M.L., Udisti, R., Becagli, S., Castellano, E., Severi, M., Wagenbach, D., Barbante, C., Gabrielli, P., Gaspari, V., 2006. Southern Ocean sea-ice extent, productivity and iron flux over the past eight glacial cycles. Nature 440, 491–496.
Xiao, C., Dou, T., Sneed, S.B., Li, R., Allison, I., 2015. An ice-core record of Antarctic sea-ice extent in the southern Indian Ocean for the past 300 years. Ann. Glaciol. 56, 451–455.
Yang, X., Pyle, J.A., Cox, R.A., Theys, N., Van Roozendael, M., 2010. Snow-sourced bromine and its implications for polar tropospheric ozone. Atmos. Chem. Phys. 10, 7763–7773.
Zreda-Gostynka, G., Kyle, P.R., Finnegan, D.L., 1993. Chlorine, fluorine, and sulfur emissions from Mount Erebus, Antarctica and estimated contributions to the Antarctic atmosphere. Geophys. Res. Lett. 20, 1959–1962.
Zreda-Gostynka, G., Kyle, P.R., Finnegan, D., Prestbo, K.M., 1997. Volcanic gas emissions from Mount Erebus and their impact on the Antarctic environment. J. Geophys. Res. 102, 15039–15055.
Zwally, H.J., Abdalati, W., Herring, T., Larson, K., Saba, J., Steffen, K., 2002. Surface melt-induced acceleration of Greenland ice-sheet flow. Science 297, 218–222.